Paper ID: TE-01

Non-isothermal Heating and Magnetic Field Effect on Non-Newtonian Power Law Fluid in Triangular Channel

Sourav Das[*], Tawfiqur Rakib, Khan Md. Rabbi, Satyajit Mojumder , Sourav Saha
Department of Mechanical Engineering, Bangladesh University of Engineering and Technology
[*]E-mail:dsourav46@yahoo.com

Abstract

In this paper, effect of external magnetic field and non-isothermal heating in a triangular cavity filled with non-Newtonian power law fluid is analyzed numerically. Cavity has a non-isothermally heated bottom wall while other walls are kept cold. Simulations are carried out for wide variety of Rayleigh numbers (Ra = 10^3 ~ 10^6), Hartmann number (Ha = 0-60) and power law index (n = 0.5, 1, 1.5). Galerkin weighted residuals method of finite analysis is adopted in this study and grid independency test is performed to ensure numerical accuracy of the solution. Results are shown on the basis of streamlines, isotherms and average Nusselt number (Nu) plots. Result indicates that distortion of isotherm ensures convective dominance thus better heat transfer at lower Hartmann number. For any Hartmann number, heat transfer rate decreases with the increment of power law index and no significant changes are observed at higher Hartmann number.

Keywords: Rayleigh number, Magnetic field, Power-law index, Non-Newtonian fluid

1. Introduction

Natural convection fluid flow by buoyancy force has been a topic of interest for many researchers [1, 2] and has various applications of engineering such as electronic cooling systems [3, 4], nuclear reactors and heat exchangers [5] etc. The interaction of induced electric currents with the applied magnetic field results in a magneto hydrodynamic (MHD) forces which influences the flow of an electrically conducting fluid in the magnetic field. An externally applied magnetic field is a media for the process of manufacturing metal [6].

MHD natural convection simulation in cavities on different fluids and boundary conditions has been studied by various numerical methods widely recently [7-10]. The flow of non-Newtonian power law fluids has wide potential application in many process industries [11], in bio-medical Engineering [12] and also under MHD convection [13]. Researches with different geometric shaped models and numerical methods were done on natural convection for non-Newtonian power law fluids. Khezzar et al. [14] investigated natural convection of non-Newtonian power-law type fluids in two-dimensional rectangular tilted enclosures numerically and indicated that the increment and decrement of average Nusselt number for non-Newtonian power law fluids depended on Rayleigh number, Prandtl number, aspect ratio and power-law index. Examining two-dimensional steady state natural convection of power-law fluids numerically, Matin et al. [15] revealed that the non-Newtonian fluids were more efficient than Newtonian fluids for cooling and insulating purposes. Transient natural convection of non-Newtonian power law fluids in a square enclosure with differentially heated vertical side walls subjected to constant wall temperatures was studied by Kim et al. [16]. They showed that the mean Nusselt number increased for the decrement of power-law index for a given set of values of *Ra* and *Pr*.

The aim of present study is to simulate MHD natural convection of non-Newtonian power-law flow in a sinusoidally heated cavity with non-isothermal heating numerically. Moreover, it is intended to analyze various magnitude of magnetic field effect on the flow and on the thermal fields evidently with the alterations of different considered parameters (Rayleigh number, power-law index).

2. Problem specification

The details of the problem are presented in Figure 1. In the figure, right angled triangular-shape geometry of unit length (*L*) for bottom and vertical wall has been considered. The inclined wall has been modeled as the

hypotenuse ($\sqrt{2}L$) of the right angle triangle. The entire cavity is filled with non-Newtonian power law fluid to transfer heat inside the cavity. Gravity is working along the negative Y axis. Both the inclined and vertical walls of the cavity are kept at low temperature ($T = T_c$), while the base is kept non-isothermally heated ($T = T_c + sin^2(\pi x)$). A uniform magnetic field with a constant magnitude B is applied in horizontal direction.
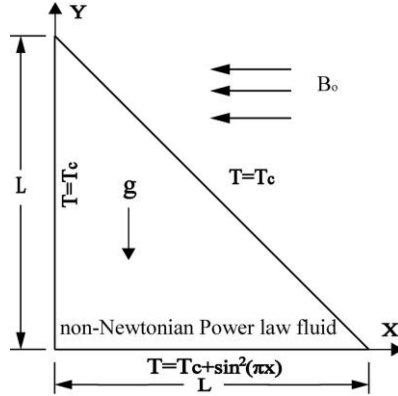

Fig. 1. Geometry of the present study

3. Mathematical formulation

A set of governing equations has been formed assuming that a two-dimensional right angled triangular enclosure filled with an incompressible non-Newtonian power-law fluid. The flow is considered to be incompressible and laminar. The density variation is approximated by the standard Boussinesq model. According to these assumptions, the governing equations like continuity, momentum and energy equation in non dimensional form can be written as follows-

$$\frac{\partial u}{\partial x} + \frac{\partial v}{\partial y} = 0. \tag{1}$$

$$\left(u\frac{\partial u}{\partial x} + v\frac{\partial u}{\partial y} \right) = -\frac{\partial P}{\partial x} + \frac{\Pr}{\sqrt{Ra}} \left[2\frac{\partial}{\partial x}\left(\frac{\mu a}{K}\frac{\partial u}{\partial x} \right) + \frac{\partial}{\partial y}\left(\frac{\mu a}{K}\left(\frac{\partial u}{\partial y} + \frac{\partial v}{\partial x} \right) \right) \right] \tag{2}$$

$$\left(u\frac{\partial v}{\partial x} + v\frac{\partial v}{\partial y} \right) = -\frac{\partial P}{\partial y} + \frac{\Pr}{\sqrt{Ra}} \left[2\frac{\partial}{\partial y}(\frac{\mu a}{K}\frac{\partial v}{\partial y}) + \frac{\partial}{\partial x}\left(\frac{\mu a}{K}\left(\frac{\partial u}{\partial y} + \frac{\partial v}{\partial x} \right) \right) \right] - \frac{\Pr Ha^2}{\sqrt{Ra}} v \tag{3}$$

$$u\frac{\partial T}{\partial x} + v\frac{\partial T}{\partial y} = \frac{1}{\sqrt{Ra}}\left(\frac{\partial^2 T}{\partial x^2} + \frac{\partial^2 T}{\partial y^2} \right) \tag{4}$$

In order to get the numerical solution of the system following scales are implemented to get the non-dimensional governing equations-

$$x = \frac{\bar{x}}{L}, y = \frac{\bar{y}}{L}, u = \frac{\bar{u}}{\left(\frac{\alpha}{L} \right)Ra^{0.5}}, v = \frac{\bar{v}}{\left(\frac{\alpha}{L} \right)Ra^{0.5}}, P = \frac{\bar{P}}{\rho\left(\frac{\alpha}{L} \right)^2 Ra}, T = \frac{\bar{T} - T_C}{T_H - T_C}. \tag{5}$$

For a purely-viscous non-Newtonian fluid according to Ostwald–DeWaele power-law [17] model the shear stress tensor can be expressed as-

$$\tau_{ij} = 2\mu_a D_{ij} = \mu_a\left(\frac{\partial \bar{u}_i}{\partial \bar{x}_j} + \frac{\partial \bar{u}_j}{\partial \bar{x}_i} \right) \tag{6}$$

where D_{ij} indicates the rate-of-deformation tensor for the two dimensional Cartesian coordinate and μ_a is the apparent viscosity that is derived for the two-dimensional Cartesian coordinates as-

$$\bar{\mu}_a = K\left[2\left[\left(\frac{\partial \bar{\mu}}{\partial \bar{x}} \right)^2 + \left(\frac{\partial \bar{v}}{\partial \bar{y}} \right)^2 \right] + \left(\frac{\partial \bar{v}}{\partial \bar{x}} + \frac{\partial \bar{u}}{\partial \bar{y}} \right)^2 \right]^{\frac{(n-1)}{2}} \tag{7}$$

In the above equations $(\bar{u}, \bar{v}), \bar{T}$ and $\bar{P}$ are the dimensional velocities, temperature and pressure respectively, ρ is the density, σ is the electrical conductivity, B is the uniform magnetic field, and n is the power law index. Therefore, the deviation of n from unity indicates the degree of deviation from Newtonian behavior. Dimensional form of the above equation is:

$$\mu_a = K\left[2\left[\left(\frac{\partial u}{\partial x}\right)^2 + \left(\frac{\partial v}{\partial y}\right)^2\right] + \left(\frac{\partial v}{\partial x} + \frac{\partial u}{\partial y}\right)^2\right]^{\frac{(n-1)}{2}} \tag{8}$$

Boundary conditions used to solve the present problem are mentioned in Table 1.

Table 1.Boundary conditions in non- dimensional form.

Boundary wall	Flow Field	Thermal Field
Vertical wall	$U = 0, V = 0$	$T = 0$
Inclined wall	$U = 0, V = 0$	$T = 0$
Bottom wall	$U = 0, V = 0$	$T = T_c + \sin^2(\pi * x)$

The non-dimensional governing parameters used are Prandtl number (Pr), Rayleigh number (Ra) and Hartmann number (Ha) these are defined below:

$$Pr = \frac{v_f}{\alpha_f}; Ha = \sqrt{\frac{\sigma_{nf} B^2 L^2}{v_{nf} \rho_{nf}}}; Ra = \frac{g\beta_f(T_h - T_c)L^3}{\upsilon_f \alpha_f}; \tag{9}$$

The characteristics of heat transfer are obtained by average Nusselt number and can be expressed as-

$$Nu_{av} = -\int_0^1 \frac{\partial T}{\partial Y} dX \tag{10}$$

4. Numerical Procedure

Numerical methods

The Galerkin weighted residual finite element method (FEM) has been deployed to the present problem to obtain a numerical solution. From Boussinesq approximation a set of algebraic equations has been formulated and the iterative process is used to solve this algebraic equation set. Triangular mesh formulation has been used to discretize the entire domain into several elements. Converging nature of the numerical solution has been confirmed and the converging criteria used is $|\Gamma^{n+1} - \Gamma^n| \leq 10^{-6}$ where n is the number of iteration and is general dependent variable.
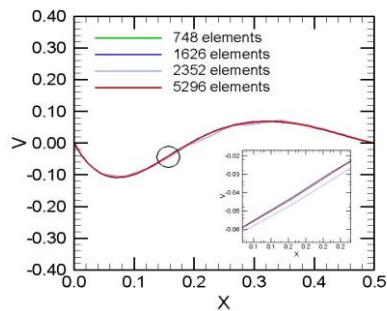

Fig. 2. Variation of mid-plane Y velocity (V) with X at $Ha = 60$, $Ra = 10^5$ and $Pr = 10$
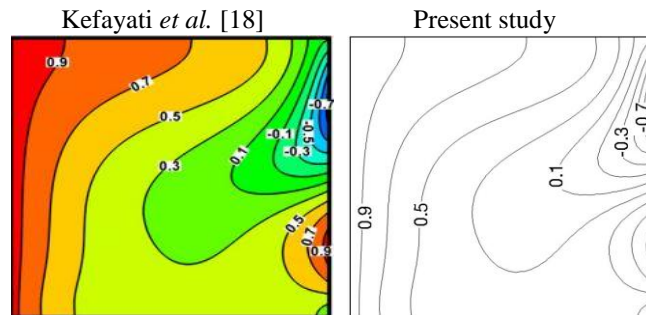
Fig. 3. Comparison of the isotherms for $Ra = 10^5$ and $Ha = 60$ between numerical results by Kefayati et al. [18] and the present results.

Grid independence

An extensive mesh testing procedure is conducted to guarantee a grid independent solution and its results have been presented in Figure 2. To check the accuracy of the numerical solution several mesh element numbers (748, 1626, 2352 and 5296) have been checked. From the figure, it is seen that mid-plane Y-velocity profiles for grid elements of 2352 and 5296 almost overlap each other thus making the solution grid independent. So, grid size of 5296 mesh elements is considered to be the optimum for the present study and other numerical simulation has been carried out taking this grid as independent.

Code validation

Code validation is done in light of isotherm and is validated with the consequences of Kefayati et al. [18] at $Ra = 10^5$ and $Ha = 60$ in Figure 3. From the figure, it is evident that present result is completely in par with the

previous study. So, the present numerical code and solution procedure are completely reliable, and so is the numerical solution.

5. Results and discussion

Effect of power law index and Hartmann number on isotherm and streamline

Fig. 4 and 5 shows the comparative analysis of streamline and isotherm contours at various Hartmann number and power law index at $Pr = 10$ and $Ra = 10^5$. The streamline shows two vortices, one anticlockwise and another clockwise. In the given problem, the working fluid gets heated at the bottom wall and moves upward using Buoyancy force. Again, the particle in contact with cold wall moves downwards and thus creates the vortices. As triangular cavity is used, it is seen that the vortex displaying clockwise rotation of the fluid is squeezed. It is considered as secondary vortex and has less strength comparable to primary vortex in the cavity. The isotherm has closely packed lines near bottom wall which indicates better convection.
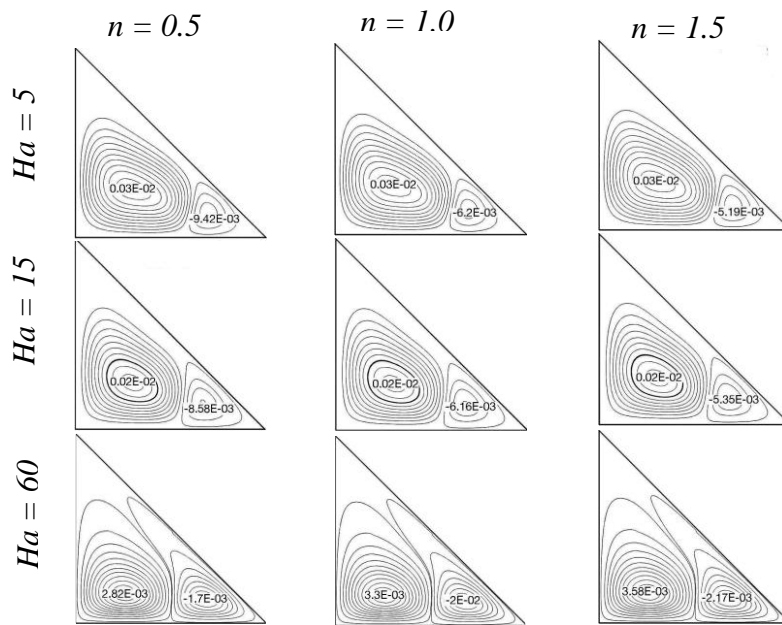

Fig. 4. Comparison of streamline at various Hartmann number and power law index for $Pr = 10$ and $Ra = 10^5$
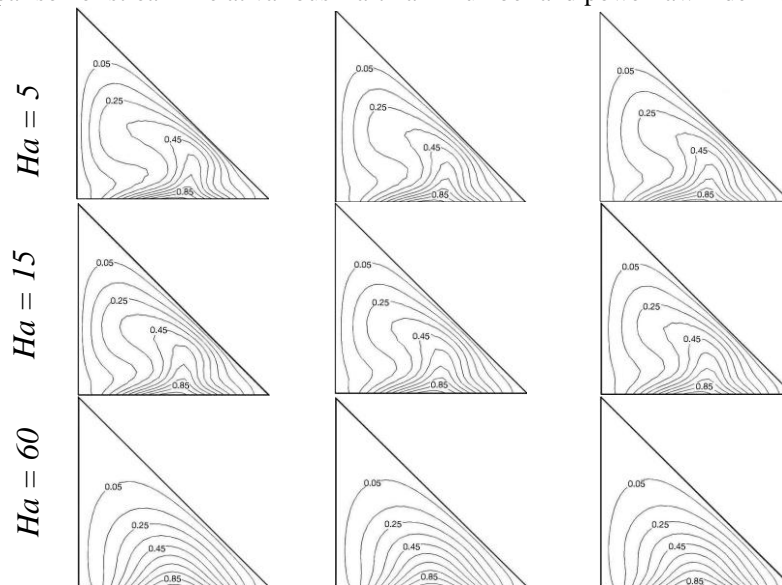

Fig. 5. Comparison of isotherm at various Hartman number and power law index for $Pr = 10$ and $Ra = 10^5$

It is evident from the isotherm (Fig. 5.) that the convective pattern is decreased due to the increase of Hartmann number. The more distortion of isotherm ensures convective dominance thus better heat transfer at lower Hartmann number. This is because the higher magnetic field distorts the vortices by suppressing

buoyancy force with the increase of power law index, the isotherm gets less distorted. So heat transfer becomes weaker. The stream function also shows a decreasing trend of value at $Ha = 5, 15$. But for $Ha = 60$, it doesn't maintain the pattern. The stream function decreases with the increase of power law index. But for $Ha = 60$, it rises. So it ensures a different behavior at $Ha = 60$. Because higher magnetic field can affects the heat transfer.

Effect of Hartmann number on average Nusselt number at different parameter

In Fig. 6(a) and 6 (b) average Nusselt number is plotted against Hartmann number at different Rayleigh number and power law index respectively for $Pr = 10$. From fig. 6(a), it can be said that Hartmann number has less effect on average Nusselt number at $Ra = 10^3$ & 10^4 as the buoyancy force was not significant for those cases. A significant change of rate of heat transfer is observed for $Ra = 10^5$ where maximum value of $Nu =$ 4.8037 is obtained in the absence of magnetic field. This is because of the higher temperature gradient at the heated wall. But as the effect of magnetic field starts to persist, the heat transfer rate diminishes gradually and becomes nearly constant at $Ha > 75$.

In fig. 6(b), it is observed that in the absence of magnetic field highest heat transfer is obtained for pseudo-plastic fluid ($n = 0.5$) with $Nu = 4.8037$ and lowest heat transfer is obtained for dilatants fluid ($n = 1.5$) with $Nu = 3.6331$. With the intensification of magnetic field, heat transfer rate shows a decreasing nature. An important change is found at nearly $Ha = 35$ where all the curves intersect. The effect Hartmann number is almost nullified and the heat transfer rate for pseudo-plastic fluid becomes lesser than that of the Newtonian ($n = 1.0$) and dilatants fluid. So it is also noticed that the lowest possible heat transfer rate is obtained for pseudo-plastic fluid at $Ha = 100$ with $Nu = 1.9454$.
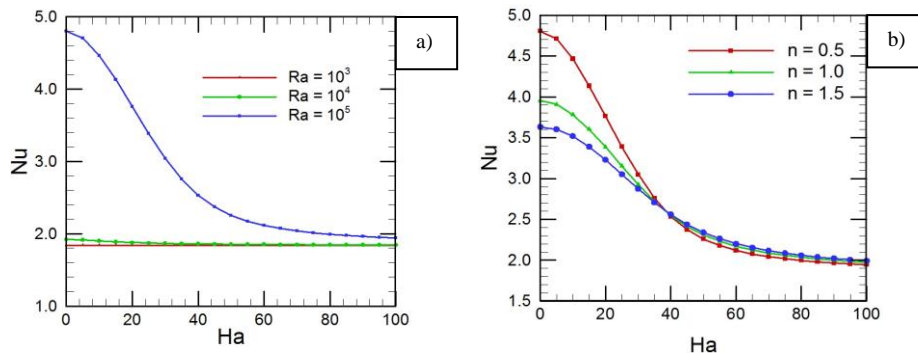

Fig. 6. Variation of the average Nusselt number due to the change of Hartmann number at different (a) Rayleigh number for $n = 0.5$ (b) Power law index for $Ra = 10^5$ at $Pr = 10$

Effect of Rayleigh number on average Nusselt number at different power law index

Fig 7 demonstrates the effect of Rayleigh number on average Nusselt number at different power law index for $Ha = 30$. It is followed that there is less effect on heat transfer rate due to the increment of Rayleigh number
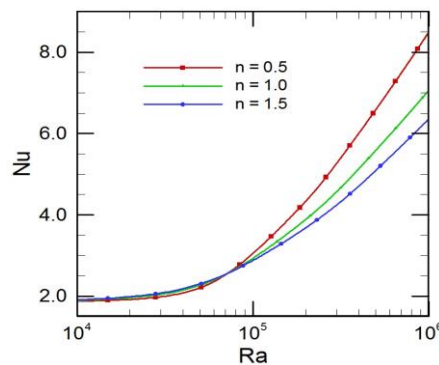

Fig. 7. Variation of average Nusselt number due to the change of Rayleigh number at different power law index for $Ha = 30$

at first. An intersection is found at near $Ra = 10^5$ for all fluids and a huge increase of heat transfer begin with the increment of Rayleigh number. The rate of increase of heat transfer for the pseudo plastic fluid is evidently the highest among all but the opposite is true for $Ra < 8 \times 10^4$.

6. Conclusion

Different pertinent parameters on this heat transfer investigation lead us to the following conclusion:
• Magnetic field is effective on overall heat transfer for higher Rayleigh number $Ra = 10^5$.

- Pseudo-plastic fluid ($n = 0.5$) should be used at lower magnetic field ($Ha < 40$) with higher buoyancy effect ($Ra > 8 \times 10^4$).
- Dilatant fluid ($n = 1.5$) would be feasible for higher intensity of magnetic induction ($Ha > 40$) at lower Rayleigh number ($Ra < 8 \times 10^4$).
- To obtain better heat transfer (more than 32%) non-Newtonian pseudo-plastic ($n = 0.5$) fluid can be used in absence of magnetic field.
- At an optimum magnetic induction ($Ha = 40$), identical heat transfer rate is found for both Newtonian fluid ($n = 1.0$) and non-Newtonian fluid ($n = 0.5, 1.5$).

7. Acknowledgement

8. References

[1] T. Basak, S. Roy, and C. Thirumalesha, "Finite element analysis of natural convection in a triangular enclosure: effects of various thermal boundary conditions", *Chemical Engineering Science*, Vol.62, No.9, pp. 2623-2640, 2007.

[2] V.A. Akinsete, and T.A. Coleman, "Heat transfer by steady laminar free convection in triangular enclosures", *International Journal of Heat and Mass Transfer*, Vol.25, No.7, pp. 991-998, 1982.

[3] S. Kakaç, H. Yüncü, and H. Hijikata, Cooling of electronic systems, *Springer Science & Business Media*, No. 258, 1994.

[4] F.P. Incropera, "Convection heat transfer in electronic equipment cooling", *Journal of Heat Transfer*, Vol. 110, No.4b, pp. 1097-1111,1988.

[5] M.G. Parent, T.H. Van der Meer, and K.G.T. Hollands, "Natural convection heat exchangers in solar water heating systems: theory and experiment", *Solar Energy*, Vol.45, No.1, pp. 43-52, 1990.

[6] M. Sathiyamoorthy, and A. Chamkha, "Effect of magnetic field on natural convection flow in a liquid gallium filled square cavity for linearly heated side wall (s)", *International Journal of Thermal Sciences*, Vol.49,No.9, pp. 1856-1865, 2010.

[7] M. Bhuvaneswari, S.Sivasankaran, and Y.J. Kim, "Magnetoconvection in a square enclosure with sinusoidal temperature distributions on both side walls", *Numerical Heat Transfer, Part A: Applications*, Vol.59, No.3, pp. 167-184, 2011.

[8] H.F. Öztop, M.M. Rahman, A. Ahsan, M. Hasanuzzaman, R. Saidur, K. Al-Salem, and N. A. Rahim, "MHD natural convection in an enclosure from two semi-circular heaters on the bottom wall", *International Journal of Heat and Mass Transfer*, Vol.55, No.7, pp. 1844-1854, 2012.

[9] M. Sheikholeslami, M. Gorji-Bandpy, D.D. Ganji, and S. Soleimani, "MHD natural convection in a nanofluid filled inclined enclosure with sinusoidal wall using CVFEM", *Neural Computing and Applications*, Vol.24, No.3-4, pp. 873-882, 2014.

[10] S.C. Kakarantzas, I.E. Sarris, A.P. Grecos, and N.S. Vlachos, "Magnetohydrodynamic natural convection in a vertical cylindrical cavity with sinusoidal upper wall temperature", *International Journal of Heat and Mass Transfer*, Vol.52, No.1, pp. 250-259, 2009.

[11] R.P. Chhabra,and J. F. Richardson, Non-Newtonian flow in the process industries: fundamentals and engineering applications, *Butterworth-Heinemann*, 1999.

[12] L.M. Srivastava, and V.P. Srivastava, "Peristaltic transport of a non-Newtonian fluid: applications to the vas deferens and small intestine", *Annals of biomedical engineering*, Vol. 13, No. 2, pp. 137-153, 1985.

[13] K.V. Prasad, and K. Vajravelu, "Heat transfer in the MHD flow of a power law fluid over a non-isothermal stretching sheet", *International Journal of Heat and Mass Transfer*, Vol.52, No.21, pp. 4956-4965, 2009.

[14] L. Khezzar, D. Siginer, and I. Vinogradov, "Natural convection of power law fluids in inclined cavities", *International Journal of Thermal Sciences*, Vol.53, pp. 8-17, 2012.

[15] M.H. Matin, and W.A. Khan, "Laminar natural convection of non-Newtonian power-law fluids between concentric circular cylinders", *International Communications in Heat and Mass Transfer*, Vol.43, pp. 112-121, 2013.

[16] G.B. Kim, J.M. Hyun, and H.S. Kwak, "Transient buoyant convection of a power-law non-Newtonian fluid in an enclosure", *International journal of heat and mass transfer*, Vol. 46, No.19, pp. 3605-3617, 2003

[17] A.F. Emery, H.W. Chi, and J.D. Dale, "Free convection through vertical plane layers of non-Newtonian Power- law fluids," *Journal of Heat Transfer*, Vol.93, No2, pp. 164-171, 1971.

[18] G.R. Kefayati, "Simulation of magnetic field effect on natural convection of non-Newtonian power-law fluids in a sinusoidal heated cavity using FDLBM", *International Communications in Heat and Mass Transfer*, Vol. 53, pp. 139-153, 2014.

Effect of magnetic field on natural convection in a rectangular enclosure with thin fin attached and having *Cu*-water nanofluid inside

Moinuddin Shuvo [1,*], Rabiul Hasan Kabir [1], Khan Md. Rabbi [1], Satyajit Mojumder [1], Sourav Saha [1]

[1] Department of Mechanical Engineering, Bangladesh University of Engineering and Technology
[1,*]E-mail: moinuddinshuvo@gmail.com

Abstract

In this study, a rectangular enclosure with thin fin attached and filled with Cu-water nanofluid under external magnetic field is numerically analyzed. A highly conductive thin fin is attached at the bottom wall. Numerical simulations have been carried out for wide variety of Rayleigh numbers (Ra = 10³ ~ 10⁶), Hartmann number (Ha = 0-100) and solid volume fraction (φ = 0 ~ 0.15). Galerkin weighted residual method of finite element analysis is used in this investigation to find the solution. Numerical accuracy is ensured by the grid independency test. Flow and thermal behavior are discussed on the basis of streamlines, isothermal lines respectively. Nusselt number (Nu) plot on cold wall and average temperature of the working fluid are shown to quantify the overall heat transfer rate. Results show that heat transfer rate increases with the increment of Rayleigh number, solid volume fraction and decreases with the increment of Hartmann number. More than 40% better heat transfer is recorded for lower strength of magnetic field. There is no significant change in overall heat transfer at Ha > 40, even with increasing Ra

Keywords: Magnetic field, Nusselt number, Rayleigh number, Nanofluid, Fin

1. Introduction

Heat transfer in natural convection mode is very crucial in this modern era of science and engineering. In order to meet the growing demand from various industries, engineers and scientists have to come up with numerical analysis of heat transfer and investigate the effect of different pertinent parameters [1-3]. Heat transfer analysis under external magnetic field has grown more attentions in this consequence. In recent times many researchers have investigated and successfully evaluated the effect of external magnetic field on natural convection. Amir Houshang Mahmoudi *et al.* [4] studied the MHD natural convection in a trapezoidal enclosure using *Cu*–water nanofluid considering two dimensional trapezoidal enclosure with partially activated wall, they found out that at Rayleigh number, $Ra = 10^4$ and 10^5 the Nusselt number increases with the Hartmann number due to the presence of nanoparticles but at higher Rayleigh number, Nusselt number reduction was also observed. Hakan F. Oztop *et al.* [5] has showed that for MHD buoyancy induced laminar in a non-isothermally heated square enclosure for different parameters as amplitude of sinusoidal function, increasing heat transfer rate is observed and Hartmann number can also be a control parameter for heat transfer rate and flow field. Recent numerical investigation also shows the importance of external magnetic field effect on heat transfer with different shapes of cavity and boundary conditions [6-8]. In this regard, Ghasemi *et al.* [9] showed that for a square enclosure filled with a water-Al_2O_3 which is influenced by magnetic field exerts stronger flow circulations and intensified isotherms near the vertical walls at higher Raleigh Number (*Ra*), lower Hartmann number (*Ha*) at a fixed solid volume fraction.

From industrial point of view energy saving and enhancement of heat transfer is a must. This calls for the replacement of conventional heat transfer fluids with nanofluid. Nanofluids are fluids containing nanometer-sized particles of metals, carbides, oxides, nitrides, or nanotubes. Related studies [10-12] show the enhanced thermophysical properties such as higher thermal conductivity and heat transfer coefficient compared to the base fluid.

Fins are thin components or appendage attached to a larger body or structure for increasing convection. Aminossadati *et al.* [13] showed in their study of MHD natural convection in a square cavity with a thin fin that the position of the fin has more effect on the hot wall then the cold wall at a higher values of Rayleigh number where the heat transfer is mainly due to convection. Also related investigations [14-16] shows that not only the positon but also the size and shape of the fin has severe impact in heat transfer mechanism.

The purpose of this investigation is to analyze natural convection under external magnetic field in a rectangular cavity. Effect of different pertinent parameters such as Rayleigh number (*Ra*), Hartmann number (*Ha*), solid

volume fraction (φ) have been shown in terms of streamline, isotherm contours and related plots. Mid-plane velocity profile is shown to justify the flow behavior under external magnetic field. Nusselt number (Nu) at the cold wall and average temperature of the nanofluid is illustrated to investigate the heat transfer.

2. Problem specification

Fig. 1 shows a schematic diagram of the rectangle enclosure filled with Cu – water nanofluid. The two vertical left and right walls have been kept adiabatic and the bottom wall is kept at high temperature ($T = T_h$) and the top wall is kept at low temperature ($T = T_c$) where $T_c < T_h$. Here, Boussinesq approximation is assumed to hold true for buoyancy effect and walls are assumed no slip. The gravitational effect is shown along the negative Y-axis. Cu - Water nanofluid is considered as the working fluid. Radiation and viscous dissipation heat transfer effects are assumed to be negligible for the simplification of the investigation.
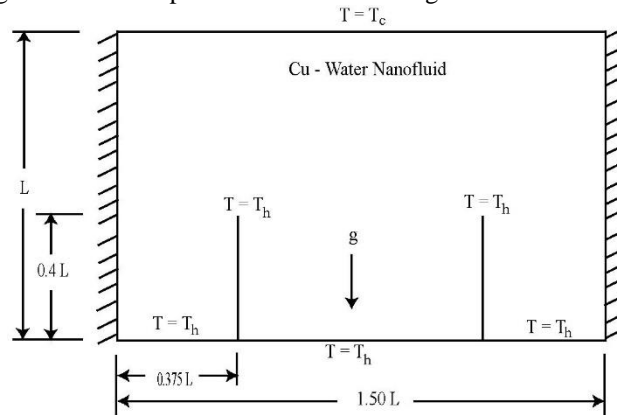

Fig. 1. Schematic diagram of a rectangular enclosure filled with Cu-Water nanofluid with thin fin attached

3. Mathematical formulation

The steady state equations that govern the conservation of energy, momentum and continuity for the natural convection of fluid in the presence of a magnetic field can be written in the following non dimensional forms.

$$\frac{\partial(U\delta)}{\partial X}+\frac{\partial(U\delta)}{\partial Y}=\frac{\partial}{\partial X}\left(\Gamma_\delta\frac{\partial\delta}{\partial X}\right)+\frac{\partial}{\partial Y}\left(\Gamma_\delta\frac{\partial\delta}{\partial Y}\right)+S_\delta. \tag{1}$$

Table 1 describes the summarized form [17].

Table 1. A summary of the terms of the non-dimensional governing equations (1).

Equation	δ	Γ_δ	S_δ
Continuity	1	0	0
U-momentum	U	$\mu_{nf}/\rho_{nf}\alpha_f$	$-\partial P/\partial X$
V-momentum	V	$\mu_{nf}/\rho_{nf}\alpha f$	$-\partial P/\partial Y + (\rho\beta)_{nf}RaPr\Theta/(\rho_{nf}\beta f) - Ha^2PrV$
Energy	Θ	α_{nf}/α_f	0

Scales are obtained to find the non-dimensional form of the governing equations which can be defined as-

$$X=\frac{x}{L},Y=\frac{y}{L},U=\frac{u}{U_o},V=\frac{v}{U_o},P=\frac{p}{\rho_pU_o{}^2},\Theta=\frac{T-T_c}{T_h-T_c}. \tag{2}$$

The non-dimensional governing parameters Rayleigh number (Ra) is an indication of the effects of buoyancy forces, Prandtl number (Pr) is the ratio of momentum diffusivity (kinematic viscosity) to thermal diffusivity and Hartmann number (Ha) corresponds to the effects of magnetic forces, can be expressed as

$$Ra=\frac{g\beta_f(T_h-T_c)L^3}{v_f^2}Pr,Pr=\frac{v_f}{\alpha_f},Ha=B_0L\sqrt{\frac{\sigma_{nf}}{\rho_{nf}v_f}}. \tag{3}$$

The thermo-physical characteristic parameters are expressed below

Effective density of nanofluid, $\quad \rho_{nf}=(1-\varphi)\rho_f+\varphi\rho_p.$ $\tag{4}$

Specific heat coefficient, $\quad (\rho C_p)_{nf}=(1-\varphi)(\rho C_p)_f+\varphi(\rho C_p)_p.$ $\tag{5}$

Thermal expansion coefficient, $(\beta\rho)_{nf}=(1-\varphi)(\beta\rho)_f+\varphi(\rho\beta)_p.$ $\tag{6}$

Dynamic viscosity [18], $\quad \mu_{nf}=\mu_f(1-\varphi)^{-0.25}.$ $\tag{7}$

Thermal conductivity [19],
$$k_{nf} = k_f \left[\frac{\left(k_p + 2k_f\right) - 2\varphi\left(k_f - k_p\right)}{\left(k_p + 2k_f\right) + \varphi\left(k_f - k_p\right)} \right]. \tag{8}$$

Here, subscript p, nf and f represent nanoparticle, nanofluid and base fluid respectively. Average verage Nusselt number can be expressed as,

$$\overline{Nu} = \frac{hL}{k_f} = -\frac{k_{nf}}{k_f} \int_0^1 \frac{\partial \Theta}{\partial Y}.dX \tag{9}$$

Boundary conditions illustrated in Fig. 1 can be written in dimensionless forms are presented in Table 2.

Table 2. Boundary condition in non-dimensional form

Boundary wall	Flow field	Thermal field
Bottom and fin wall	U = 0, V = 0	$\Theta = 1$
Top wall	U = 0, V = 0	$\Theta = 0$
Side wall	U = 0, V = 0	$\frac{\partial \Theta}{\partial X} = 0$

Here, U, V, Θ represent non dimensional x-direction velocity, y-direction velocity and temperature respectively. Again σ, υ, β and B_o represent electrical conductivity, kinematic viscosity, thermal expansion co-efficient and magnetic flux density respectively.

4. Numerical procedure
Grid Independency test
To examine the accuracy of the numerical results grid independency test is carried out. Mid-plane velocity profile of the vertical mid-plane is inspected at $Ra = 10^4$, $Ha = 30$, $\varphi = 0.15$ (see Fig 2). As shown in the following Fig. 2 mesh elements for the test are 1334, 2548, 6329, 10377. From the figure it is observed that mid-plane x-velocity profiles for 6329 and 10377 mesh elements are almost overlapping each other. As a result we take 6329 mesh elements as the optimum grid elements for present study.
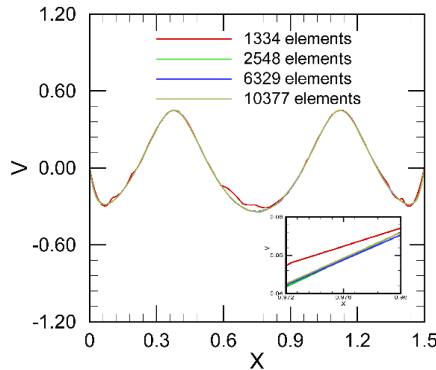

Fig. 2. Variation of mid-plane Y-velocity (V) with X at $Ha = 20$, $Ra = 10^5$ and $\varphi = 0.15$
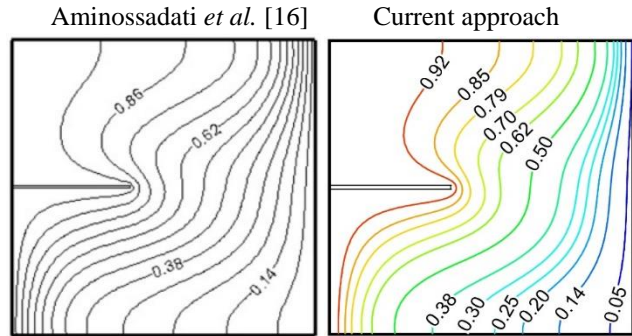
Fig. 3. Comparison of isotherm contours between Aminossadati *et al.* [16] and present code at $Ra = 10^5$, $Ha = 50$, $L_p = 0.4$, $Y_p = 0.5$

Code Validation
The non-dimensional governing equations along with the boundary conditions are solved numerically. The previous study by Aminossadati *et al.* [16] is compared with the present code (see Fig. 3). For comparing the results isothermal lines are plotted for $Ra = 10^5$ and $Ha = 50$ when the length of the fin $L_P = 0.4$ and position of the fin $Y_P = 0.5$. According to figure, we can say that the validation study holds a very good agreement.

5. Result and discussion
Effect of Hartmann number (*Ha*) on streamlines and isotherm contours
From the Fig. 4, it is evident that that increment of Hartmann number (*Ha*) tends to decrease the strength of flow field no matter what the Rayleigh number (*Ra*) is. This is due to the fact that, the fluid particles do have the unique magnetic susceptibility property which results in Lorentz force. So domination of this force opposes the reason of its generation. Thus the net force applied on the working fluid is affected which eventually weakens the flow field in terms of values of stream function. Thus weaker vortices can be found at lower $Ra = 10^4$ and higher at Hartmann number (*Ha* = 50). But at higher *Ra*, the vortices previously formed in the cavity tend to absorb more energy, get larger in size thus get accumulate within the cavity. Stronger vortices with higher value of stream function created
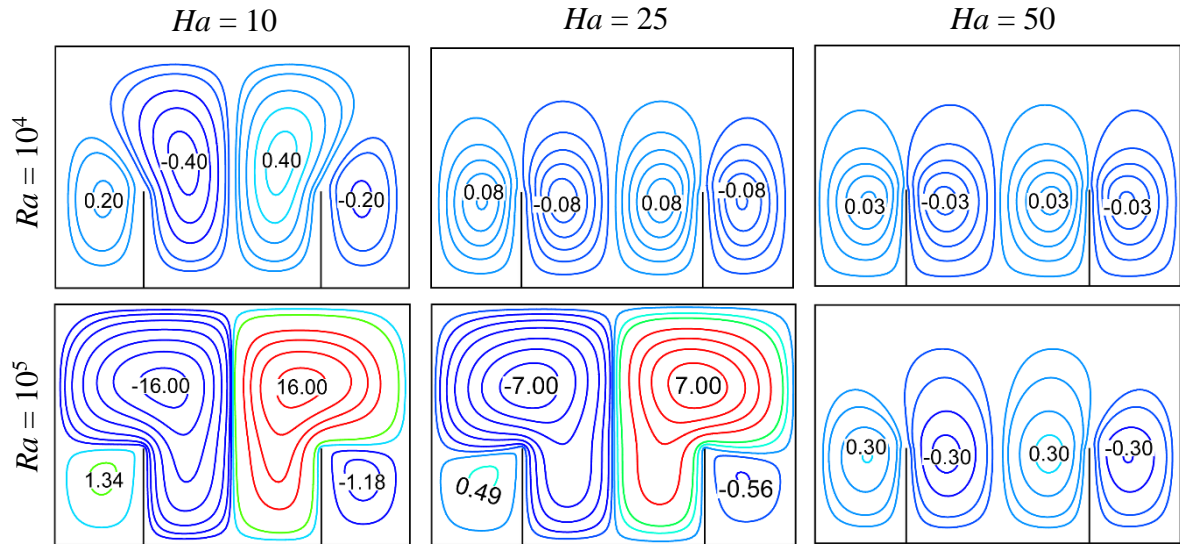
3

Fig. 4. Effect of *Ha* on streamlines in upper row for *Ra* =10^4 and in lower row for *Ra* =10^5 at $\varphi = 0.15$
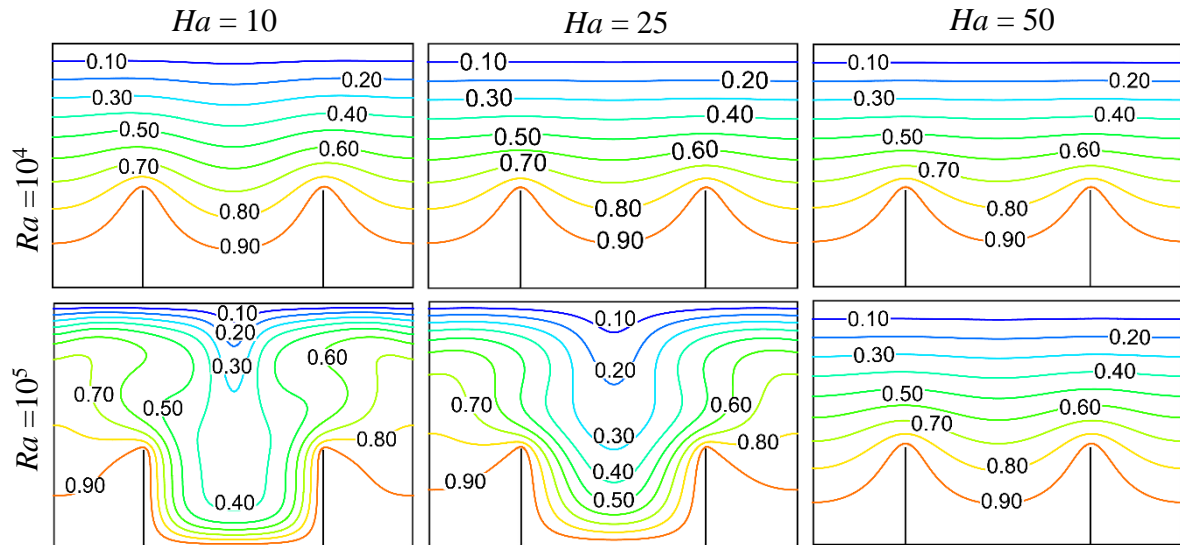

Fig. 5. Effect of *Ha* on isotherm contours in upper row for *Ra* = 10^4 and in lower row for *Ra* =10^5 at $\varphi = 0.15$

at *Ra* = 10^5 certainly have impact on the overall heat transfer rate which will be backed up by Nusselt number plots.

Fig. 5 represents the thermal field of the working fluid inside the cavity. At lower *Ra* = 10^4, isotherm patterns do not attain much variation with Hartmann number (*Ha*). This is because, in this case buoyancy force is too low to be suppressed by external magnetic field. But at higher *R*a = 10^5, when buoyancy flow is higher, more distorted lines are found which results in convective heat transfer phenomenon. With the increment of *Ha*, parallel lines suggest conduction mode of heat transfer. One interesting note is revealed that, being exposed to higher magnetic field (*Ha* = 50), isotherm contours become similar in pattern for *R*a = 10^4 and 10^5. Thus the thermal field suggests that higher magnetic field has always a negative impact on the heat transfer mechanism.

Effect Hartmann number on mid-plane velocity profile

Variation of Y-component of the velocity field of the working fluid is illustrated in Fig. 6. As *Ha* is increased, the velocity profile tends to be diminished and shows almost no variation for higher Hartmann number (*Ha* = 50). This is because when the *Ha* is increased, an influence of Lorentz force is occurred on the convective flow. In this case, lower Rayleigh number (*Ra* = 10^4) is chosen because the influence of magnetic field is more prominent on weaker convective flow.
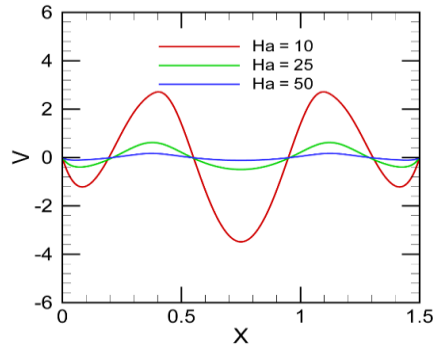
Fig. 6. Variation of Y-velocity (V) at mid-section of the enclosure with X-length for $Ra = 10^4$, $\varphi = 0.15$

Effect of Hartmann number on average Nusselt number and average temperature of the working fluid

Fig. 7 depicts the effect of Hartmann number on average Nusselt number (Nu). Nusselt number is quantified at the cold wall. This is because, the isothermal lines are more intensified at that wall. It is seen that Nu shows no variation at lower Rayleigh numbers ($Ra = 10^3$, 10^4) due to less convection phenomena. For higher Rayleigh number ($Ra = 10^5$) and $Ha = 0$, temperature gradient in the cold wall is higher and therefore Nusselt number (Nu) is maximum. It is observed that Nu tends to fall rapidly upto $Ha = 40$. An interesting observation is made that for $Ha > 40$, Ra shows no significant effect on overall heat transfer which is due to the dominance of conductive regime.

Table 3 shows the effect of Ra and Ha on the average temperature of the fluid. For inspecting the effect, $Ha = 10$, $Ha = 25$ and $Ha = 50$ have been observed where Ra is varied from 10^3 to 10^5. It is evident that for $Ha = 10$, $Ha = 25$ and $Ha = 50$ the value of the average temperature does not change that much with the increase of Ra from 10^3 to 10^5 but slightly decrease at higher value of Hartmann number.
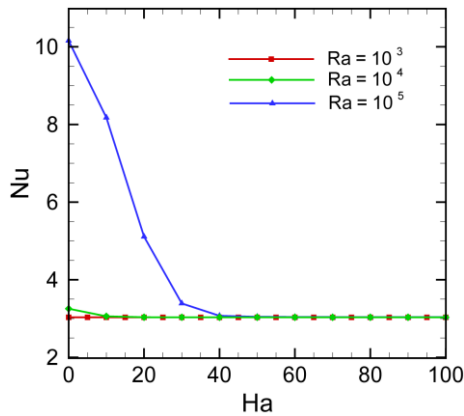

Fig. 7. Variation of average Nusselt number with Ha at $\varphi = 0.15$

Table 3. Variation of average temperature of the fluid for different Ha and Ra at $\varphi = 0.15$

Ra	Ha		
	10	25	50
1×10^3	0.907	0.908	0.908
5×10^3	0.906	0.907	0.908
1×10^4	0.904	0.907	0.907
5×10^4	0.902	0.889	0.906
1×10^5	0.902	0.877	0.905

Effect of solid volume fraction of nanofluid on average Nusselt number

Fig. 8 illustrates the effect of solid volume fraction (φ) on the average Nusselt number (Nu). It illustrates that value of Nu increases with the increase of φ and the rate of increase of Nu increases with the increase of φ. The addition of solid nanoparticle (Cu) to the base fluid (water) results in an increase of μ_{nf}/ρ_{nf} in the diffusion term which describes better buoyancy circulation. Such buoyancy current eventually increases the heat transfer rate. Thus maximum average Nusselt number at the cold wall is attained at solid volume fraction ($\varphi = 0.15$)
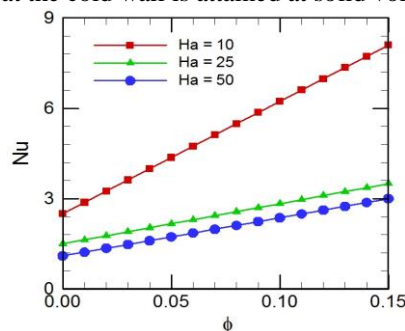

Fig. 8. Variation of average Nusselt number (Nu) with the solid volume fraction (φ) at $Ra = 10^5$

6. Conclusion
From the results discussed before, the following conclusion for this investigation can be drawn-
- Study shows the strength of flow decreases with the increment of magnetic field.
- The isothermal lines get less distorted as the magnetic field gets stronger. It signifies the increase of conduction mode of heat transfer.
- Strength of magnetic field has severe effect on amplitude of velocity profile of the working fluid.
- More than 40% better heat transfer is recorded for lower strength of magnetic field.
- Solid volume fraction of nanoparticle has a positive impact on heat transfer rate in terms of average Nusselt number.
- There is no significant variation in overall heat transfer at Ha > 40, even with increasing Ra.

7. Acknowledgement

8. References
[1] H. Nemati, M. Farhadi ∗, K. Sedighi, H.R. Ashorynejad, E. Fattahi,"Magnetic field effects on natural convection flow of nanofluid in a rectangular cavity using the Lattice Boltzmann model", *Scientia Iranica*, Vol.19, No.2, pp.303–310 , 2012.

[2] L.F. Jina, K.W. Tou, C.P. Tso, ,"Effects of rotation on natural convection cooling from three rows of heat sources in a rectangular cavity", *International Journal of Heat and Mass Transfer*, Vol. 48, No.19–20, pp. 3982–3994, 2005.

[3] Rejane De C. Oliveski, Mario H. Macagnan, Jacqueline B. Copetti, "Entropy generation and natural convection in rectangular cavities", *Applied Thermal Engineering*, Vol. 29, No.8–9, pp. 1417–1425, 2009.

[4] A.H. Mahmoudi, I. Pop, M. Shahia, F. Talebia, "MHD natural convection and entropy generation in a trapezoidal enclosure using *Cu*–water nanofluid", *Computers and Fluids*, Vol.72, pp. 46–62, 2013.

[5] Hakan F. Oztop, Mesut Oztop, Yasin Varol, ", Numerical simulation of magnetohydrodynamic buoyancy-induced flow in a non-isothermally heated square enclosure", *Communications in Nonlinear Science and Numerical Simulation*, Vol.14, pp. 770–778, 2009.

[6] K.M. Rabbi, T. Ahmad, S. Mojumder, S. Saha, M.Z. Hossain, "Geometric Effect on Magnetohydrodynamic Convection in a Half-moon Shaped Cavity Filled with Water Having Semi-circular Bottom Heater", *Procedia Engineering*, Vol. 105, pp. 73-80, 2015.

[7] L.Th. Benos, S.C. Kakarantzas, I.E. Sarris, A.P. Grecos, N.S. Vlachos, "Analytical and numerical study of MHD natural convection in a horizontal shallow cavity with heat generation", *International Journal of Heat and Mass Transfer*, Vol.75, pp.19–30, 2014.

[8] M. Sheikholeslami , M. Gorji-Bandpy, D.D. Ganji, "MHD free convection in an eccentric semi-annulus filled with nanofluid", *Journal of the Taiwan Institute of Chemical Engineers*, Vol. 45,No. 4, pp.1204–1216, 2014.

[9] B. Ghasemi, S.M. Aminossadati, A. Raisi, "Magnetic field effect on natural convection in a nanofluid-filled square enclosure", *International Journal of Thermal Sciences*, Vol. 50, pp. 1748-1756, 2011.

[10] A.G. Agwu Nnanna, "Experimental model of temperature-driven nanofluid", *Journal of Heat Transfer*, Vol. 129, No. 6, pp. 697-704, 2007.

[11] H.F. Oztop, E. Abu-Nada, "Numerical study of natural convection in partially heated rectangular enclosuresfilled with nanofluids", *International Journal of Heat and Fluid Flow*, Vol. 29, No. 5, pp. 1326-1336, 2008.

[12] S.M. Aminossadati, B. Ghasemi,"Natural convection cooling of a localised heat source at the bottom of a nanofluid-filled enclosure", *European Journal of Mechanics B/Fluids*, Vol. 28, No. 5, pp. 630-640, 2009.

[13] S.M. Aminossadati, B. Ghasemi, A. Kargar, "Computational analysis of magnetohydrodynamic natural convection in a square cavity with a thin fin", *European Journal of Mechanics B/Fluids*, Vol. 46, pp.154–163, 2014.

[14] Qiu-Wang Wang, , Mei Lin, Min Zeng,"Effect of lateral fin profiles on turbulent flow and heat transfer performance of internally finned tubes", *Applied Thermal Engineering*, Vol. 29,No. 14–15, pp. 3006–3013, 2009.

[15] M. Dogan, M. Sivrioglu, "Experimental investigation of mixed convection heat transfer from longitudinal fins in a horizontal rectangular channel: In natural convection dominated flow regimes", *Energy Conversion and Management*, Vol. 50,No. 10, pp. 2513–2521, 2009.

[16] Tri Lam Ngo, Yasuyoshi Kato, , Konstantin Nikitin, Takao Ishizuka, "Heat transfer and pressure drop correlations of microchannel heat exchangers with S-shaped and zigzag fins for carbon dioxide cycles", *Experimental Thermal and Fluid Science*, Vol. 32,No. 2, pp. 560–570, 2007.

[17] M.M. Rahman, S. Mojumder, S. Saha, A.H. Joarder, R. Saidur, A.G. Naim, "Numerical and statistical analysis on unsteady magnetohydrodynamic convection in a semi-circular enclosure filled with ferrofluid", *International Journal of Heat and Mass Transfer*, Vol. 89, pp. 1316-1330, 2015.

[18] H.C. Brinkman, "The viscosity of concentrated suspensions and solutions", *Journal of Chemical Physics*, Vol. 20, pp 571-581, 1952.

[19] J.C. Maxwell, A Treatise on Electricity and Magnetism, second ed., Oxford University Press, Cambridge, pp. 435-441, 1904.

Pure Mixed Convection inside Square Ventilated Cavity Containing Rotating Adiabatic Cylinder: Influence of Working Fluid

Mir Jalal Ahmad[1], Nandita Chakrabarty Jhumur, Sourav Saha[2], Satyajit Mojumder, Khan Rabbi

Department of Mechanical Engineering, Bangladesh University of Engineering and Technology, Dhaka-1000.

E-mail: [1]mja.sujon@gmail.com
[2]souravsahame17@gmail.com

Abstract

Mixed convection has been one of the major topics of research in the field of heat transfer for many years. Mixed convection from open or ventilated cavity deserves particular attention for their more common occurrence in practical field. In this paper, mixed convection in a square cavity, having inlet and outlet ports at bottom and top walls respectively and containing a rotating circular cylinder at center, is analyzed thoroughly under pure mixed convective regime for a plain fluid (water) and a nanofluid (Al_2O_3-water) with solid volume fraction (φ) of 0.1. For pure mixed convection (Richardson number, Ri =1), both aiding and opposing flow convection mechanisms are analyzed by varying speed (Ω = 0 – 100) and direction of rotation of cylinder keeping Reynolds (Re) and Grashof (Gr) numbers constant at 100 and 10^4. Moreover, effect of addition of nanofluid is observed by comparing average Nusselt number (Nu) at heated boundary and average fluid temperature (T_{av}), as well as, flow and thermal fields for both water and nanofluid. At Ri = 1, Gr is varied from 0.1 to 10^5 for both kinds of fluid to find out the impact of transition of mixed convection regimes. It has been observed that, for opposing flow mixed convection heat transfer rate is significantly low up to a certain value of Ω. However, significant increment of heat transfer rate is possible for high rotational speed of cylinder, higher Re and Gr. Almost invariably, addition of nanofluid augments heat transfer rate.

Keywords: Mixed convection, ventilated cavity, rotating cylinder, nanofluid, pure mixed convection.

1. Introduction

Pure mixed convection, combination of natural and forced convection, has many occurrences such as in nuclear reactor, solar receiver, heat exchanger, thermal storage, semiconductors, etc. [1], [2]. Other applications include rotating-tube heat exchangers, rotating shafts, drilling of oil-wells, nuclear reactor fuel rods, steel suspension bridge cables, etc. [3]

A nanofluid contains nanometer-sized particles, called nanoparticles, suspended in base fluids (water, ethylene glycol, etc). These nanoparticles are generally made of metals, metal oxides, carbides or carbon nanotubes. Roslan *et al.* [3] studied the effect of a rotating cylinder on heat transfer in a square enclosure, filled with nanofluid. They showed that the maximum heat transfer can be found at a high nanoparticle concentration. Teng *et al.* [4] made a study on the effect of Al_2O_3-water nanofluid particle size on thermal conductivity. The results showed a correlation between small nanoparticle size and higher temperature. Sebdani *et al.* [5] carried out a study on the effect of Al_2O_3-water nanofluid on mixed convection in a square cavity. They found that the rate of heat transfer decreased with the increase of nanoparticle volume fraction for a constant Reynolds (*Re*) number and high Rayleigh (*Ra*) numbers. Costa and Raimundo [6] studied on steady mixed convection in a differentially heated square enclosure with an active rotating circular cylinder. They found that the rotating cylinder affected the thermal performance and the thermo-physical properties of the cylinder were important on the overall heat transfer process.

Basak *et al*. [7] considered mixed convection in a square cavity with uniform and non-uniform heating of bottom wall. The local Nusselt (*Nu*) number plot showed that the heat transfer rate was very high at the edges of the bottom wall, but it decreased at the center of the wall for uniform heating. Rahman *et al*. [8] carried out a numerical study on opposing mixed convection in a ventilated enclosure. They found that the rate of heat transfer from the heated wall depended on the position of the inlet port. Mehrizi *et al*. [9] made a study on mixed convection in a ventilated cavity with hot obstacle. They showed that the heat transfer rate was the maximum with different locations of outlet port at different Richardson numbers.

In our present work, pure mixed convection inside a square ventilated cavity is studied. A rotating adiabatic cylinder is at the center of the cavity. The cavity has inlet and outlet ports with the flow of Al_2O_3 –water

Nomenclature

a	Length of inlet and outlet	*Greek symbols*		
C_p	Constant pressure specific heat	α	Thermal diffusivity	
g	Gravitational acceleration	β	Coefficient of volume expansion	
Gr	Grashof number	μ	Dynamic viscosity	
k	Thermal conductivity	v	Kinematic viscosity	
L	Length of square cavity	ρ	Density	
Nu	Nusselt number	ω	Angular rotational velocity	
p	Pressure	Ω	Dimensionless Angular rotational velocity	
P	Dimensionless pressure	θ	Dimensionless temperature	
Pr	Prandtl number			
r	Radius of cylinder			
R	Dimensionless radius of cylinder	Subscripts		
Re	Reynolds number	c	Cold (lower value)	
Ri	Richardson number	f	Fluid	
T	Temperature	h	Hot (higher value)	
u,v	Cartesian velocity components	nf	Nanofluid	
U,V	Dimensionless velocity components	o	Initial value	
x,y	Cartesian co-ordinates	0	At the center of the cylinder	
X,Y	Dimensionless co-ordinates			

nanofluid. The cylinder can rotate with different speeds and directions. The Reynolds (Re) and Grashof (Gr) numbers are kept constant at 100 and 10^4 respectively, whereas the Richardson (Ri) number is kept 1. Qualitative analyses are carried out by comparing thermal and flow fields in terms of isotherm and streamlines while quantitative analyses are done by presenting Nusselt number (Nu) at the heated wall and average fluid temperature inside the cavity.

2. Problem Formulation

2.1. Physical Modeling

The present configuration consists of a two-dimensional square enclosure of the same width and height, L. A rotating adiabatic cylinder of radius R is placed at the center (X_0, Y_0) of the square cavity, which rotates with an angular velocity, ω. The physical model is shown in Fig. 1 along with the important geometric parameters. The origin of a Cartesian coordinate is at the lower left corner of the computational domain. Both the lower and the upper horizontal walls are assumed to be adiabatic along with an inlet at the left corner and an outlet at the right corner respectively. The vertical side left wall is assumed to have an isothermal temperature (T_h) higher than the temperature (T_c) of the opposite right wall. No slip condition is assumed at the walls. Under the influence of the vertical gravitation field, the vertical walls with different temperatures lead to a natural convection problem. Again, due to the non-slip boundary condition for velocity on its surface, the rotating adiabatic cylinder induces a forced flow. The overall situation results in a mixed convection problem. The free space of the cavity is filled with a water-based nanofluid containing Al_2O_3 nanoparticles. The flow is assumed to be laminar. Thermal radiation and viscous dissipation are neglected.
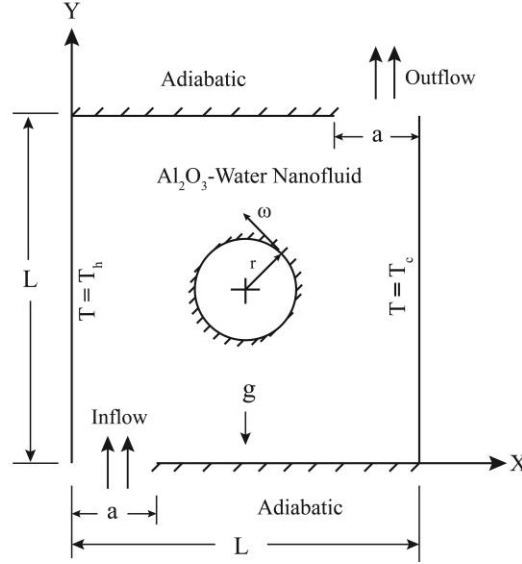
Fig. 1. Schematic diagram of the square ventilated cavity with problem specifications.

2.2. Mathematical Modeling

Mixed convection fluid flow inside the cavity follows the continuity equation that reads, in its dimensionless form

$$\frac{\partial U}{\partial X} + \frac{\partial V}{\partial Y} = 0 \tag{1}$$

The momentum equations,

$$U\frac{\partial U}{\partial X} + V\frac{\partial U}{\partial Y} = -\frac{\partial P}{\partial X} + \frac{\mu_{nf}}{\rho_{nf}\nu_f}\frac{1}{\mathrm{Re}}\left(\frac{\partial^2 U}{\partial X^2} + \frac{\partial^2 U}{\partial Y^2}\right) \tag{2}$$

$$U\frac{\partial V}{\partial X} + V\frac{\partial V}{\partial Y} = -\frac{\partial P}{\partial Y} + \frac{\mu_{nf}}{\rho_{nf}\nu_f}\frac{1}{\mathrm{Re}}\left(\frac{\partial^2 V}{\partial X^2} + \frac{\partial^2 V}{\partial Y^2}\right) + \frac{(\rho\beta)_{nf}}{\rho_{nf}\beta_f}Ri\theta \tag{3}$$

The energy equation,

$$U\frac{\partial \theta}{\partial X} + V\frac{\partial \theta}{\partial Y} = \frac{\alpha_{nf}}{\alpha_f}\frac{1}{\mathrm{Re}\,\mathrm{Pr}}\left(\frac{\partial^2 \theta}{\partial X^2} + \frac{\partial^2 \theta}{\partial Y^2}\right) \tag{4}$$

The dimensionless parameters appearing in the above equations are the space coordinates, the velocity components, the temperature and the driving pressure, defined, respectively, as

$$(X,Y) = (x,y)/L; (U,V) = (u,v)/u_o \tag{5}$$

$$\theta = \frac{T-T_c}{T_h-T_c}; P = \frac{p}{\rho_{nf}u_o^2}; \mathrm{Pr} = \frac{(\mu C_p)_f}{k_f}; \mathrm{Re} = \frac{\rho_f u_o L}{\mu_f}; Gr = \frac{g\rho_f^2\beta_f(T_h-T_c)L^3}{\mu_f^2}; Ri = \frac{Gr}{\mathrm{Re}^2}. \tag{6}$$

For the rotating adiabatic cylinder, the dimensionless governing parameters are as

$$R = r/L; \Omega = \omega L^2/\alpha_f; U = -\Omega(Y-Y_0); V = -\Omega(X-X_0) \tag{7}$$

Over the surface of the cylinder, the absolute value of velocity can be evaluated as [3]

$$|V| = |\Omega|R. \tag{8}$$

Boundary conditions for analysis of pure mixed convection in a square ventilated cavity, containing rotating adiabatic cylinder are presented in non-dimensional form in Table 1.

Table 1. Boundary conditions for this problem in non-dimensional form

Boundary Wall	Flow Field	Thermal Field
Top Wall	U = V = 0	$\partial\Theta/\partial n = 0$
Bottom Wall	U = V = 0	$\partial\Theta/\partial n = 0$
Left Side Wall	U = V = 0	$\Theta = 1$

3

Right Side Wall	U = V = 0	Θ = 0
Rotating Cylinder	U= -Ω(Y-Y$_0$), V= -Ω(X-X$_0$)	∂Θ/∂n = 0
Inlet	U = 0, V = 1	Θ = 0
Outlet	P = 0, ∂U/∂Y = 0, ∂V/∂Y = -∂U/∂X	Θ = Θ/A, Θ = -(Nuc* Θx)/A

The heat transfer rate from the high temperature vertical wall to fluid is represented by the overall Nusselt number (*Nu*), defined as

$$Nu = \frac{k_{nf}}{k_f} \int_0^L -(\frac{\partial \theta}{\partial X})_{X=0} dY. \tag{9}$$

Average temperature of the flow field can be calculated as,

$$\theta_{av} = \frac{1}{A} \int_A \theta dA \tag{10}$$

Here, area of the cavity, $A = L^2 - \pi r^2$ $\tag{11}$

3. Numerical Scheme

3.1. Numerical Procedure

Galerkin weighted residual scheme of finite element method (FEM) has been used to get the solution of this specific problem. Six nodded triangular mesh has been employed to discretize the entire cavity. Fine mesh has been applied near the boundary walls. An iterative method has been used to find out the solution by the UMPFACK solver and relative tolerance of 10^{-5} has been set for the error estimation.

3.2. Grid Independency Test

A grid independency test has been performed to economize the solution process by taking least number of elements for satisfactory solution. The grid independency test result is presented in Fig.2. From the figure it is evident that for the lower grid element numbers, the Nusselt number varies significantly. Nusselt number is calculated at the left vertical heated wall. When the number of grid elements reaches to 5000, the Nusselt number becomes more or less constant. For higher elements the grid shows constant Nusselt number. So the grid having 5000 elements has been taken for the entire numerical simulation of the specified problem.
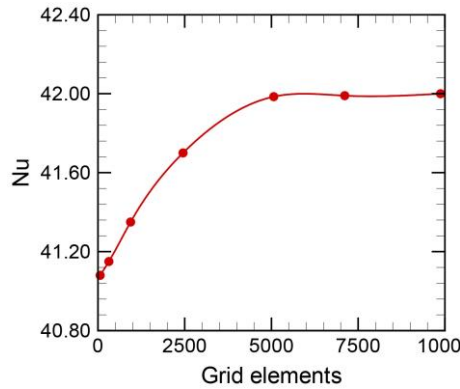

Fig. 2. Variation of Nusselt number with grid size for $Gr = 10^4$ and $\Omega = 50$.

4. Results and Discussions

Results are generated for water as plain fluid and nanofluid (Al_2O_3 –Water) with 0.1 solid volume fraction (φ). Firstly isotherm and streamline contours for both fluids are presented for $0 < \Omega < 100$. Ω indicates the rotational speed of cylinder. Then isotherm and streamlines for both fluids are presented for different Grashof number, *Gr*. Then average temperature for the cavity and average Nusselt number at the heated left vertical wall between the geometries have been presented with varying *Gr* and Ω.

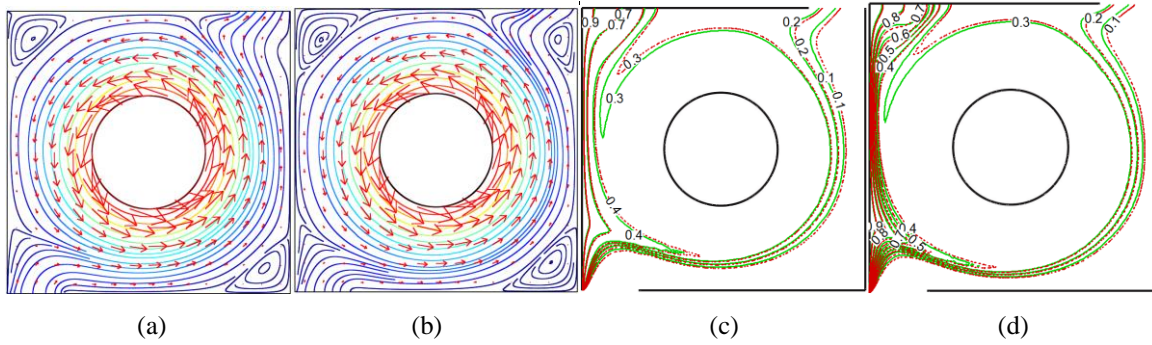### 4.1. Effect of Rotational Speed (Ω) and Grashof Number (*Gr*)

Fig. 3. Streamlines for (a) Ω = 50, (b) Ω =100. Isotherms for (c) Ω =50, (d) Ω =100. At Ri = 1, Re =100 and Gr = 10^4.
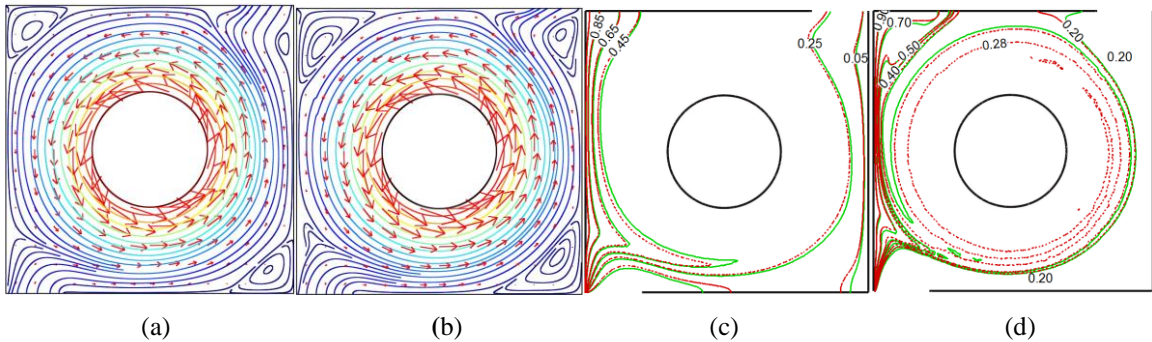

Fig. 4. Streamlines for (a) Gr = 10^3, (b) Gr =10^5. Isotherm for (c) Gr =10^3, (d) Gr =10^5 at Ri = 1, Ω=100.

Fig. 3 has been generated for different Ω, specifically for 50 and 100 in the range of 0< Ω <100. Also Grashof (Gr) and Reynolds (Re) numbers, Re are fixed to 10^4 and 100 respectively thus making Richardson number (Ri) equal to 1. Fluid flow takes place in the free space between the cylinder and the enclosure for pure mixed convection specifically the fluid flows towards the outlet port from the inlet port. The rotating motion of the cylinder creates a vortex which rotates in the counterclockwise direction. There is also a small vortex at the right corner of the cavity. At low rotational speed of cylinder this small vortex becomes weaker. Only primary vortex is created due to pure mixed convection. Streamline plots for Ω =50 and 100 are shown in Fig. 3(a) and 3(b) and isotherm plots are shown in Fig. 3(c) and 3(d). Fig. 4 has been generated for Grashof number 10^3 and 10^5. Streamline and isotherm plots in Fig. 4 indicate that, increasing the Grashof number from 10^3 to 10^5 the natural convection is increased compared to forced convection.

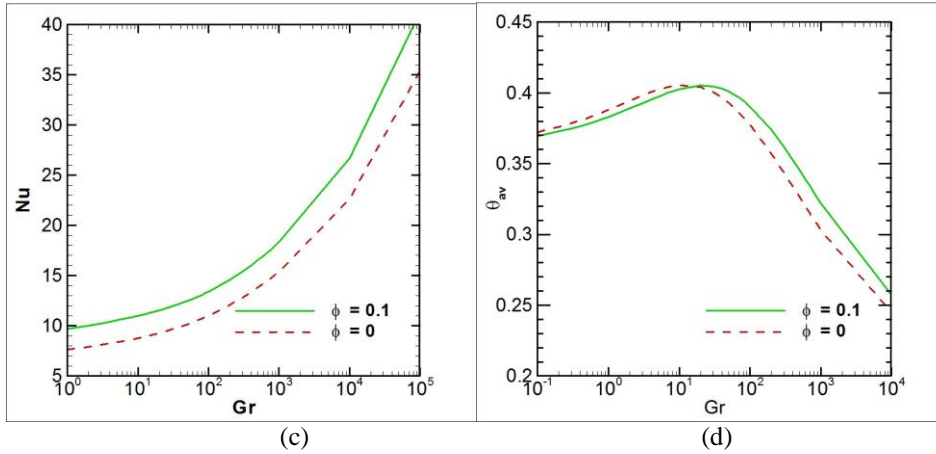## 4.2. Variation of Average Nusselt Number (Nu) and Average Temperature (θ_{av})

(a)   (b)
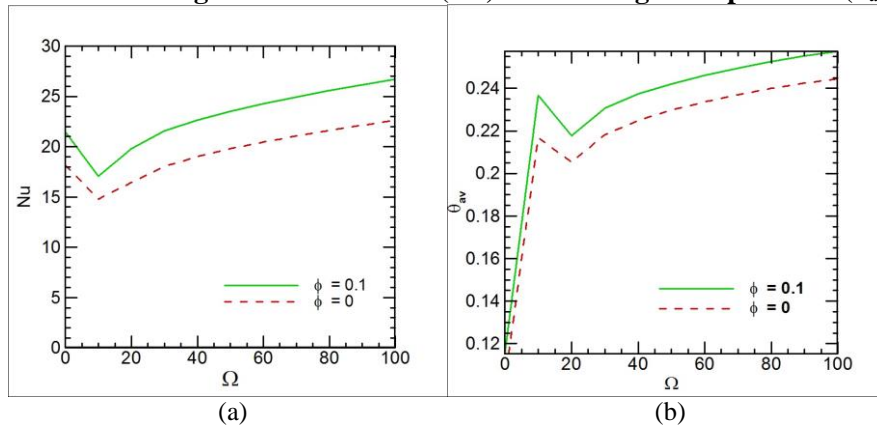
Fig. 5. Variation of (a) *Nu* and (b) θ_{av} with Ω at $Gr=10^3$. Variation of (c) *Nu* and (d) θ_{av} with *Gr* at Ω =50. Dashed lines are for water and solid lines for *Al$_2$O$_3$-water.*

In the figure, variation of *Nu* and θ_{av} are analyzed. The solid volume fraction, φ in nanofluid is 0.1 and 0 in plain fluid. Ω was varied in the range of $0 < \Omega < 100$ for Fig. 5(a) and 5(b). *Gr* was varied in the range of $0.1 < Gr < 10^5$ for figure 5(c) and 5(d). With the increase of Ω, *Nu* and θ_{av} both increase. With the increase of *Gr*, *Nu* increases but θ_{av} decreases. Although, inclusion of solid nanoparticles yields the higher thermal conductivity that eventually leads to higher energy and thus increases the average temperature. So, in Fig. 5(a) and 5(c), it is seen that Nusselt number for nanofluid is greater than plain fluid. Numerically from Fig. 5(a), Nusselt number is 26.75 for nanofuid and 22.5 for plain fluid. In Fig. 5(b) and 5(d), it is seen that average temperature for nanofluid is greater than plain fluid.

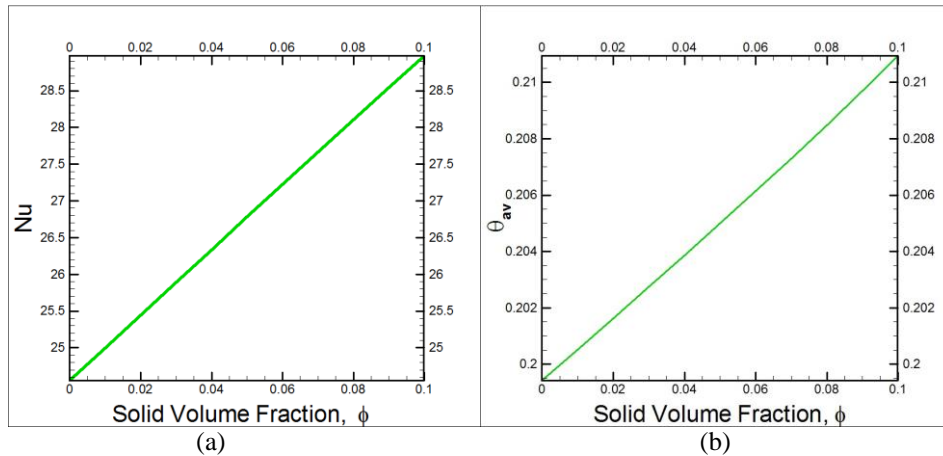## 4.3. Effect of Solid Volume Fraction (φ) on Average Nusselt Number (*Nu*) and Average Temperature ($\boldsymbol{\theta_{av}}$)

Fig. 6. Variation of (a) *Nu* and (b) θ_{av} with φ at $\Omega = 50$, $Gr = 1000$.

In Fig. 6, it is seen that addition of solid volume fraction increases the *Nu* and θ_{av} proportionally. The addition of solid nanoparticles increases the heat conductivity of the fluid and thus increases the energy of the fluid.

5. Conclusions

In this paper a thorough discussion has been made on the problem specification, its background literature and numerical solution procedures. From the result analysis the following conclusions can be drawn:

- Addition of rotating speed, Ω results in a recirculating cell in the cavity which circulates in the opposite to the natural convection flow.

- Higher value of Gr increases the natural convection rate rather than forced convection.

- Inclusion of nanoparticles increases the Nusselt number and average temperature of the fluid.

Since the geometry shows a lot of promise and has got attention lately, the authors hope that the present paper will help the researcher around the world to have a better insight on the problem.

6. Acknowledgement

7. References

[1] Param Jeet Singh, S. Roy, "Mixed convection along a rotating vertical slender cylinder in an axial flow'', *International Journal of Heat and Mass Transfer*, Vol. 51 pp. 717–723, 2008.

[2] M.M. Rahman, R. Saidur, N.A. Rahim , "Conjugated effect of joule heating and magneto-hydrodynamic on double-diffusive mixed convection in a horizontal channel with an open cavity'', *International Journal of Heat and Mass Transfer*, Vol. 54, pp. 3201–3213, 2011.

[3] R. Roslan, H. Saleh, I. Hashim, "Effect of rotating cylinder on heat transfer in a square enclosure filled with nanofluids", *International Journal of Heat and Mass Transfer*, Vol. 55, pp. 7247–7256, 2012.

[4] Tun-Ping Teng, Yi-Hsuan Hung, Tun-Chien Teng, Huai-En Mo, How-Gao Hsu, "The effect of alumina/water nanofluid particle size on thermal conductivity", *Applied Thermal Engineering*, Vol. 30, No. 14–15, pp. 2213–2218, 2010.

[5] Saeed Mazrouei Sebdani, Mostafa Mahmoodi, Seyed Mohammad Hashemi, "Effect of nanofluid variable properties on mixed convection in a square cavity", *International Journal of Thermal Sciences*, Vol. 52, pp. 112–126, 2012.

[6] V. Costa, A. Raimundo, "Steady mixed convection in a differentially heated square enclosure with an active rotating circular cylinder", *International Journal of Heat and Mass Transfer*, Vol. 53, pp. 1208–1219, 2010.

[7] Tanmay Basak, S. Roy, Pawan Kumar Sharma, I. Pop, "Analysis of mixed convection flows within a square cavity with uniform and non-uniform heating of bottom wall", *International Journal of Thermal Sciences*, Vol. 48, No. 5, pp. 891–912, 2009.

[8] M. M. Rahman, M. A. Alim, M. A. H. Mamun, M. K. Chowdhury, A. K. M. S. Islam, "Numerical study of opposing mixed convection in a ventilated enclosure", *ARPN Journal of Engineering and Applied Sciences*, Vol. 2, No. 2, 2007.

[9] A. Abouei Mehrizi, M. Farhadi, H. Hassanzade Afroozi, K. Sedighi, A.A. Rabienataj Darz, "Mixed convection heat transfer in a ventilated cavity with hot obstacle: Effect of nanofluid and outlet port location", *International Communications in Heat and Mass Transfer*, Vol. 39, pp. 1000–1008, 2012.

Natural convection in circular headed cavity with discrete bottom heat sources filled with Ferro-fluid

Anwarul Karim [1,*], Asif Reza Chowdhury [1], Khan Md. Rabbi [1]

[1] Department of Mechanical Engineering, Bangladesh University of Engineering and Technology
*E-mail: anwarul2buet@gmail.com *, rezaasif93@gmail.com , khanrabbi92@gmail.com*

Abstract

Natural convection in a two dimensional circular headed cavity filled with Ferro-fluid (water + Fe_3O_4) is numerically investigated for different heater positions. In this study, two discrete heat sources at constant temperature are located on the bottom wall. The vertical and circular top walls are cooled at constant low temperature. The Ferro-fluid is assumed to be homogenous and Newtonian. The physical problem is represented mathematically by sets of governing equations and the developed mathematical model is solved by employing Galerkin finite element formulation. The influence of pertinent parameter such as Rayleigh number (Ra) ranges from 10^3 to 10^6 for different aspect ratios (λ) of 0, 0.4 and 0.7 and also the solid volume fraction of Ferro-fluid (φ) from 0 to 0.15 on heat transfer are studied. The present study analyzes and discusses the flow patterns (streamline structures and isotherm distributions) set up by the buoyancy force and the heat transfer rate is quantified by the average Nusselt number (Nu) along the heat source. The results show that the heat transfer rate increases with the increase of the Rayleigh number and solid volume fraction of Ferro-fluid. It is also evident from results that heat transfer is maximum for λ=0.7 up to Ra=10^6 but the increasing rate of heat transfer is higher for λ=0.4 beyond Ra=10^4.

Keywords: Circular headed cavity, Natural convection, Ferro-fluid , Discrete heat source.

1. Introduction

Natural convection heat transfer is significantly applied in various fields like industries, scientific and engineering applications. Researchers have begun to experimentally and numerically investigate the natural convection of nanofluid in recent few years in order to extract the advantages of nanofluid. The numerical method to analyze natural convection in square cavity was first used by Vahl Davis [1]. Further natural convection for different cavities were investigated widely [2-4]. Choi [5] first found the term "Nanofluid". Nanofluid is suspension of nanoparticles (size up to about 1-100nm) in a base fluid as they exhibit enhanced thermal conductivity and convective heat transfer coefficient compared to the base fluid. The variety of nanofluid advantages can be related in many natural convection heat transfer applications such as in micro-electro-mechanical systems (MEMS), in heat exchangers,boilers,cooling engines,in fuel cells, solar energy,crystal growth etc. Ferrofluid is a stable colloidal suspension of sub-domain magnetic particles in a base liquid. The particles are coated with a stabilizing dispersing agent, which prevents particle agglomeration even when a strong magnetic field gradient is applied to the ferrofluid [6, 7]. The shape of cavity is also a considerable factor affecting the heat transfer and fluid flow phenomena. The variety of shape actually depends on the real life physical problems. The common shapes are square, rectangular, circular etc. The effect of multiple sources also has immense influence on heat transfer. Effect of multiple sources and sinks on natural convection is investigated with importance [8-10].

The literature reviews show that despite lots of work on convection, there is lack of information on effect of heater position along with ferro-fluid for cavity having circular head. In this paperwork, a ferrofluid filled circular headed cavity with discrete bottom heat sources is investigated for different positions of heat sources (aspect ratio). The effect of different Rayleigh number for different aspect ratios is shown in terms of flow and thermal field. Heat transfer effectiveness and average temperature are also presented in result. The model has been validated against established results and the results have been briefly discussed.

2. Problem formulation

2.1 Physical modeling

The geometry of the problem is depicted in *Fig.1*. The system consists of a two-dimensional cavity of sides *L* and the top circular head of diameter *L*. The bottom surface is heated by two heat sources of constant high temperature T_h. The vertical side walls and circular top wall are kept at constant low temperature T_c $(< T_h)$ and the remaining walls are adiabatic. The length of each heat source is *a* and the difference between them is *b*. The ratio *b/L* is taken as aspect ratio which is varied as *0, 0.4* and *0.7*. The entire cavity is filled with ferrofluid *(water + Fe₃O₄)*. The gravity is acting in the negative y-direction. The radiation effect and viscous dissipation are neglected for the simplification of the problem.

Nomenclature

|			
g	acceleration due to gravity (m/s^{-2})	Greek symbol	
k	thermal conductivity (W m^{-1}K^{-1})	λ	aspect ratio (b/L)
T	temperature (K)	ρ	density (kgm^{-3})
L	length of the cavity (m)	α	thermal diffusivity (m^{2}s^{-1})
p	pressure (Pa)	β	volume expansion coefficient (K^{-1})
P	dimensionless pressure	ν	kinematic viscosity (m^{2}s^{-1})
(u, v)	velocity components (ms^{-1})	φ	solid volume fraction
(U, V)	dimensionless velocity components	Ψ	stream function
(x, y)	dimensional coordinates (m)	Θ	dimensionless temperature
(X, Y)	dimensionless coordinates	Subscript	
Ra	Rayleigh number	h	hot
Pr	Prandtl number	c	cold
Nu	Nusselt number	ff	ferrofluid
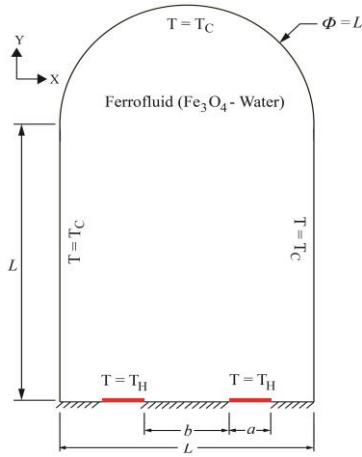
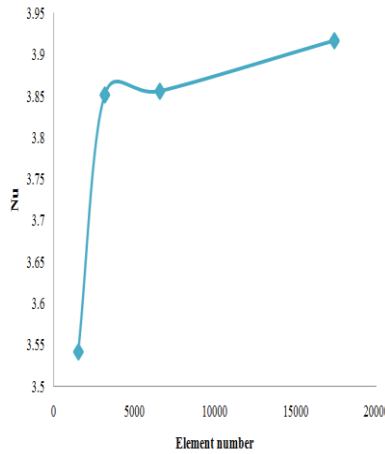**Fig. 1**. Schematic diagram of circular headed cavity with discrete heat source.

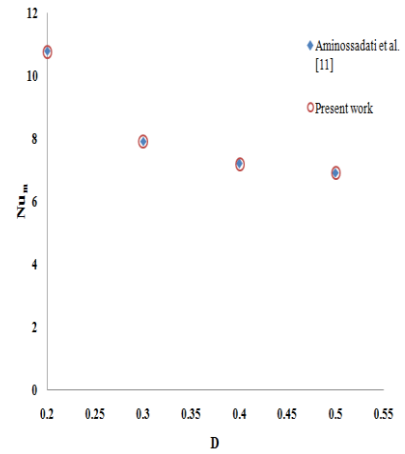**Fig. 2**. Grid refinement test on average Nusselt number for Ra=10^5 and φ=0.1.

Fig. 3. Comparison of present work with Aminossadati et al. [11] for Ra=10^5, φ=0.1 and B=0.4.

2.2 Mathematical modeling

The two-dimensional steady state continuity, momentum and energy equations are applied to model this problem for flow and thermal fields. The working fluid is assumed to be incompressible Newtonian with constant properties and thermal equilibrium between the ferromagnetic particles and the base fluid are assumed. The density variation of the fluid is modeled by the Boussinesq approximation by the buoyancy term.

From the above stated assumptions, the non-dimensional governing equations take the form as-

$$\frac{\partial(U\delta)}{\partial X} + \frac{\partial(V\delta)}{\partial Y} = \frac{\partial}{\partial X}\left(\Gamma_\delta \frac{\partial\delta}{\partial X}\right) + \frac{\partial}{\partial Y}\left(\Gamma_\delta \frac{\partial\delta}{\partial Y}\right) + S_\delta \qquad (1)$$

Here non-dimensional dependent variables are designated by δ and corresponding diffusion and source term are defined by Γ_δ and S_δ respectively and those are summarized in Table 1,

Table 1. A summary of the terms of the non-dimensional governing equations (1).

Equations	δ	Γ_δ	S_δ
Continuity	1	0	0
U-momentum	U	$\mu_{ff} / \rho_{ff} \alpha_f$	$-\partial P / \partial X$
V-momentum	V	$\mu_{ff} / \rho_{ff} \alpha_f$	$-\partial P / \partial Y + (\rho\beta)_{ff} Ra \Pr \Theta / (\rho_{ff} \beta_f)$
Thermal energy	Θ	α_{ff} / α_f	0

The non-dimensional parameters, which are adopted to obtain the above non-dimensional governing equation, are presented below-

$$X = \frac{x}{L}, Y = \frac{y}{L}, U = \frac{uL}{\alpha_f}, V = \frac{vL}{\alpha_f}, P = \frac{(p + \rho_f gy)L^2}{\rho_{ff} \alpha_f^2}, \Theta = \frac{(T - T_c)}{(T_h - T_c)} \qquad (2)$$

here U, V, P and Θ are non-dimensional velocities, pressure and temperature respectively. Here subscripts 'ff' and 'f' stand for the properties of the ferrofluid and the base fluid respectively.

The non-dimensional governing parameters Rayleigh number (Ra), Prandtl number (Pr) and Hartmann number (Ha) can be defined as below-

$$Ra = \frac{g\beta_f L^3 (T_h - T_c)}{\alpha_f \nu_f}, \Pr = \frac{\nu_f}{\alpha_f} \qquad (3)$$

The density of ferrofluid which is assumed to be constant can be expressed as-

$$\rho_{ff} = (1 - \varphi)\rho_f + \varphi\rho_s \qquad (4)$$

Here property of solid ferromagnetic particles is represented by subscript 's'. In the above equation, solid volume fraction (φ) has significant effect on thermal diffusivity of ferrofluid which is quite different from the base fluid and can be modeled as-

$$\alpha_{ff} = \frac{k_{ff}}{(\rho c_p)_{ff}} \qquad (5)$$

where heat capacitance of ferrofluid $(\rho c_p)_{ff}$ can be found by

$$(\rho c_p)_{ff} = (1 - \varphi)(\rho c_p)_{ff} + \varphi(\rho c_p)_s \qquad (6)$$

In addition, the thermal expansion coefficient (β_{ff}) of the ferrofluid can be obtained as

$$(\rho\beta)_{ff} = (1 - \varphi)(\rho\beta)_{ff} + \varphi(\rho\beta)_s \qquad (7)$$

Moreover, dynamic viscosity of the ferrofluid (μ_{ff}) can be expressed as

$$\mu_{ff} = \frac{\mu_f}{(1 - \varphi)^{2.5}} \qquad (8)$$

Effect of thermal conductivity of ferrofluid can be described as

$$\frac{k_{ff}}{k_f} = \frac{k_s + 2k_f - 2\varphi(k_f - k_s)}{k_s + 2k_f + \varphi(k_f - k_s)} \qquad (9)$$

The thermophysical properties of the base fluid (kerosene) and the ferromagnetic particle (cobalt) are given in Table 2.

Table 2. Thermophysical properties of ferrofluid.

Property	Fe_3O_4 (nanoparticles)	Water (base fluid)
Heat capacitance, c_p ($JKg^{-1}K^{-1}$)	670	4179
Density, ρ (Kgm^{-3})	5200	997.1
Thermal conductivity, k ($Wm^{-1}K^{-1}$)	6	0.613
Thermal expansion coefficient, β (K^{-1})	1.18×10^{-5}	2.1×10^{-4}
Dynamic viscosity, μ (Nsm^{-2})	-	0.001003

The corresponding dimensionless boundary conditions for the above problem are given by:
On vertical walls: U=0, V=0, Θ=0.

On top circular wall: U=0, V=0, Θ=0.
On bottom wall: U=0, V=0, Θ=1 (at heat sources) or $\partial\Theta/\partial Y = 0$ *(at wall other than sources).*

Average Nusselt number is evaluated for horizontal bottom heated walls and calculated from following expression

$$\mathrm{Nu} = -\frac{k_{ff}}{k_f} \int_0^1 \frac{\partial\Theta}{\partial y} \, dX \tag{10}$$

Average fluid temperature inside the cavity can also be found by the following expression

$$\Theta_{av} = \frac{1}{A} \int \Theta dA \tag{11}$$

where A is non dimensional area which can be evaluated by A=L^2(1+π/8).

Flow field of the present problem is visualized through streamline obtained from stream function. Stream function is defined from velocity components U and V. Relation between the stream function and velocity components for 2-D flow are given by,

$$U = \frac{\partial\psi}{\partial Y}, V = -\frac{\partial\psi}{\partial X} \tag{12}$$

3. Numerical procedure

Galerkin weighted residual method of finite element analysis is applied study to obtain the numerical solution. The entire domain is discritized into triangular mesh elements of different size. Non-dimensional governing equations are transformed into a set of algebraic equations. $P_2 - P_1$ Lagrange finite elements are used to discretize pressure and velocity components and Lagrange-quadratic finite elements are chosen for temperature. Iteration technique is employed to find the converged solution. The convergence criterion is set to 10^{-6}, so that $|z^{p+1} - z^p| \leq 10^{-6}$, where z is the general dependent variable and p is the number of iteration.

4. Grid independency test

A grid sensitivity test is performed for $Ra=10^5$ and $\varphi=0.1$ for aspect ratio of $\lambda=0.4$ to ensure the numerical accuracy of this computation. The test is performed for different element numbers as 1528, 3167, 6576 and 17393. It is evident from *Fig.2* that after reaching element number 6576, average Nusselt number becomes insensitive. So for the present problem, grid having element number 6576 is taken as the optimum grid and all the simulations are carried out at this specified grid.

5. Code validation

A code validation is necessary for checking the reliability of the present code. The present code is compared with the results of Aminossadati et al. [11] on the basis of average Nusselt number for Ra=10^5 and $\varphi=0.1$ where heat source length B=0.4. As indicated from *Fig.3*, obtained result shows good agreement with literature result.

6. Result and discussion

The main objective of investigation is to analyze the effect of different heater configurations on natural convection for varying Rayleigh number inside a circular headed cavity filled with ferro fluid. Heat transfer performance is compared for aspect ratios (λ) of 0, 0.4 and 0.7 while varying Raleigh number from 10^3 to 10^6 with constant solid volume fraction φ=0.02 in terms of streamline and isotherm contours, average Nusselt number (*Nu*) and average temperature (θ$_{av}$) of the fluid inside cavity. The effect of different solid volume fraction (φ=0, 0.05, 0.07, 0.1 and 0.15) is also quantified for various Rayleigh number.

6.1 Effect of Rayleigh number on different aspect ratio

Effect of Rayleigh number (*Ra*) on flow and thermal fields for aspect ratio *λ=0, 0.4 and 0.7* is depicted in terms of stream function and isothermal contours in *Fig.4*. The study is carried out for solid volume fraction of *φ=0.02* and *Ra= 10³, 10⁵and 10⁶*. A counter clockwise (CCW) vortex at left and a clockwise (CW) vortex at right half of cavity are evaluated for all *λ* for Ra=10³. But the vortices for *λ=0.7* is more elongated in vertical direction compared to other two aspect ratios. This leads to higher buoyancy effect when the distance between the sources are maximum (*λ=0.7*). The isotherm contours are stratified in parallel lines for *λ=0* which are a bit distorted for *λ=0.4* and *0.7*. The vortices are stretched vertically for all *λ* when Ra=10⁵ in *Fig.4 [(g)~(i)]*. For the distant heater position, streamline elongated most. The isotherm contours also show immense changes as Ra updated to 10⁵. The isotherms near heater become thinner which indicates increasing convection heat transfer. The greater deflection of isotherms is noticed in case of *λ=0.4*. This indicates rapid growth of heat transfer rate for *λ=0.4* when Ra=10⁵. The vortices engulf almost all the cavity as Rayleigh number is updated to 10⁶ for all λ at *Fig.4 [*
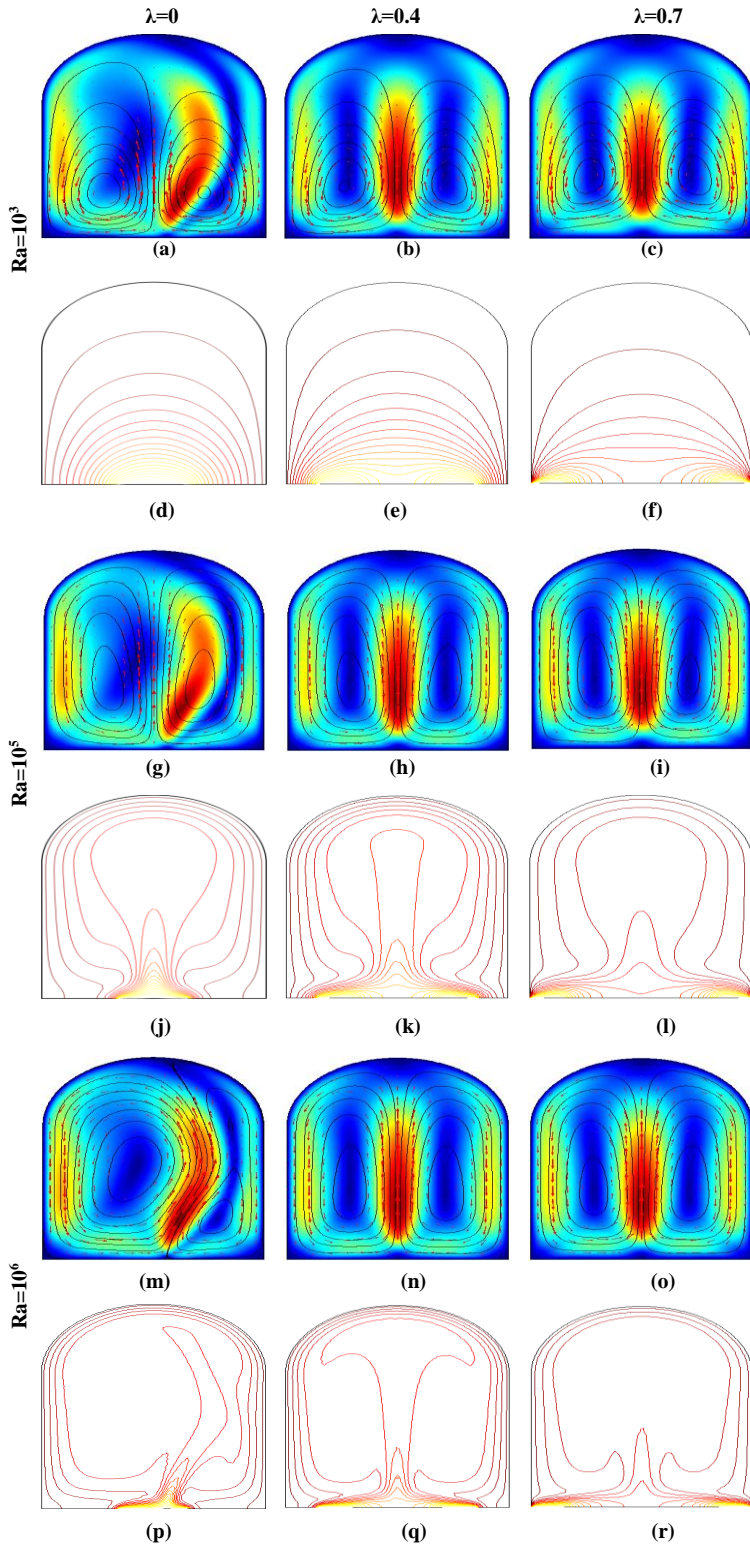
Fig.4 Variation of streamlines for Ra=10^3 at [(a), (b), (c)]; Ra=10^5 at [(g), (h), (i)]; Ra=10^6 at [(m), (n), (o)] and isotherm contours for Ra=10^3 at [(d), (e), (f)]; Ra=10^5 at [(j), (k), (l)]; Ra=10^6 at [(p), (q), (r)]

Fig.5 Variation of *Nu* with *Ra* for λ=0, 0.4 and 0.7

Fig.6 Variation of Θ_{av} with *Ra* for λ=0, 0.4 and 0.7

Fig.7 Variation of *Nu* with *Ra* for φ=0, 0.05, 0.07, 0.1 and 0.15

(m) ~(r)]. For *λ=0* the left side vortex elongated more in vertically and horizontally indicating that convection is dominant in CCW direction in this case. The streamline patterns are almost same for the other two aspect ratios. The isotherm lines become thinner than previous which represents higher convection in all *λ*. The distortion of isotherms is noticeable for *λ=0*. For *λ=0.4* isotherms diffuse through the entire cavity which denotes the increasing rate of convection. Heat transfer also increases in case of *λ=0.7* as the thermal boundary layer becomes thinner.
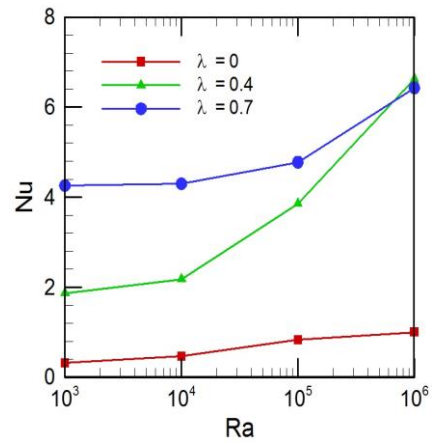
5

6.2 Variation of Nusselt number and average temperature

Nusselt number defines the effectiveness of convection heat transfer. The variation of Nusselt number with Rayleigh number for various aspect ratio ($\lambda=0, 0.4, 0.7$) is depicted in *Fig.5*. It is seen from the figure that Nu value increases as Ra increase. Nu value is maximum for $\lambda=0.7$ up to Ra<10^6. This implies that heat transfer is maximum when the heat sources are in distant position. The minimum heat transfer happens for $\lambda=0$ when the sources are in close position. It is also noticed that the increasing rate of convection is higher for $\lambda=0.4$. The average temperature inside the cavity increases for increment of Ra=10^3 to Ra=10^4 and more or less constant for further increasing value of Ra for all three aspect ratios seen from *Fig.6*. Maximum average temperature is found for $\lambda=0.4$ and the minimum for $\lambda=0.7$.

6.3 Effect of solid volume fraction

The effect of solid volume fraction of ferrofluid (φ) on heat transfer is shown in *Fig.7*. For φ of 0, 0.05, 0.07, 0.1 and 0.15 Nusselt number is found for different *Ra*. The graph indicates that higher solid volume fraction results in higher *Nu* i.e. higher convection heat transfer. This indicates that the addition of more nanoparticle (Fe_3O_4) with base fluid increases fluid solid interaction hence increases convection.

7. Conclusion

The results of numerical analysis on flow field, thermal field and effectiveness of heat transfer with varying Rayleigh number for different aspect ratio and solid volume fraction are computationally analyzed in a ferrofluid filled circular headed cavity with discrete heat sources. The outcomes are listed as follows:

- Heat transfer increases with Rayleigh number for all heater positions or aspect ratio.
- The configuration of heat sources in distant position ($\lambda=0.7$) provides better heat transfer than the adjacent one ($\lambda=0$). But heat transfer rate is rapid for $\lambda=0.4$.
- The addition of ferro particle (increasing solid volume fraction) increases heat transfer significantly.

8. References

[1] de Vahl Davis, G. "Natural convection of air in a square cavity: a bench mark numerical solution." International Journal for numerical methods in fluids 3.3 (1983): 249-264.

[2] Dixit, H. N., and V. Babu. "Simulation of high Rayleigh number natural convection in a square cavity using the lattice Boltzmann method." International journal of heat and mass transfer 49.3 (2006): 727-739.

[3] Oztop, Hakan F., and Eiyad Abu-Nada. "Numerical study of natural convection in partially heated rectangular enclosures filled with nanofluids." International Journal of Heat and Fluid Flow 29.5 (2008): 1326-1336.

[4] Grosan, T., et al. "Magnetic field and internal heat generation effects on the free convection in a rectangular cavity filled with a porous medium." International Journal of Heat and Mass Transfer 52.5 (2009): 1525-1533.

[5] S.U.S. Choi, J.A. Eastman, Enhancing thermal conductivity of fluids with nanoparticles, in: Proceedings of the 1995 ASME Int. Mech. Eng. Cong. And Expo, ASME, San Francisco, USA, (1995).

[6] C. Chang, W.Cheng, W.Liu, H.Cheng, C.Huang, S.Du, Thermal flow of fluid with magnetic particles in the presence of magnetic field, Int.Commun.Heat Mass Transfer37(2010)801–808.

[7] M. Ghasemian,Z.Najafian Ashrafi, M.Goharkhah,M.Ashjaee, Heat transfer characteristics of Fe3O4 ferrofluid flowing in a mini channel under constant and alternating magnetic fields, Journal of Magnetism and Magnetic Materials 381(2015)158–167.

[8] V.C. Mariani, A. Da Silva, Natural convection: analysis of partially open enclosures with an internal heated source, Numer. Heat Transfer, Part A 52 (2007) 595–619.

[9] I. Dagtekin, H.F. Oztop, Natural convection heat transfer by heated partitions within enclosure, Int. Commun. Heat Mass Transfer 28 (2001) 823–834.

[10] Aminossadati, S. M., and B. Ghasemi. "Natural convection of water–CuO nanofluid in a cavity with two pairs of heat source–sink." *International Communications in Heat and Mass Transfer* 38.5 (2011): 672-678.

[11] Aminossadati, S. M., and B. Ghasemi. "Natural convection cooling of a localised heat source at the bottom of a nanofluid-filled enclosure." *European Journal of Mechanics-B/Fluids* 28.5 (2009): 630-640.

Paper ID: TE-07

Production, Characterization and Performance Study of Cottonseed Biodiesel in a Diesel Engine

Md. Wahedul Islam[1], Mafia Naher Afroj[1*], Romana Jannat[1]

[1] Department of Mechanical Engineering, Rajshahi University of Engineering and Technology
Corresponding Author E-mail: mafianaherafroj@yahoo.com

Abstract

The energy crisis and environmental concerns of the world has led the researchers to the search of feasible alternatives of fossil fuel. Biodiesel, also known as fatty acid methyl ester is an alternative, nontoxic, biodegradable, harmless and environmentally benevolent fuel. This paper represents an assessment of the production of biodiesel from non-edible renewable cotton (Gossypium herbaceum) seed oil and its characterization and performance. Cottonseed oil was used for biodiesel production by the transesterification process followed by the determination of various fuel properties. The variation of biodiesel production can be caused due to variation in the process parameters. It was observed that for 1% NaOH catalyst, 20% methanol, 58^0C reaction temperature and 60 min reaction heating time yield maximum (96%) biodiesel production. The engine performance test was conducted in a diesel engine using pure diesel and biodiesel blending with diesel in various ratios. Assorted parameters such as speed, fuel consumption and brake power were measured at different loads and their effects were discussed in this paper. From the results achieved it is noticed that cottonseed biodiesel has great potential to be used as alternative fuel in diesel engine.

Keywords: Biodiesel, cottonseed oil, transesterification, properties, performance test.

1. Introduction

Biodiesel is an alternative fuel formulated exclusively for diesel engines. Biodiesel is defined as the mono-alkyl esters of vegetable oils or animal fats, produced by using a bio-chemical method known as transesterification. Biodiesel and its blends with petroleum-based diesel fuel can be used in diesel engines without any significant modifications to the engines. The advantages of biodiesel are that it displaces petroleum thereby reducing global warming gas emissions, tail pipe particulate matter, hydrocarbons, carbon monoxide, and other air Toxics. Biodiesel improves lubricity and reduces premature wearing of fuel pumps [1]. It is important to explore the feasibility of substitution of diesel with an alternative fuel, which can be produced within the country on a massive scale for commercial utilization. At present the potential alternative fuels are Alcohols (Methanol and Ethanol), Liquefied Petroleum Gas (LPG), Compressed Natural Gas (CNG), Hydrogen and Vegetable Oils [2, 3, 4]. The cotton seed oil, a non-edible type vegetable oil is chosen as a potential alternative for producing biodiesel. After ginning process of cotton, cottonseed remains, which is used to produce cottonseed oil. Cottonseed oil is a waste product of cotton industry. Cottonseed oil does not have food value. It is one of the most sprayed crops in the world due the industrial value of cotton. Therefore, there is a plentiful supply of cottonseed as it comes as a byproduct of cotton cultivation [5]. At present 100 percent biodiesel is not used in place of diesel fuel to run the engine, because 100 percent biodiesel cause significant reduction of brake thermal efficiency, higher specific fuel consumption and excessive NOx formation. This problem can be greatly minimized by using diesel biodiesel blend. The most widely used blends are B10 (10%biodiesel, 90% diesel) and B20 (20% biodiesel, 80% diesel). Diesel biodiesel doesn't cause a significant increase of NOx and reduction of brake thermal efficiency. In the meantime the other performance parameter of the engine is similar to that of diesel fuel. In view of the fact that the cost of raw materials accounts about 60–80% of the total cost of biodiesel production, choosing a proper feedstock is very important. The method of production also plays very vital role in its production as the yield differs from process to process. The process parameters have great influence on the yield of biodiesel. That's why the optimum conditions are suggested in this paper.

2. Experimental

2.1 Materials and Method

There are various methods of extracting oil from oil producing seeds and these to a large extent determine the quality of the oil. The various methods include; mechanical extraction, pyrolysis, solvent extraction, etc. [6].The

raw cottonseed was collected from the Cotton Development Board. The raw cottonseed was dried and then the crude oil was extracted by expeller machine. The cleaned seed meats were first passed through a series of press rolls to produce thin flakes, after which the flakes were cooked under steam pressure, which ruptures the oil cells. Subsequently, the flakes were processed in expellers which remove the oil under high pressure.

2.2 Transesterification

When vegetable oil is mixed with methanol and a catalyst in the presence of heat, it produces methyl ester and glycerol. Biodiesel was prepared from cotton seed oil by alkali catalyzed transesterification. NaOH was used as the catalyst amounting 1.0% on a mass basis and 20% methanol was treated with the cottonseed oil. The oil was preheated and mixed with a solution of 20% methanol and 1% NaOH. The mixture was kept on a magnetic stirrer cum hot plate for proper mixing. The reaction was carried out in 55-60^{0}c for one hour. It was then placed in the separating funnel for separating the layers of biodiesel and glycerin impurities for 24 hours. The upper layer was biodiesel and lower layer was of glycerin. The method was repeated for different percentages of sodium hydroxide. It was found that maximum amount of biodiesel was produced at about 1% of NaOH. Fig.1 represents the flow chart for the transesterification process. The chemical equation of transesterification is below.
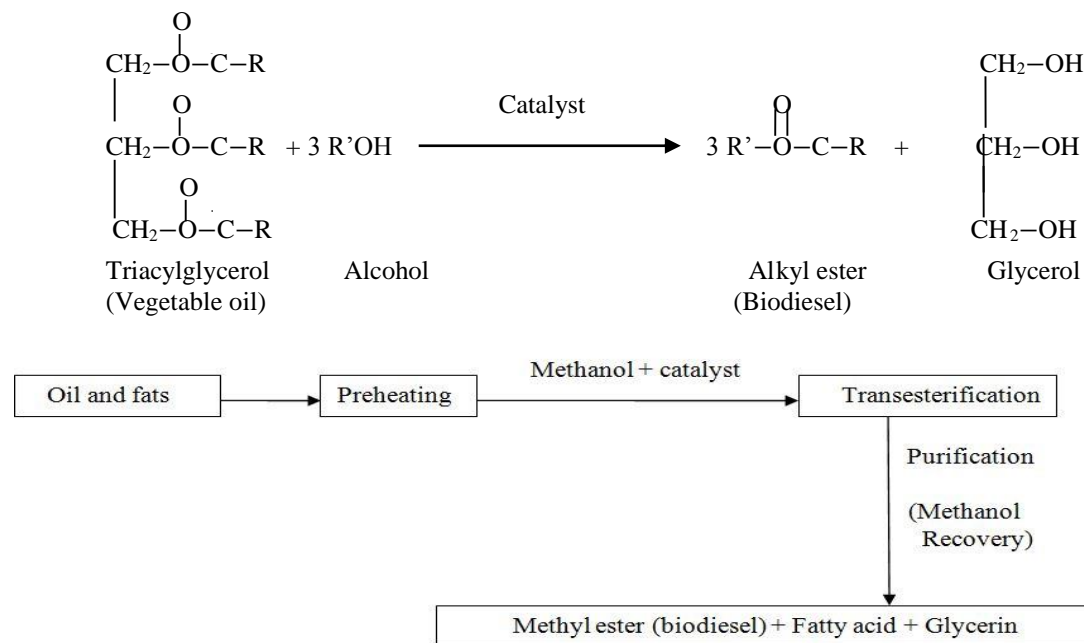

Triacylglycerol   Alcohol   Alkyl ester   Glycerol
(Vegetable oil)   (Biodiesel)

Fig.1. Flow chart for Transesterification process

2.3 Process Variables in Transesterification

Fig.2 represents the variation of % volume of biodiesel with % methanol. As the percentage of methanol increases, production of biodiesel increases. Maximum(96%) production of biodiesel occurs for 20% of methanol. For lower percent of methanol more reaction time is required. For higher percent of methanol biodiesel production decreased due to poor separation of glycerol.
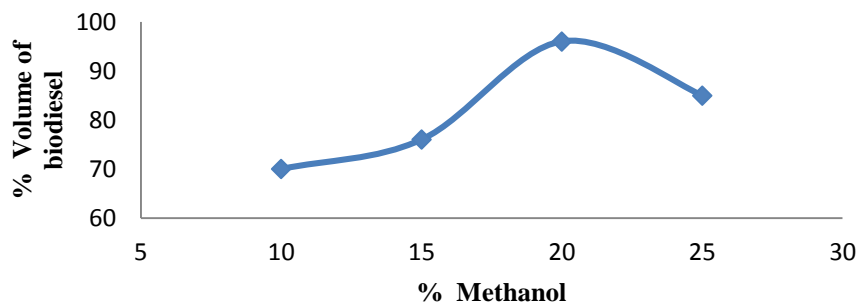

Fig. 2. The variation of % volume of biodiesel with % methanol

Fig.3. represents the variation of % volume of biodiesel with % NaOH. NaOH was used in transesterification. As the percentage of NaOH catalyst increases, production of biodiesel increases. Maximum(96%) production of

biodiesel occurs for 1% of NaOH. Further increase in percentage of catalyst causes reduction of biodiesel production. It was found that higher amounts of NaOH catalyst were required for higher FFA oil.
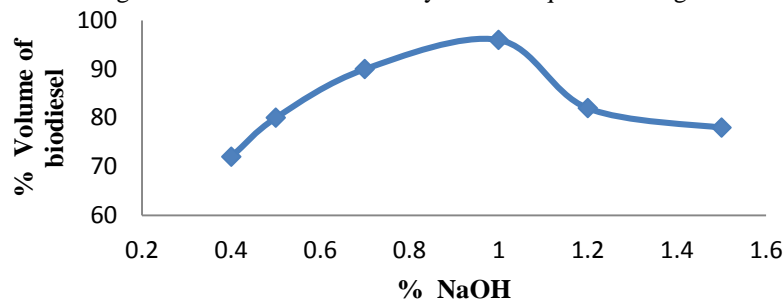

Fig. 3. The variation of % volume of biodiesel with % NaOH.

Fig.4. represents the variation of % volume of biodiesel with reaction time(min). As the reaction time increases, production of biodiesel increases. Maximum (96%) production of biodiesel occurs for 60 minutes of heating time. Further increase in time causes reduction of biodiesel production by producing higher amount of glycerol.
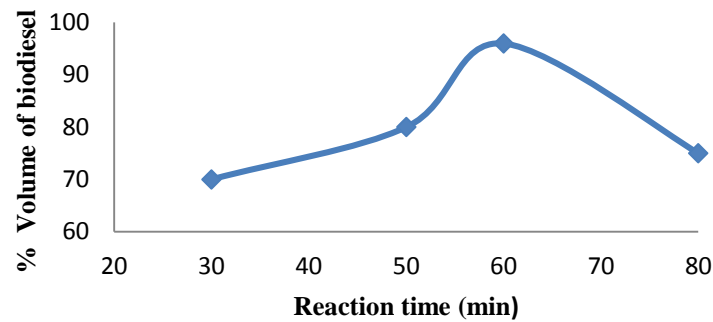

Fig. 4. The variation of % volume of biodiesel with reaction time(min).

Fig.5. represents the variation of % volume of biodiesel with reaction temperature. The rate of reaction is strongly influenced by the reaction temperature. Generally the reaction was conducted close to the boiling point of methanol (50^0C to 60^0C) at atmospheric pressure. As the temperature increases, production of biodiesel increases. Maximum(96%) production of biodiesel occurs at 58^0C. Further increase in temperature causes reduction of biodiesel production.
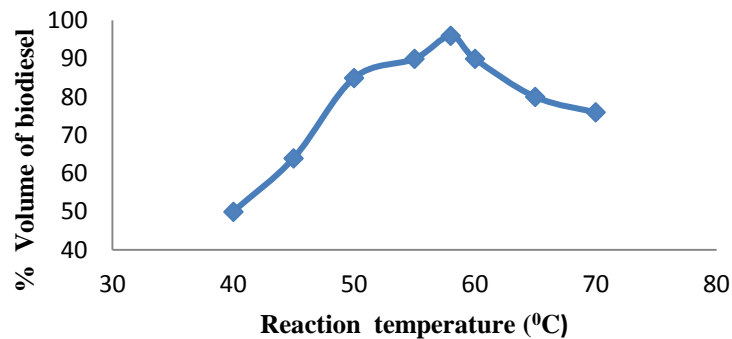

Fig. 5. The variation of %volume of biodiesel with reaction temperature.

2.4 Economical aspect of producing biodiesel as diesel substitute in Bangladesh

- The Textile industry plays an important role in the economy of Bangladesh. The textile industry in Bangladesh currently accounts for 45% of industrial employment and contributes 5% of total national income. The environment and soil in Bangladesh are very suitable for Cottonseed cultivation. If this crop can be cultivated on large scale production, yielding non-conventional oil that can be usefully converted into biodiesel.

- The country produced a record of 0.152 million bales of cotton in the just-concluded fiscal year (2014-15), marking a 5.47 percent growth as compared to the previous year's production. According to BCDB data, 152,534 bales of cotton were produced from about 42,700 hectares of land. These yield 20064.59 tons of cotton seed which produce 1575 tons of biodiesel [7].
- After the experimental work the net cost of biodiesel production from cottonseed oil was found 50 taka per liter in Bangladesh.
- Cottonseed oil is a wasted product of textile industry. It doesn't have any other significant use. If cottonseed biodiesel can be used as a substitution of diesel fuel it can save around 280 million taka per year in addition of its economical advantage.

2.5 Engine Performance

Performance tests were conducted on a four stroke diesel engine with various biodiesel blends in order to optimize the blend concentration for usage in CI engines. The engine specifications are given in Table 1. To achieve this, three samples of cottonseed biodiesel-diesel blends i.e. B5 (5% cottonseed biodiesel, 95% diesel), B10 (10%cottonseed biodiesel, 90% diesel) and B20 (20% cottonseed biodiesel, 80% diesel) were prepared to be fueled into a diesel engine.

Table 1: Engine Specification

Engine type	4-stroke CI engine
Number of cylinders	one
Bore x stroke	80 x 110 mm
Swept volume	553 cc
Cooling	water cooling
Compression ratio	16.5
Rated pressure	4.476 KW@1800 rpm
Injection pressure	14 Mpa (low speed, 900-1099rpm)
	20 Mpa (high speed, 1100-2000rpm)
Injection timing	24^0 BTDC

3. Results and Discussions

3.1 Properties

Table 2 presents the physicochemical properties of the extracted crude cottonseed oil, produced biodiesel and conventional diesel fuel. The calorific value which shows the energy density in the fuel was found 40562.72 KJ/Kg for biodiesel which is close to diesel. The density of biodiesel is slightly higher than diesel. The cottonseed biodiesel has high viscosity. This is why pure biodiesel is not used in an engine for combustion. It is used in engine after blending with diesel in various proportions. The biodiesel can be directly used in lubrication system. Since the specific gravity and API gravity are related to heat of combustion it has a major effect on engine fuel consumption. The API gravity of hydrocarbon diesel fuel is a reliable indication of the heat energy released when the fuel is burnt [8]. The flash and fire points indicate the temperature below which oil can be handled without danger of fire. High free fatty acid content can reduce the quality and yield of biodiesel production. The amount of FFA value in cottonseed biodiesel is 2.82% which is low. The acid value is a measure of acidic or alkaline contents of oil. The cloud and pour points indicate the temperature below which the flow of fuel will be difficult. These give the temperatures above which oil should be handled in cold environments. Carbon residue content and ash contents is the pointer to the deposit characteristics of the oil. Cottonseed biodiesel has low carbon residue content and ash content which indicates low deposition. But the formation of deposits is strongly affected by the design of the engine, the fuel used, and the operating conditions. The cetane rating of a diesel fuel is a measure of its ability to auto ignites quickly when it is injected into the compressed and heated air in the engine [9].

Table 2: Properties of Diesel, Cotton Seed Oil biodiesel and Cotton Seed Oil (Crude oil)

Properties	Crude oil	Biodiesel	Diesel
Calorific value, KJ/Kg	3056.76	40562.72	44500
Density, gm/cc, at 27.7 ^{0}C	0.94	0.88	0.8445
Viscosity, cP, at 27.7 ^{0}C	70	26.3	7.3
Specific gravity	0.94	0.87	0.84
API gravity	19.03	37.56	34.52
Flash point, ^{o}C	216	97	65

Properties	Crude oil	Biodiesel	Diesel
Fire point,^{0}C	224	112	105
Acid value, mgNaOH/g	11.50	5.61	0.34
FFA value, %	5.75	2.82	0.17
Cloud point	1	2	-12
Pour point	-2	-3	-20
Carbon residue content, %	4.9	0.04	0.05
Ash content, %	1.5	0.005	0.02
Cetane number	49	51	52

3.2 Performance Parameters

3.2.1 Speed Optimization

From the Fig.6 it is observed that brake thermal efficiency of an engine increases with increase of engine speed. After reaching the maximum value the efficiency of the engine also decreases. This is due to the fact that initially with the increase in engine rpm the torque produced by the engine increases, so the efficiency also increases. But at higher rpm(>850) the amount of fuel injected into the engine cylinder per cycle increases and due to higher engine speed this fuel doesn't get sufficient time to burn completely which reduce the efficiency of the engine.
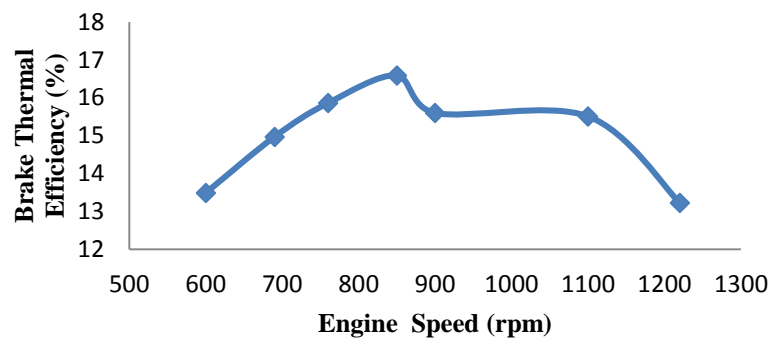

Fig. 6. The variation of brake thermal efficiency with engine speed.

3.2.2 Brake Thermal Efficiency

The change of brake thermal efficiency of the engine with break power output is presented in Fig.7. The brake thermal efficiency of the engine presented very similar affinity for all the fuel samples. It is apparent that the B20 blend shows the nearest break thermal efficiency to that of pure diesel. From the graph it is detected that the brake thermal efficiency increases with the rise in engine load (brake, power) to a maximum point then decrease with the increase in the brake power.
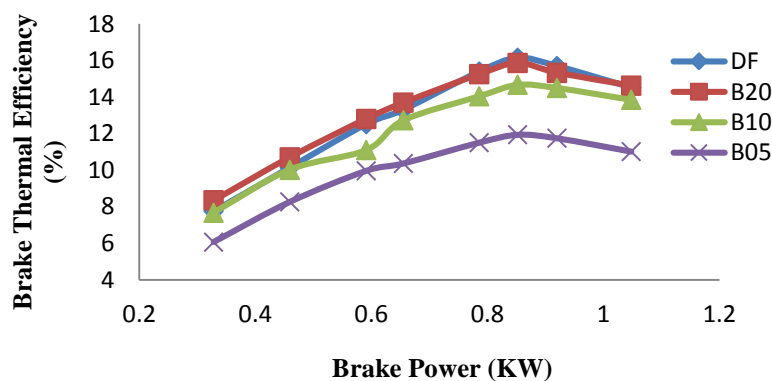

Fig. 7. The variation of brake thermal efficiency with brake power.

From the equation of brake thermal efficiency it can be found that with the increase in engine load the engine brake power increases which increases the thermal efficiency of the engine. At higher loads, i.e. at higher brake power more amount of fuel is injected into the engine cylinder which is not completely burned [8]. It causes higher BSFC and low thermal efficiency. The B20 blend has the highest efficiency among all the blends for the brake power 0.852KW.

3.2.3 Brake Specific Fuel Consumption

In Fig.8 the variation of brake specific fuel consumption (BSFC) with brake power is represented. The BSFC decreases with the brake power increase to a certain point, then again increases with the increase in brake power. The B05 blend has the lowest BSFC among the blends. With the increase in engine load break power increases. As an outcome the brake specific fuel consumption decreases. The BSFC for the same amount of power produced, for biodiesel is slightly higher than that of diesel fuel. This is due to the poor volatility, higher viscosity, higher density and lower calorific value of biodiesel [10].
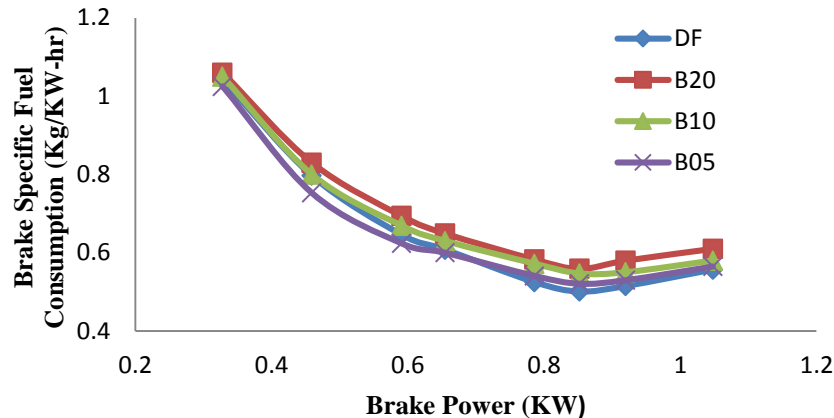

Fig. 8. The variation of BSFC with brake power

4. Conclusion

The following conclusions could be drawn according to the analysis and summary of the current investigational work:

1. The cost analysis of the cottonseed biodiesel production process shows that it is more economical than conventional diesel fuel. According to the production of cotton in the year 2014-15, if the waste cottonseed oil can be converted to biodiesel it can save around 280 million taka per year.
2. The maximum production of biodiesel from cottonseed oil came up with 1% NaOH and 20% methanol in the transesterification process.
3. The optimum temperature for transesterification process is 58^0C with 60 min of heating time.
4. Although the brake specific fuel consumption is slightly higher than the diesel for 20% biodiesel and 80% diesel blend, but it shows the nearest brake thermal efficiency of that of pure diesel.

5. References

[1] Joshi Rushang M. et al. "Flow properties of biodiesel fuel blends at low temperatures", *Elsevier,* Vol. 86, No. 1-2, pp.143- 151, 2007.
[2] K. VinuKumar, "Production of bio-diesel used in diesel engines", *Innovare Journal of Engineering & Technology,* Vol.1, No.1, 2013.
[3] Syed Ameer Basha , K. Raja Gopal, S. Jebaraj, " A review on biodiesel production, combustion, emissions and performance", *Renewable and Sustainable Energy Review,* Vol.13, No. 6-7, pp. 1628–1634,2009.
[4] A.S.Ramadhas,S Jayaraj, C. Muraleedharan, "Use of vegetable oils as I.C. engine fuels—a review", *Renewable Energy,* Vol. 29,No.5, pp. 727– 742,2004.
[5] Fangrui Ma[a], Milford A. Hanna[b], "Biodiesel production: a review", *Bioresource Technology,* Vol. 70, pp. 1-15, 1999.
[6] Orhevba Bosede Adelola [1] and Efomah Andrew Ndudi [2] "Extraction and Characterization of Cottonseed (*Gossypium*) Oil", *IJBAS,* Vol. 01, No. 02, Oct 2012.
[7] www.thefinancialexpress-bd.com/2015/07/10/99910/print, 2015/10/10.
[8] MN Nabi, MM Rahman, MS Akhter, "Biodiesel from cottonseed oil and its effect on engine performance and exhaust emissions", *Applied Thermal Engineering*, Vol. 29, No. 11,pp. 2265-2270,2009.
[9] M.L.Mathur, R.P, Sharma, Internal Combustion Engines, *Dhanpat Rai Publications,* 2011-2012, pp.306-307, 503.
[10] Dr.V. Naga prasad naidu, Prof. V. Pandu rangadu, "A Comparative Study of Performance and Emission Characteristics of Four Stroke Diesel Engine with Mahua and Cotton Seed Biodiesel Blended with Diesel", *IJITR,* Vol. 2, No.5, pp. 1223 – 1227, 2014.

Finite Element Analysis of Bio-heat Transfer Problems with Different Heating Condition on Skin Surface

Abul Mukid Mohammad Mukaddes and Sannyal Mridul
Department of Industrial and Production Engineering
Shahjalal University of Science and Technology, Sylhet
Email: mukaddes1975@gmail.com

Abstract:

Most of the therapy aims to raise the temperature of the cancerous tissue above a therapeutic value to kill or destroy it. One of the main concerns of these therapies is to minimize the damage of the unaffected cells. Therefore acknowledgement of temperature profile of living tissue is necessary before the treatment starts. This needs the heat transfer analysis of biological body. Pennes bio-heat equation represents the heat transfer model of the human body. In this paper, a one-dimensional finite element model has been developed to analyse the bio-heat transfer problems based on the Pennes equation. A C program has been coded to solve the developed model. Using the developed program, the temperature profile in the human body subject to constant and sinusoidal spatial heating on skin surface has been computed. The point and stochastic heating on the skin surface are also investigated. Numerical results are compared with the analytical result for the steady state case. The developed finite element code can be used to measure the temperature of human tissue with different heating and cooling conditions.

Keywords: Finite element, Bio-heat, Pennes equation, Spatial heating.

1. Introduction:

Heat transfer in living tissue has become a very interesting topic for scientists and engineers because of its broad application in bioengineering and designing of medical equipments. Many therapeutic applications need the proper thermal description of the human body. Again many medical operations rely on engineering methods to determine safety and risk level involved in surgeries. At present mathematical modelling of Bio heat transfer is widely used in treating tumours, cryosurgery, laser eye surgery and many other applications. The success of hyperthermia treatment greatly depends on the proper knowledge of heat transfer in blood perfused tissue [1].

Among the various model proposed to study the heat transfer in biological bodies, the most widely used ine is proposed by Pennes [2]. Though initially it was developed to predict heat transfer in human forearm later it was implemented in various biological research works due to its simplicity i.e. uniform thermal conductivity, perfusion rate and metabolic heating.

Numerous analytical and numerical solutions of the bio-heat transfer problem are found in the literature. Analytical solution using Green function is presented in [3]. In some cases time dependent surface heat flux, oscillatory heat flux and sometimes cooling of the skin [3] are considered as boundary conditions. In some numerical analysis sinusoidal spatial heating, point heating [4] was used as external heating.

In this paper a finite element model (FEM) [5] has been developed for the numerical solution of the 1D unsteady Pennes equations with different spatial heating and boundary conditions. The Crank-Nicolson method is used for the time discretization. A C code has been developed which can be used to measure the temperature distribution in the human tissue.

2. Bio Heat Transfer:

For the study of bio-heat transfer in human tissue the most useful one is Pennes equation which is:

$$c\rho \frac{\partial T}{\partial t} = \left\{ \frac{\partial}{\partial x}\left(K \frac{\partial T}{\partial x}\right) + \omega_b \rho_b C_b (Ta - T) + Q_m + Q_r \right\} \tag{1}$$

where ρ, c, K are respectively the density, the specific heat, and the thermal conductivity of the tissue; ρ_b, C_b denote density and specific heat of blood; ω_b the blood perfusion; T_a the known arterial temperature, and $T(x,t)$ is unknown tissue temperature; Q_m is the metabolic heat generation, and $Q_r(x,t)$ the heat source due to spatial heating with respect to time t.

For a one dimensional problem of length L, let $T(x,o) = T_0(x)$ is initial temperature, T_c is the body core temperature, h_0 is the heat convection coefficient between the skin surface and the surrounding air, T_f is the surrounding air temperature. Thus the boundary conditions

$$T = T_0(x) = T_c, \quad \text{at } x = L \tag{2(a)}$$

$$-k\frac{dT_0(x)}{dx} = h_0[T_f - T(x)], \quad \text{at } x = 0 \tag{2(b)}$$

In some cases boundary condition is time dependent .So time dependent boundary conditions can be introduced as

$$-k\frac{dT_0(x)}{dx} = f_1(t) \quad \text{at } x = 0 \tag{3}$$

Where f₁(t) is the time dependent surface heat flux. Here, the skin surface is defined at $x = 0$ and the body core at $x = L$.

3. Finite element discretization:

The first step of the finite element discretization is to develop a weak form that is a weighted-integral statement and is equivalent to both the governing equation as well as certain type of boundary conditions. The simplest form of the equation (1) is

$$c\rho \frac{\partial T}{\partial t} - \left\{ \frac{\partial}{\partial x}\left(k \frac{\partial T}{\partial x}\right) + CT + q \right\} = 0 \tag{4}$$

Where $\quad C = w_b \rho_b C_b \quad$ and $\quad q = CTa + Q_m + Q_r$

The weak form of the differential equation (Applying weighted residual method) is derived as

$$\int_{xa}^{xb} \left[Wc\rho \frac{dT}{dt} - k \frac{dW}{dx}\frac{dT}{dx} + CWT - Wq \right] + (WQ)x_a + (WQ)x_b = 0 \tag{5}$$

Where W is the weighted function and Q is the secondary variable.
In this paper a linear element is considered whose temperature function is given by

$$T_h^e(x) = \sum_{j=1}^{2} \varphi_j^e(x) T_j^e \tag{6}$$

Using the linear approximation function of equation as (6) finally a linear equation was derived of the following form

$$[C]\{\dot{T}\} + [K]\{T\} = \{q\} + \{Q\} \tag{7}$$

Where C is the capacitance matrix, K is heat conductive matrix and T is unknown temperature and others are known vectors.

4. Time Discretization Scheme

A simple time integration scheme to solve equation (7) was derived by assuming that C and K are constant. In such case, matrix differential equation can be discretized on time as:

$$C\frac{T^{n+1}-T^n}{\Delta T}+\alpha KT^{n+1}+(1-\alpha)KT^n=0 \tag{8}$$

Where T^{n+1} and T^n are the vectors of unknown nodal values at times $n\Delta T$ and $(n+1)\Delta T$ respectively. α is a weighting factor which must be chosen in between 0 and 1. In equation (8) the standard approximation for time derivative was used.

$$\dot{T}=\frac{T^{n+1}-T^n}{\Delta T}$$

When the value of α is considered 0.5, the process is called the popular Crank-Nicolson method. The discretized equation (8) can be written as:

$$\left(\frac{1}{\Delta T}C+\alpha K\right)T^{n+1}=\left(\frac{1}{\Delta T}C-(1-\alpha)K\right)T^n+Q+q \tag{9}$$

The equation (9) was solved using an iterative procedure. The initial temperature is known and then temperature of the next step can be calculated from the solution of equation (9) via the Gauss elimination technique.

5. Analysis and Numerical Results:

A FEM code has been developed using C language to solve the numerical solution of the finite element model described in the previous section. In this paper, a tissue of length 3mm from the skin surface is considered for the calculation. The tissue properties and parameters of the boundary conditions (Table 1) are applied as given in [3, 6].

The initial temperature (at t=0) of all nodes is considered as constant (37°C). As the body core temperature remains constant at all-time thus the body core temperature is considered as 37^0 C.

Table 1.Thermal Properties

Parameters	Symbol	value
Thermal conductivity	K	0.5 w/m^2
Convection Coefficient	h_o	10 w/m^2
Forced convection coefficient	h_f	100 w/m^2
Environmental Temperature	T_f	25 °C
Temperature of the Artery	T_a	37 °C
Body core temperature	T_c	37 °C
Metabolic heat generation	Q_m	33800 w/m^2
Density of blood	ρ_b	1000 kg/m^3
Density of tissue	ρ	1000 kg/m^3
Specific heat of blood	C_b	4200 J/kg.°C
Specific heat of tissue	C	4200 J/kg.°C
Blood perfusion	ω_b	0.0005 ml/s/ml

Investigation-1: Surface adiabatic condition and sinusoidal spatial heating

In case of heating by laser, microwave, the expression for specific absorption rate can be simplified as $Q_r=\eta P_0(t)\exp(-\eta x)$ in which heat flux decays exponentially with respect to distance from the skin surface [6, 7]. Here $P_o(t)$ is the time dependent heating power on skin surface and η is the scattering coefficient.
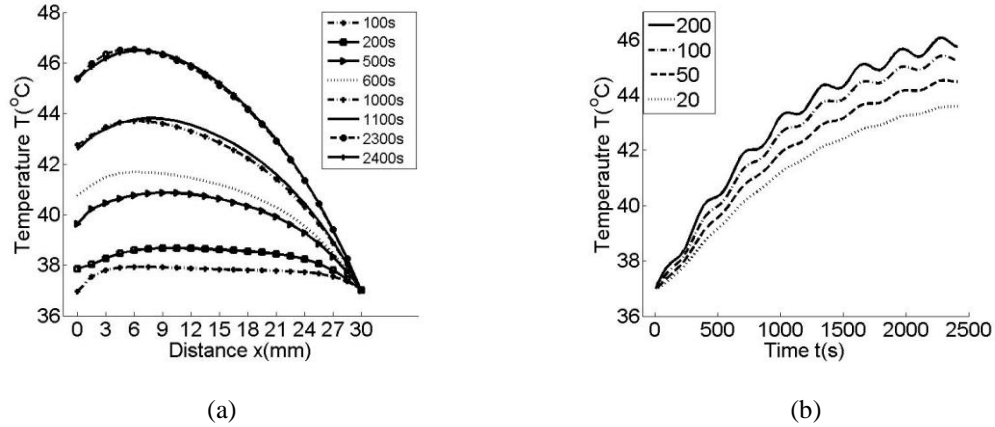
(a)   (b)

Fig. 1. Temperature distribution subjected to sinusoidal spatial heating of human tissue;

$(P_o(t)=250+200\cos(0.02t)$ W/m^2); (a) at different times; (b) at different scattering coefficient.

Fig. 1(a) shows the temperature distribution with respect to distance from the skin surface at different times. In this figure there is cross of temperature curve at different times which indicates the temperature oscillation inside tissue. Fig. 1(b) shows the effect of scattering coefficient (for four different values of scattering coefficient). Clearly this curve indicates the sinusoidal effect and also demonstrates that the higher frequency results in higher amplitude.

Investigation-2: Surface heating

Here, we analysed the thermal behaviour of living tissue subjected to time dependent surface heat flux. This is very beneficial in case of thermal injury analysis i.e. thermal burn analysis [8].The calculated tissue temperature for three different constant surfaces heating is shown in Fig. 2(a). Curves A, B, C indicates the temperature at f_1 = 1000 W/m^2, f_1 = 500 W/m^2, f_1 = 200 W/m^2 respectively (when $P_o(t)=250$). These curves indicate that the larger heat flux brings higher temperature. Moreover temperature increases as time increases.

Transient temperature at three positions subject to surface step heating (Considering $Q_r=0$) is shown in Fig 2(b).

Where $f_1(t)= \begin{cases} 1000 \ \frac{w}{m2}, t \le 1200s \\ 0 \quad \frac{w}{m2}, t > 1200s \end{cases}$. The practical application of these types of heating can be found in eye

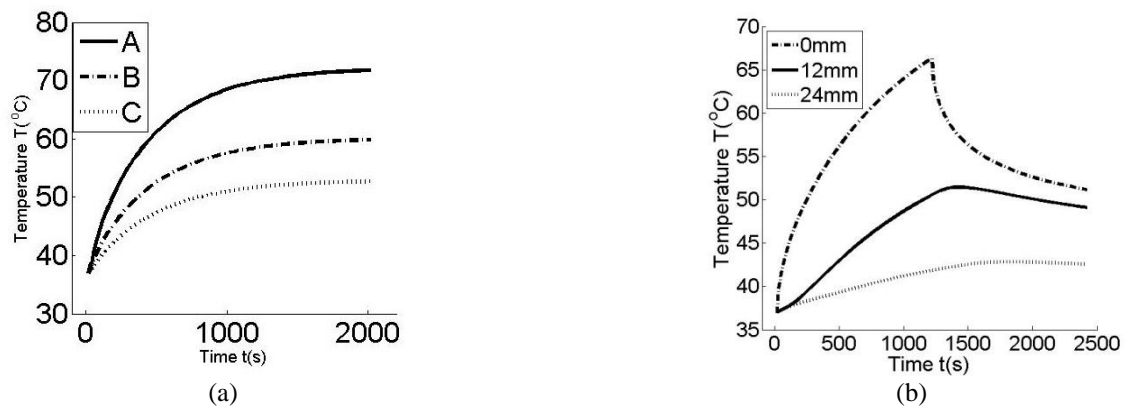surgery or skin burn due to a flash fire, hot plate, liquid or hot gas for a short period [8].

(a)   (b)

Fig. 2. Tissue temperature response on surface heat flux; (a) Constant surface heat flux; (b) Step heating

4

Fig. 2(a) indicates that larger heat flux brings higher temperature. Moreover temperature increases as time increases. Fig. 2(b) shows that as time increases temperature also increases but this becomes reverse after 1200s when $f_1(t) = 0$.

Investigation-3: Effect of heating frequency and blood perfusion

The calculated result for different heating frequency and blood perfusion is shown in Fig. 3 when simultaneously constant spatial heating (when $P_o(t)=250$) and sinusoidal surface heating is applied. The sinusoidal heating at the skin surface can be expressed as $f(t)=q_0+q_w\cos(\omega_1 t)$. Where q_0 and q_w are the constant term and oscillation amplitude of sinusoidal heat flux respectively and ω_1 represents the heating frequency.

Here curve A and B we use blood perfusion as 0.0005, where in curve C & D it is 0.004. When in curve A and C we uses a heating frequency of value 0.02 where in B & D it is 0.01.
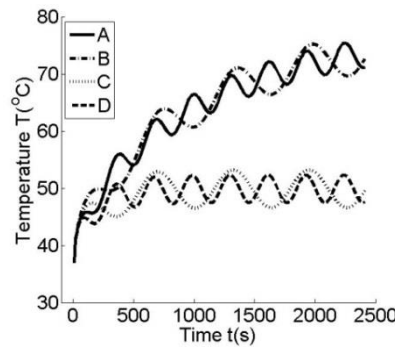

Fig. 3 Effect of heating frequency and blood perfusion on tissue temperature.

This figure indicates that higher blood perfusion leads to lower temperature. This curve also indicates that frequency of the temperature varies with that of the surface heating.

Investigation-4: Point and Stochastic heating

Point heating is adopted when a deep tumour is selected and treatment is applied to thermally kill it. In this heating the target region is heated up to a certain high temperature within a short period [9]. So acknowledgement of temperature distribution under such heating condition is necessary. In contrast to previous heating style where heat flux decays exponentially here the point heating term is expressed as $Q_r(x,t) = P_1(t)\delta(X - X_0)$. Where $P_1(t)$ is the point heating power and $\delta(x-x_0)$ is the Dirac delta function.
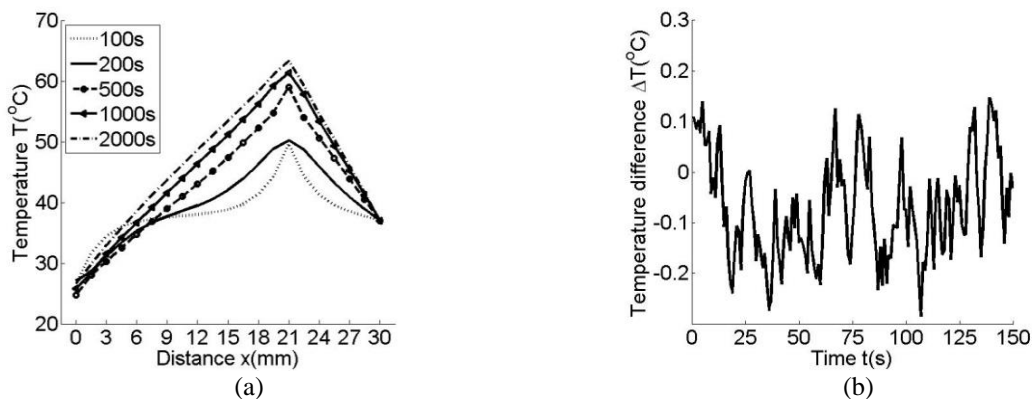$\delta(x-x_0)$ has a value 1 at $x = x_0$ and 0 elsewhere in x.

Fig. 4 Impact of point and stochastic heating on tissue temperature distribution;
(a) Point heating; (b) Stochastic heating;

In Fig. 4(a) temperature distribution at different times is shown where point heating with a point heat source of $P_1(t)=2500$ W/m^2 at a distance 21mm ($x_0 = 21$mm) below the skin surface is applied. In this figure at skin surface convection boundary condition is applied ($h_f=100$ W/m^2 and $T_f=15$ °C).This figure demonstrates that due to

point heat source the position of the maximum temperature remain constant at the site of the point source at different time. Here the maximum temperature is more than 60^0C thus it can be helpful in case of thermal ablation.

Previously we considered environmental temperature as a constant value but in practical cases it does not remain constant at all. It generally fluctuates over time so it is necessary to study the impact of such variance.

In Fig. 4(b) stochastic heating is shown where surrounding fluids temperature is usually a stochastic value and it is taken as $T_e = T_f + \lambda_t(0.05 - \sigma_i)$, where λ_t is a constant which is taken as 5^0C and σ_i the random number between 0 and 1. Clearly the figures demonstrate that due to irregular cooling medium temperature the tissue temperature fluctuates within a narrow range. This may be helpful in thermal comfort analysis as it indicates that the biological body trends to keep its temperature stable.

6. Conclusion:

A system for finite element analysis of bio-heat transfer has been developed. Various types of heating pattern i.e. spatial heating, surface heating, point heating, stochastic heating and their impacts are investigated and briefly discussed in this paper. The effect of heating frequency, blood perfusion and scattering coefficient are also shown. It is found that for destroying a target cell point heating is more suitable than other heating as it increases the temperature of the target region and it has relatively low impact on nearby unaffected cells. As heating apparatus such as laser or microwave may have different power and scattering coefficient. Results obtained in this paper can be used to select suitable apparatus. During treatment, fluctuation of environmental fluid temperature may be out of considered as its impact on tissue temperature is almost negligible as shown in stochastic heating. Results described in this paper could be useful to accurately predict the thermal behaviour of living tissues and can be extended to such application as parameter estimation, clinical treatment and medical protocols design and to optimize for surgical treatment.

7. Acknowledgement:

References:

[1] Khanafer, K., and K. Vafai. "Synthesis of mathematical models representing bioheat transport." *Advances in Numerical Heat Transfer* 3 (2009): 1-28.

[2] Pennes, Harry H. "Analysis of tissue and arterial blood temperatures in the resting human forearm." *Journal of applied physiology* 1.2 (1948): 93-122.

[3] Deng, Zhong-Shan, and Jing Liu. "Analytical study on bioheat transfer problems with spatial or transient heating on skin surface or inside biological bodies."*Journal of biomechanical engineering* 124.6 (2002): 638-649.

[4] Karaa, Samir, Jun Zhang, and Fuqian Yang. "A numerical study of a 3D bioheat transfer problem with different spatial heating." *Mathematics and Computers in Simulation* 68.4 (2005): 375-388.

[5] Reddy, J.N. An Introduction to the Finite Element Method, 3rd edition, McGraw Hill, Inc, (2006).

[6] Sharma, P. R., Sazid Ali, and V. K. Katiyar. "Transient heat transfer analysis on skin surface and inside biological tissue." *Journal of Applied Mathematics and Mechanics* 5.5 (2009): 36-47.

[7] Cheung, Augustine Y., and Ali Neyzari. "Deep local hyperthermia for cancer therapy: external electromagnetic and ultrasound techniques." *Cancer research*44.10 Supplement (1984): 4736s-4744s.

[8] Torvi, D. A., and J. D. Dale. "A finite element model of skin subjected to a flash fire." *Journal of biomechanical engineering* 116.3 (1994): 250-255.

[9] Huang, Huang-Wen; Liauh, Chihng-Tsung, Review: Therapeutical Application of Heat in Cancer Theraphy, Journal of Medical and Biological Engineering Vol-32(1),P.1-11(2011)

[10] Shen, Wensheng, Jun Zhang, and Fuqian Yang. "Modeling and numerical simulation of bioheat transfer and biomechanics in soft tissue." *Mathematical and computer modelling* 41.11 (2005): 1251-1265.

[11]Shih, Tzu-Ching, et al. "Analytical analysis of the Pennes bioheat transfer equation with sinusoidal heat flux condition on skin surface." *Medical Engineering & Physics* 29.9 (2007): 946-953.

Double Diffusive Natural Convection in a Porous Wavy Triangular Enclosure Filled with Nanofluid in Presence of Magnetic Field

R. Chowdhury[a,b,*], S. Parvin[b], M. A. H. Khan[b]

[a]*Department of Natural Science, Stamford University Bangladesh, Dhaka-1217, Bangladesh.*
[b]*Department of Mathematics, Bangladesh University of Engineering & Technology, Dhaka-1000, Bangladesh.*
[*]*E-mail: raju_chy_23@yahoo.com*

Abstract

The current numerical study is conducted to analyze double diffusive natural convection flow in a triangular enclosure with a sinusoidal wavy bottom surface filled in a porous medium saturated by nanofluid in presence of magnetic field. The wavy bottom surface of the cavity is heated constantly and maintained at higher concentration while left and right inclined walls are at cold temperature and maintained at lower concentration. The transport governing equations are solved by finite element formulation based on the Galerkin method of weighted residuals. The implications of thermal Rayleigh number (Ra$_T$), Hartmann number (Ha), Lewis number (Le) and number of undulations (λ) on the flow structure, heat and mass transfer characteristics are investigated in detail while, Prandtl number (Pr), buoyancy ratio (N) and solid volume fraction (φ) is considered fixed. The results are presented in terms of streamlines, isotherms, isoconcentrations, Nusselt number (Nu) and Sherwood number (Sh). Results of this investigation illustrates that the rate of heat and mass transfer are affected by the considering parameters.

Keywords: Double diffusion, Natural convection, Sinusoidal wavy triangular enclosure, Magnetic field, Nanofluid.

1. Introduction

   Natural convective heat and mass transfer in cavities becomes most important issues from industrial and energy perspectives. In the past few decades, experimentally, analytically and numerically extensive researches have been performed on this topic by many researchers [1]-[4]. Combined convective heat and mass transfer is refereed to buoyancy driven flows by both temperature and concentration gradients. Combined heat and mass transfer occurs in a wide range of applications in both nature and industry. In nature, such flows are occurred in oceans, lakes, shallow coastal water, and the atmosphere. In industry, these type of flows are the chemical process, crystal growth, solidification, food processing and migration of impurities in non-isothermal material processing applications. Ostrach [5] and Viskanta et al. [6] have reported complete reviews on the subject.

   Double-diffusive natural convection in nanofluids is an important fluid dynamics topic that describes the convection driven by two different density gradients with different rates of diffusion [4]. Thermal buoyancy-induced flow and heat transfer inside a porous medium has been investigated enormously in the literature due to its relevance in many natural and industrial applications. The magnetic field effect on the convective heat transfer and the free convection flow of the fluid are very important in engineering. Effect of magnetic field and heat generation on free convection in a porous media filled equilateral triangular cavity has been studied by Chowdhury et al. [7]. Adjlout et al. [8] have studied laminar natural convection in an inclined cavity with a wavy wall. Molla et al. [9] have investigated natural convection flow along a vertical wavy surface with uniform surface temperature in presence of heat generation/observation. Das and Mahmud [10] have conducted numerical investigation of natural convection inside a wavy enclosure. Das et al. [11] have analyzed effect of surface waviness and aspect ratio on heat transfer inside a wavy enclosure. Amiri et al. [12] have investigated effect of sinusoidal wavy bottom surface on mixed convection heat transfer in a lid-driven cavity.

   Heat transfer in a triangular model can be a simple model for many engineering applications. Although many studies have reported natural convection in triangular cavities [7], studies in combined heat and mass transfer in wavy triangular enclosures filled with nanofluid are very limited. The aim of the present study is to investigate the flow pattern, heat and mass transfer in a porous wavy triangular enclosure filled with nanofluid exposed to both temperature and concentration gradients. Double-diffusive conditions is maintained by taking the bottom wall as heated wall and the source for solute concentration and the left and right inclined wall is cold and lower concentration.

Nomenclature		**Greek Letters**	
B_0	magnetic field $[T]$	α	thermal diffusivity $[ms^{-2}]$
c	concentration $[mol\ m^{-3}]$	β_T	volumetric coefficient of thermal expansion $[K^{-1}]$
C	dimensionless concentration	β_s	volumetric coefficient of solutal expansion $[m^3 kg^{-1}]$
Cp	specific heat $[Jkg^{-1}K^{-1}]$	λ	undulation number
D	mass diffusivity $[m^2/s]$	μ	dynamic viscosity $[kgm^{-1}s^{-1}]$
g	gravity acceleration $[m/s^2]$	θ	dimensionless temperature
k	thermal conductivity $[Wm^{-1}K^{-1}]$	ν	kinematic viscosity $[m^2 s^{-1}]$
L	height of the triangle $[m]$	ρ	density $[kgm^{-3}]$
N	buoyancy ratio, $\beta_S \nabla c / \beta_T \nabla T$	φ	nanoparticle volume fraction
p	fluid pressure $[Pa]$	**Subscript**	
P	dimensionless fluid pressure	c	cold
u, v	x, y component of velosity $[ms^{-1}]$	h	hot
U, V	x, y component of dimensionless velocity	f	fluid
T	temperature $[K]$	p	nanoparticle
		nf	nanofluid

2. Governing Equations

Fig. 1 shows the schematic diagram of wavy triangular enclosure subjected to the non-dimensional boundary conditions. The bottom wall of the cavity is heated uniformly at temperature T_h, the left and right inclined wall is considered to be cold at temperature T_c. The concentration c_h, is higher at wavy bottom wall and lower c_c, at left and right inclined wall. The working fluid consider in the system is water based Al_2O_3 nanofluid. The properties of water and Al_2O_3 are presented in Table 1. The physical properties of the fluid are assumed to be constant except the density in the buoyancy force term. The non-dimensional governing equations for nanofluids can be written as:
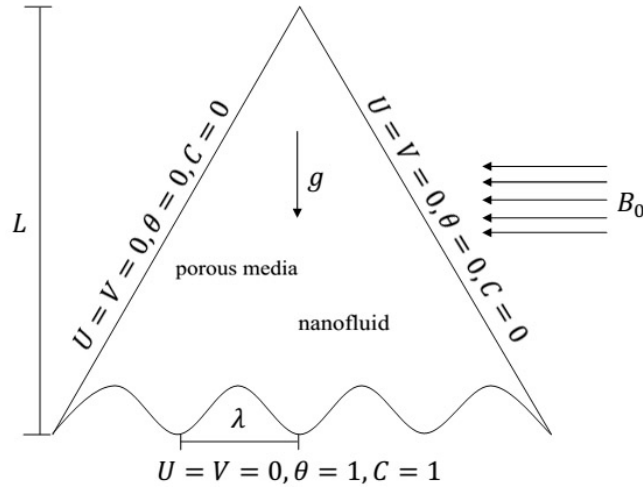

Fig. 1: Physical model of the problem with corresponding non-dimensional boundary conditions.

$$\frac{\partial U}{\partial X} + \frac{\partial V}{\partial Y} = 0 \tag{1}$$

$$\left(U\frac{\partial U}{\partial X} + V\frac{\partial U}{\partial Y}\right) = -\frac{\partial P}{\partial X} + \frac{\mu_{nf}}{\rho_{nf}\alpha_f}\left(\frac{\partial^2 U}{\partial X^2} + \frac{\partial^2 U}{\partial Y^2}\right) - \frac{\mu_{nf}}{\rho_{nf}\alpha_f}\frac{1}{Da}U \tag{2}$$

$$\left(U\frac{\partial V}{\partial X} + V\frac{\partial V}{\partial Y}\right) = -\frac{\partial P}{\partial Y} + \frac{\mu_{nf}}{\rho_{nf}\alpha_f}\left(\frac{\partial^2 V}{\partial X^2} + \frac{\partial^2 V}{\partial Y^2}\right) - \frac{\mu_{nf}}{\rho_{nf}\alpha_f}\frac{1}{Da}V + Ra_T Pr(\theta + NC) - Ha^2 V \tag{3}$$

$$\left(U\frac{\partial \theta}{\partial X} + V\frac{\partial \theta}{\partial Y}\right) = \frac{\alpha_{nf}}{\alpha_f}\left(\frac{\partial^2 \theta}{\partial X^2} + \frac{\partial^2 \theta}{\partial Y^2}\right) \tag{4}$$

$$\left(U\frac{\partial C}{\partial X} + V\frac{\partial C}{\partial Y}\right) = \frac{1}{Le}\left(\frac{\partial^2 C}{\partial X^2} + \frac{\partial^2 C}{\partial Y^2}\right) \tag{5}$$

where the thermal Rayleigh number $Ra_T = \frac{g\beta_f\rho_f(T_h - T_c)L^3}{\alpha_f\mu_f}$, the solutal Rayleigh number $Ra_S = \frac{g\beta_S\rho_f(C_h - C_c)L^3}{\alpha_f\mu_f}$,

Prandtl number $Pr = \frac{v_f}{\alpha_f}$, Darcy number $Da = \frac{K}{L^2}$, Hartmann number $Ha = B_0 L \sqrt{\frac{\sigma_f}{\rho_{nf}\alpha_f}}$, Buoyancy ratio $N = \frac{Ra_S}{Ra_T}$ and Lewis number $Le = \frac{\alpha_f}{D_f}$.

The non-dimensional boundary conditions are:
On the left and right wall: $U = V = 0, \theta = 0, C = 0$
On the bottom sinusoidal wall: $U = V = 0, \theta = 1, C = 1$.

The following dimensionless variables are used to non-dimensionalize the governing equations:
$$X = \frac{x}{L}, Y = \frac{y}{L}, U = \frac{uL}{\alpha_f}, V = \frac{vL}{\alpha_f}, P = \frac{pL^2}{\rho_{nf}\alpha_f^2}, \theta = \frac{T-T_c}{T_h-T_c}, C = \frac{C-C_c}{C_h-C_c} \tag{6}$$

Table 1: Thermophysical properties of water and nanoparticles

Physical Properties	$Cp(J/kgK)$	$\rho(kg/m^3)$	$k(W/mK)$	$\beta_T (1/K)$
Water	4179	997.1	0.613	21×10⁻⁵
Al_2O_3	765	3970	40	0.8×10⁻⁵

The effective thermal conductivity of the nanofluid is approximated by the Hamilton-Crosser model [13] expressed as
$$k_{nf} = k_f \frac{k_p + 2k_f - 2\varphi(k_f - k_p)}{k_p + 2k_f - \varphi(k_f - k_p)}$$
The viscosity of nanofluid $\mu_{nf} = \frac{\mu_f}{(1-\varphi)^{2.5}}$, volumetric coefficient of thermal expansion $(\rho\beta_T)_{nf} = (1-\varphi)(\rho\beta_T)_f + \varphi(\rho\beta_T)_p$, density $\rho_{nf} = (1-\varphi)\rho_f + \varphi\rho_p$, thermal diffusivity $\alpha_{nf} = \frac{k_{nf}}{(\rho C_p)_{nf}}$, and heat capacitance $(\rho C_p)_{nf} = (1-\varphi)(\rho C_p)_f + \varphi(\rho C_p)_p$.
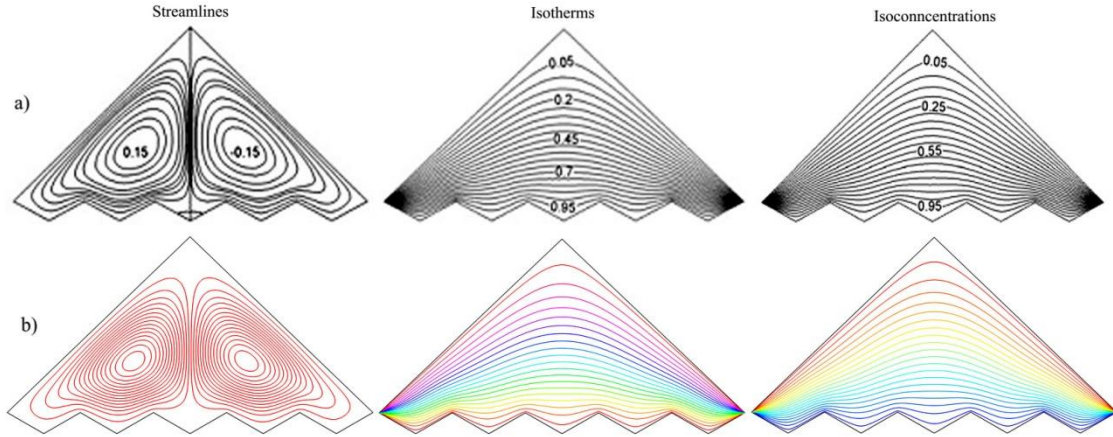

Fig. 2: A comparison for streamlines (left column), isotherms (middle column) and isoconcentration (right column) between Rahman et al. [14] (top row) and present study (bottom row) for $Ra_T = 10^4, Pr = 7.0, \varphi = 0, Le = 2$ and $N = 0$.

The local and average Nusselt number along the heated bottom wall can be calculated as
$$Nu_b = -\frac{k_{nf}}{k_f}\left(\frac{\partial\theta}{\partial n}\right), Nu = -\left(\frac{k_{nf}}{k_f}\right)\frac{1}{L}\int_0^L \left(\frac{\partial\theta}{\partial n}\right) dL \tag{7}$$
The local and average Sherwood number along the heated bottom wall can be calculated as
$$Nu_b = -\left(\frac{\partial C}{\partial n}\right), Nu = -\frac{1}{L}\int_0^L \left(\frac{\partial C}{\partial n}\right) dL. \tag{8}$$

3. Numerical Method
The numerical procedure used in this study is based on the Galerkin weighted residual method of finite element method. In this method, the solution domain is discretized into finite element meshes, which are composed of non-uniform triangular elements. Then the nonlinear governing partial differential equations are transferred into a system of integral equations by applying Galerkin weighted residual method. The integration involved in each term of these equations is performed by using Gauss's quadrature method. The nonlinear algebraic equations so obtained are modified by imposition of boundary conditions. These modified nonlinear equations are transferred into linear algebraic equations by using Newton's method. Finally, these linear equations are solved by using Triangular Factorization method.

4. Validation

A test has been performed to valid the present study by comparing with earlier study Rahman et al.[14]. Fig. 2 represents the results in terms of streamlines, isotherms and isoconcentrations obtained by the present code and the results presented by [14]. The comparison shows in Fig. 2 and it can be clearly seen that there is good agreement between the results.
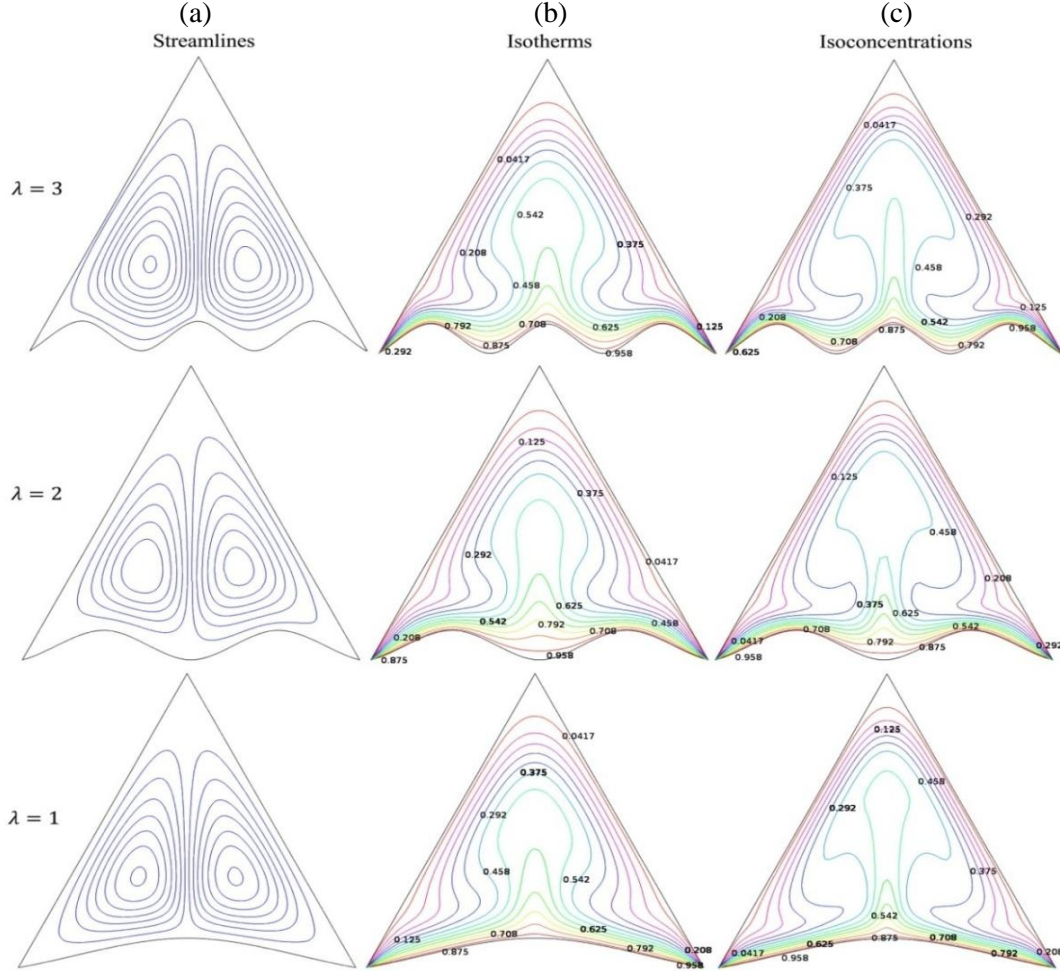

Fig. 3: a) Streamlines, b) Isotherms and c) Isoconcentrations for different values of undulation number λ with $Ra_T = 10^5, Pr = 7.0, \varphi = 10\%, Le = 2, Ha = 25, N = 1, Da = 10^{-3}$.

5. Result and Discussion

The natural convection inside a porous wavy triangular cavity filled with nanofluid including magnetic effect is influenced by the controlling parameters $10^4 \leq Ra_T \leq 10^6, 0 \leq \lambda \leq 3, 0 \leq Ha \leq 50$ and $1 \leq Le \leq 10$. The results are represented in terms of streamlines, isotherms, isoconcentrations, average Nusselt number (Nu) and average Sherwood number (Sh) for controlling parameters while $Pr = 7.0, \varphi = 10\%, N = 1, Da = 10^{-3}$ are kept fixed.

Fig. 3 (a)-(c) represents the flow strength, heat transport and species transport profile for different values of undulation number λ while $Ra_T = 10^5, Pr = 7.0, \varphi = 10\%, Le = 2, Ha = 25, N = 1, Da = 10^{-3}$. At Fig. 3 (a), it can be shown that two symmetrically distributed cells are created within the cavity for $\lambda = 1$. The cell near the left inclined wall rotates clockwise direction while the other cell rotates in anticlockwise direction. The cell of rightside increases and dominates the cell of leftside for $\lambda = 2$. The opposite results can be shown for further increasing of undulation number ($\lambda = 3$) where the right cells dominates the left one. In Fig. 3 (b), a symmetrical plumwise temperature distribution is started due to moving fluid to the upper direction of the cavity as buoyancy driven flow moves the fluid from the hotter to colder. This flow becomes stronger with increasing the undulation number. Hat of the plume becomes thinner for concave wave ($\lambda = 2$) and wider for convex wave ($\lambda = 1, \lambda = 3$) at the centre of the bottom wall. A subplume are started from the wavy bottom wall and moves to the upper direction of the cavity for all values of λ. The similar distribution can be shown for concentration that can be noticed from the Fig. 3. A wavy solutal boundary layer forms for all undulation

numbers. The symmetrical temparature and concentration distribution occures as the left and right inclined wall are maintained at the similar boundary condition. The thermal and solutal boundary layer near the bottom
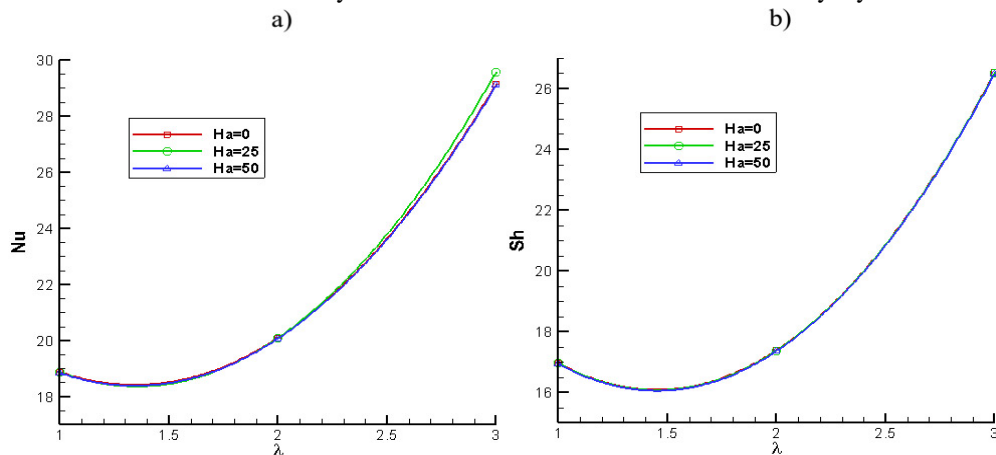

Fig. 4: The variation of *a*) average Nusselt number (*Nu*) and *b*) average Sherwood number (*Sh*) at the heated bottom wavy wall for different undulation number and *Ha* with $Pr = 7.0, \varphi = 10\%, Ra_T = 10^5, Le = 2, N = 1$ and $Da = 10^{-3}$.
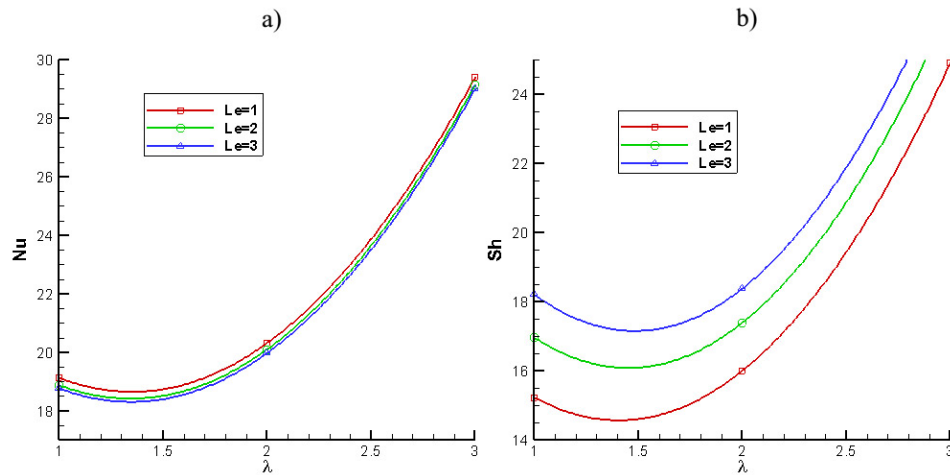

Fig. 5: The variation of *a*) average Nusselt number (*Nu*) and *b*) average Sherwood number (*Sh*) at the heated bottom wavy wall for different undulation number and *Le* with $Pr = 7.0, \varphi = 10\%, Ra_T = 10^5, Ha = 25, N = 1$ and $Da = 10^{-3}$.
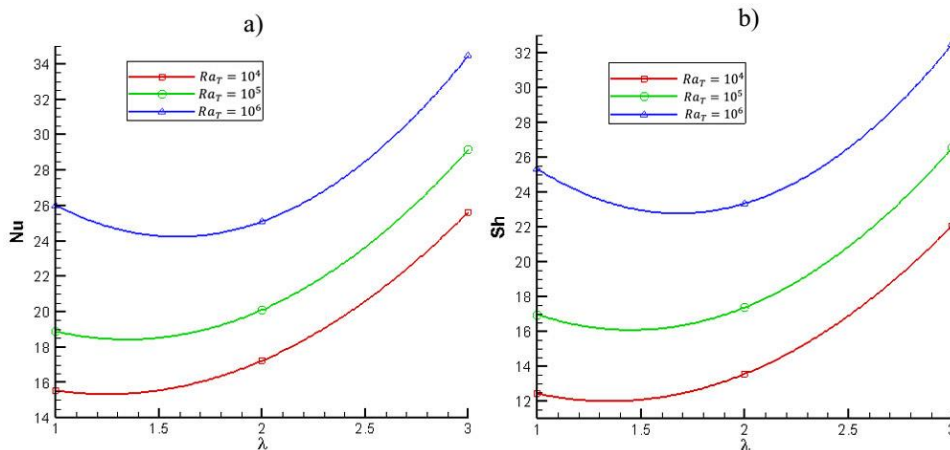

Fig. 6: The variation of *a*) average Nusselt number (*Nu*) and *b*) average Sherwood number (*Sh*) at the heated bottom wavy wall for different undulation number and Ra_T with $Pr = 7.0, \varphi = 10\%, Le = 2, Ha = 25, N = 1$ and $Da = 10^{-3}$.

surface becomes slightly compressed when the number of waves increases.

Fig. 4-6 describes the investigation of the effect of Hartmann number, Lewis number and thermal Rayleigh number on the heat and mass transfer rate on the wavy bottom wall which is heated uniformly for different values of undulation number while $Pr = 7.0, \varphi = 10\%, N = 1, Da = 10^{-3}$. In the Fig. 4-6, the graph demonstrates that the Nusselt number and Sherwood number on the heated bottom wavy wall increase

remarkably with the increase of λ for all Hartmann number, Lewis number and thermal Rayleigh number. The effect of Hartmann number is negligible for *Nu* and does not affect on the average Sherwood number that can be shown in Fig. 4 (a)-(b). Fig. 5 demonstrates that The average nusselt number is slightly decreased while the average Sherwood number increase considerably with the increasing of Lewis number. The average Sherwood number increases as the thermal resistance is higher than the solutal resistance and therefore the mass transfer rate is higher than the heat transfer rate for increasing the value of *Le* .The average Nusselt number and the average Sherwood number increase considerably with the increasing of thermal Rayleigh number that represents by the graphs in Fig. 6. This is because the flow strength increases with the increasing of thermal Rayleigh number.

6. Conclusion

In this study, a numerical simulation has been conducted to investigate the effect of Hartmann number, thermal Rayleigh number, undulation number and Lewis number on flow pattern, temperature and concentration profile in a wavy triangular cavity filled porous media saturated nanofluid. The outcomes of the existing analysis are as follows:

a. The flow pattern, temperature and solutal profile changes with raising the number of waves in the bottom wall.
b. The average Nusselt number and Sherwood number increases for increasing the undulation number and thermal Rayleigh number.
c. The magnetic field effect is negligible on the average Nusselt number and Sherwood number.
d. The heat transfer rate slightly decreases while the mass transfer rate increase significantly for increasing Lewis number.

7. Acknowledgements

References

[1] C. Pang, J.W. Lee, Y.T. Kang, "Review on combiened heat and mass transfer charicteristics in nanofluids", *Int. J. Therm. Sci.*, Vol. 87, pp. 49-67, 2015.
[2] O.V. Trevisan, A. Bejan, "Combined heat and mass transfer by natural convection in a vertical enclosure", *J. Heat Transfer*, Vol. 109, pp. 104-112, 1987.
[3] A. Mojtabi, M.C. Charrier-Mojtabi, "Double-diffusive convection in porous media", *In. Vafai K (ed) Handbook of Porous Media*, New York, Dekker, 2000.
[4] K. Khanafer, K. Vafai, M. Lightstone, "Buoyancy-driven heat transfer enhancement in a two dimensional enclosure utilizing nanofluids", *Int. J. Heat Mass Trans.* Vol. 46, pp. 3639-3653, 2003.
[5] S. Ohtrach, "Natural convection with combined driven forces", *Physico Chem.Hydodynamics*, Vol. 1, pp. 233-247, 1980.
[6] R. Viskanta, T.L. Bergman, F.P. Incropera, "Double-diffusive natural convection, in: S. Kakac, W. Aung, R. Viskanta (Eds.), Natural Convection: Fundamentals and Applications", Hemisphere, Washington, DC, pp.1075-1099, 1985.
[7] R. Chowdhury, S. Parvin, M.A.H. Khan, "Effect of Magnetic Field and Heat Generation on Free Convection in a Porous Media Filled Equilateral Triangular Cavity", *Int. J. Energy Tech.*, Vol. 7, pp. 49-61, 2015.
[8] L. Adjlout, O. Imine, A. Azzi, M. Belkadi, "Laminar natural convection in an inclined cavity with a wavy wall", *Int. J. Heat Mass Trans.*, Vol. 45, pp. 2141–2152, 2002.
[9] M. M. Molla, M.A. Hossain, L.S. Yao, "Natural convection flow along a vertical wavy surface with uniform surface temperature in presence of heat generation/absorption", *Int. J. Therm Sci.*, Vol. 43, pp. 157–163, 2004.
[10] P.K. Das, S. Mahmud , "Numerical investigation of natural convection inside a wavy enclosure", *Int. J. Therm. Sci.*, Vol. 42, pp. 397–406, 2003
[11] P.K. Das, S. Mahmud, S.H. Tasnim, A.K.M. Sadrul Islam, "Effect of surface waviness and aspect ratio on heat transfer inside a wavy enclosure", *Int. J. Num. Methods Heat Fluid Flow*, Vol. 13 No. 8, pp. 1097-1122, 2003.
[12] A. Al-Amiri, K. Khanafer, J. Bull, I. Pop, "Effect of sinusoidal wavy bottom surface on mixed convection heat transfer in a lid-driven cavity", *Int. J. Heat Mass Trans.*, Vol. 50, pp. 1771–1780, 2007.
[13] R.L. Hamilton, O.K. Crosser, "Thermal conductivity of heterogeneous two component system, I & EC Fundamentals", Vol. 1, pp. 187-191, 1962.
[14] M.M. Rahman, H.F. Oztop, A. Ahsan, J. Orfi, "Natural convection effects on heat and mass transfer in a curvilinear triangular cavity", *Int. J. Heat Mass Trans.*, Vol. 55, pp. 6250-6259, 2012.

3D Finite Element Analysis for Heat Transfer in a Solar Collector: Effect of Solar Irradiation

Rehena Nasrin*, Salma Parvin and M.A. Alim

Department of Mathematics, Bangladesh University of Engineering and Technology, Dhaka-1000, Bangladesh
E-mail: rehena@math.buet.ac.bd

Abstract

Due to renewable and nonpolluting nature of solar energy it is often used in applications such as electricity generation, thermal heating and chemical processing. "Flat-plate" type solar collectors are the most cost effective. Water based copper nanofluid is used as the heat transfer medium. Three-dimensional heat transfer model is developed in which direct sunlight is incident on transparent glass cover of a flat plate solar collector (FPSC). The governing partial differential equations are solved using finite element method with Galerkin's weighted residual technique. In order to evaluate the temperature and velocity profiles within the collector, the energy balance equation and Navier Stokes equation are solved numerically. Average Nusselt number (Nu) at the heated surface, average temperature (T_{av}), average velocity (V_{av}), mean output temperature (T_{out}) and collector efficiency (η) for both nanofluid and base fluid as well as mid-height temperature (T) for nanofluid through the flat plate solar collector are presented as function of the solar irradiation. It is observed that the solar radiation variation increases the rate of heat transfer and thermal efficiency for nanofluid more than that of pure water. Comparison is also shown between the results obtained using 2D and 3D simulations. Code validation is also shown with the literature available.

Keywords: Flat plate solar collector, finite element method, nanofluid, solar irradiation.

1. Introduction

Solar radiation is radiant energy emitted by the sun. Solar flat plate collectors are commonly used for domestic and industrial purposes and have the largest commercial application amongst the various solar collectors. This is mainly due to simple design as well as low maintenance cost. The heat transfer rate per unit area as thermal radiation is called radiative heat flux. The fluids with solid-sized nanoparticles suspended in them are called "nanofluids". Applications of nanoparticles in thermal field are to augment warmth transport from solar collectors to luggage compartment tanks, to pick up proficiency of coolants in transformers.

Numerical simulation was carried on a solar flat plate collector using [1-2]. Manjunath et al. [3] analyzed three dimensional conjugate heat transfers through unglazed solar flat plate collector. They used finned tubes and the heat transfer simulation due to solar irradiation to the fluid medium, increased with an increase in the mass flow rate. Vestlund [4] studied gas-filled flat plate solar collector. The gases examined were argon, krypton and xenon in his thesis paper. CFD analysis of solar flat plate collector was conducted by [5-7] where the numerical results obtained using the experimentally measured temperatures are compared to the temperatures determined by the CFD model. Struckmann [8] and Kalogirou [9] conducted project and survey reports on solar thermal collectors respectively. Very recently, Nasrin and Alim [10-12] developed a semi-empirical relation for forced convective analysis through a solar collector. A new correlation was derived from their obtained results and it was easy to use heat transfer purposes.

From the above literature review it is mentioned that a very few 3D numerical studies have been completed using traditional fluid that is water, gas, air etc. The overall goal of this study is to numerically simulate 3D model of heat transfer by nanofluids through a flat plate solar collector. The investigation is to be carried out at different values of solar irradiation (I) using 2% concentrated water/Cu nanofluid as well as water.

2. Formulation

The glass top surface is exposed to solar irradiation. It is made up of borosilicate which has thermal conductivity of 1.14 W/mK and refractive index of 1.47, specific heat of 750 J/kgK and coefficient of sunlight transmission of 95%. The wavelength of visible light is roughly 0.7 μm. Thickness of glass cover is 0.005m. There is an air gap of 0.005m between glass cover and absorber plate. Length, width and thickness of the absorber plate are 1m, 0.15m and 0.0005m respectively. The riser pipe has inner diameter 0.01 m and thickness 0.0005m. Coefficients of heat absorption and emmision of copper absorber are 95% and 5% respectively. A

trapezium shaped bonding conductance of copper metal is located from middle one-third part of width of the absorber plate. It covers the three-fourth part of the riser pipe. It is as long as the absorber plate and tube. The computation domain is the copper absorber plate containing a fluid passing copper riser pipe with bonding conductance. Figure 1 shows the computational domain in 3D view.
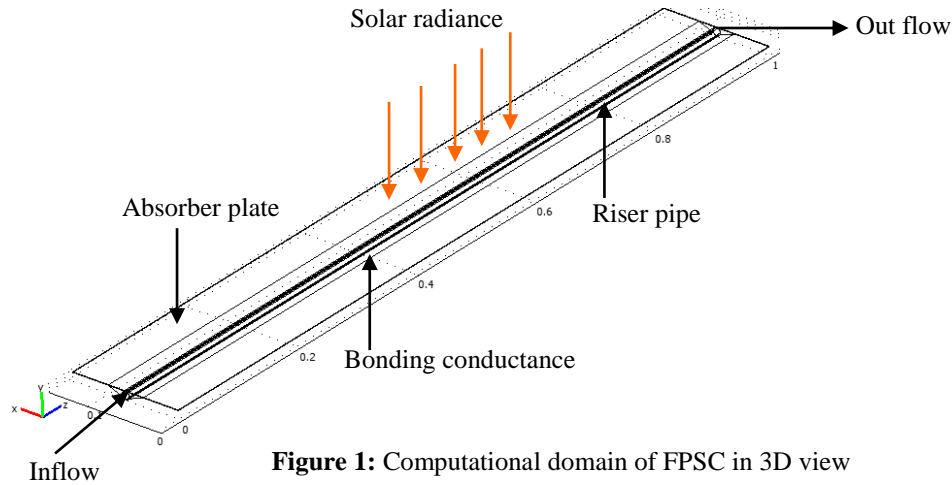

Figure 1: Computational domain of FPSC in 3D view

Let *I* be the intensity of solar radiation and *A* be any surface area, then the amount of energy received by any surface is: $Q_i = I.A$ (1)

This equation is modified for solar collector surface as it is the product of the rate of transmission of the cover (τ) and the absorption rate of the absorber (α). Thus, $Q_{recv} = I(\tau\alpha)A$ (2)

Some heat is lost to the atmosphere by convection and radiation process. The rate of heat loss (Q_{loss}) depends on the collector overall heat transfer coefficient (U_l) and the collector temperature.

$$Q_{loss} = U_l A(T_{col} - T_{amb}) \tag{3}$$

The rate of useful energy extracted by the collector (Q_{usfl}) is: $Q_{usfl} = Q_{recv} - Q_{loss} = I(\tau\alpha)A - U_l A(T_{col} - T_{amb})$ (4)

Another form of rate of heat extraction from the collector can be measured as $Q_{usfl} = mC_p(T_{out} - T_{in})$ (5)

where *m*, C_p, T_{in} and T_{out} are the mass flow rate per unit area, the specific heat at constant pressure, inlet and outlet fluid temperatures respectively.

To calculate the collector average temperature is difficult. The equation (4) may not be convenient. It is convenient to define a quantity that relates the actual useful energy gain of a collector to the useful gain if the whole collector surface is at the fluid inlet temperature. This quantity is known as "the collector heat removal factor (F_R)" and is expressed as: $F_R = \dfrac{mC_p(T_{out} - T_{in})}{A[I(\tau\alpha) - U_L(T_{in} - T_{amb})]}$ (6)

The maximum possible useful energy gain in a solar collector occurs when the whole collector is at the inlet fluid temperature. The actual useful energy gain (Q_{usfl}), is found by multiplying the collector heat removal factor (F_R) by the maximum possible useful energy gain. Thus equation (4) can be modified as follows:

$$Q_{usfl} = F_R A[I(\tau\alpha) - U_L(T_{in} - T_{amb})] \tag{7}$$

Equation (7) is known as the "**Hottel-Whillier-Bliss equation**". The heat flux per unit area of absorber surface (*q*) is now denoted as $\dfrac{Q_{usfl}}{A} = q = I\tau\alpha - U_L(T_{in} - T_{amb})$. The 3D governing equations are as follows

$$\frac{\partial u}{\partial x} + \frac{\partial v}{\partial y} + \frac{\partial w}{\partial z} = 0 \tag{8}$$

$$\rho_{nf}\left(u\frac{\partial u}{\partial x} + v\frac{\partial u}{\partial y} + w\frac{\partial u}{\partial z}\right) = -\frac{\partial p}{\partial x} + \mu_{nf}\left(\frac{\partial^2 u}{\partial x^2} + \frac{\partial^2 u}{\partial y^2} + \frac{\partial^2 u}{\partial z^2}\right) \tag{9}$$

$$\rho_{nf}\left(u\frac{\partial v}{\partial x} + v\frac{\partial v}{\partial y} + w\frac{\partial v}{\partial z}\right) = -\frac{\partial p}{\partial y} + \mu_{nf}\left(\frac{\partial^2 v}{\partial x^2} + \frac{\partial^2 v}{\partial y^2} + \frac{\partial^2 v}{\partial z^2}\right) \tag{10}$$

$$\rho_{nf}\left(u\frac{\partial w}{\partial x} + v\frac{\partial w}{\partial y} + w\frac{\partial w}{\partial z}\right) = -\frac{\partial p}{\partial z} + \mu_{nf}\left(\frac{\partial^2 w}{\partial x^2} + \frac{\partial^2 w}{\partial y^2} + \frac{\partial^2 w}{\partial z^2}\right) \tag{11}$$

$$u\frac{\partial T}{\partial x}+v\frac{\partial T}{\partial y}+w\frac{\partial T}{\partial z}=\frac{\alpha_{nf}}{\alpha_f}\frac{1}{Pr}\left(\frac{\partial^2 T}{\partial x^2}+\frac{\partial^2 T}{\partial y^2}+\frac{\partial^2 T}{\partial z^2}\right) \tag{12}$$

$$\left(\frac{\partial^2 T_a}{\partial x^2}+\frac{\partial^2 T_a}{\partial y^2}+\frac{\partial^2 T_a}{\partial z^2}\right)=0 \tag{13}$$

Here, $\alpha_{nf}=k_{nf}\big/\left(\rho C_p\right)_{nf}$ is the thermal diffusivity, $\rho_{nf}=\left(1-\phi\right)\rho_f+\phi\rho_s$ is the density, $\left(\rho C_p\right)_{nf}=\left(1-\phi\right)\left(\rho C_p\right)_f+\phi\left(\rho C_p\right)_s$ is the heat capacitance, $\mu_{nf}=\dfrac{\mu_f}{\left(1-\phi\right)^{2.5}}$ is the viscosity of Brinkman model [13], $k_{nf}=k_f\dfrac{k_s+2k_f-2\phi\left(k_f-k_s\right)}{k_s+2k_f+\phi\left(k_f-k_s\right)}$ is the thermal conductivity of Maxwell Garnett (MG) model [14] and $Pr=\dfrac{v_f}{\alpha_f}$ is the Prandtl number. The boundary conditions of the computation domain are:

at all solid boundaries of the riser pipe: $u=v=w=0$, at the solid-fluid interface: $k_f\left(\dfrac{\partial T}{\partial N}\right)_{fluid}=k_a\left(\dfrac{\partial T}{\partial N}\right)_{solid}$, at the inlet boundary of the riser pipe: $T=T_{in}$, $w=w_{in}$, at the outlet boundary: convective boundary condition $p=0$, at the top surface of the absorber: heat flux $-k_a\dfrac{\partial T_a}{\partial z}=q=I\tau\alpha-U_L\left(T_{in}-T_{amb}\right)$, at the other surfaces of absorber plate: $\dfrac{\partial T_a}{\partial N}=0$, at the outer boundary of riser pipe: $\dfrac{\partial T_a}{\partial N}=0$, at the outer boundary of bonding conductance: $\dfrac{\partial T_a}{\partial N}=0$, where N is the distances either along x or y or z directions acting normal to the surface respectively.

The average Nusselt number at the inner surface of riser pipe is $Nu=\dfrac{\iint_S \overline{Nu}\,ds}{\iint_s dS}=-\dfrac{1}{\pi DL}\dfrac{k_{nf}}{k_f}\iint_S \sqrt{\dfrac{\partial^2\theta}{\partial X^2}+\dfrac{\partial^2\theta}{\partial Y^2}+\dfrac{\partial^2\theta}{\partial Z^2}}\,ds$ where L is the height of absorber tube. The above equations are non-dimensionalized by using the following dimensionless quantities $X=\dfrac{x}{D}$, $Y=\dfrac{y}{D}$, $Z=\dfrac{z}{D}$, $\theta=\dfrac{\left(T-T_{in}\right)k_f}{qD}$. The instantaneous thermal efficiency of the collector is:

$$\eta=\frac{\text{useful gain}}{\text{available energy}}=\frac{Q_{usfl}}{AI}=\frac{F_R A\left[I\left(\tau\kappa\right)-U_L\left(T_{in}-T_{amb}\right)\right]}{AI}=F_R\left(\tau\kappa\right)-F_R U_L\frac{\left(T_{in}-T_{amb}\right)}{I}$$

3. Numerical Modeling

The Galerkin finite element method [15-16] is used to solve the non-dimensional governing equations along with boundary conditions for the considered problem. Conservation equations are solved for the finite element method to yield the velocity and temperature fields for the water flow in the absorber tube and the temperature field for the absorber plate. The equation of continuity has been used as a constraint due to mass conservation and this restriction may be used to find the pressure distribution. Then the velocity components (u, v, w) and temperatures (T, T_a) of governing equations (8-13) are expanded using a basis set. The Galerkin finite element technique yields the subsequent nonlinear residual equations. Gaussian quadrature technique is used to evaluate the integrals in these equations. The non-linear residual equations are solved using Newton–Raphson method to determine the coefficients of the expansions. The convergence of solutions is assumed when the relative error for each variable between consecutive iterations is recorded below the convergence criterion such that $\left|\psi^{n+1}-\psi^n\right|\le 1.0\mathrm{e}^{-6}$, where n is the number of iteration and Ψ is a function of any one of u, v, w, T and T_a.

3.1 Mesh Generation

The computational domains with irregular geometries by a collection of finite elements make the method a valuable practical tool for the solution of boundary value problems arising in various fields of engineering. Figure 2 displays the 3D finite element mesh of the present physical domain.
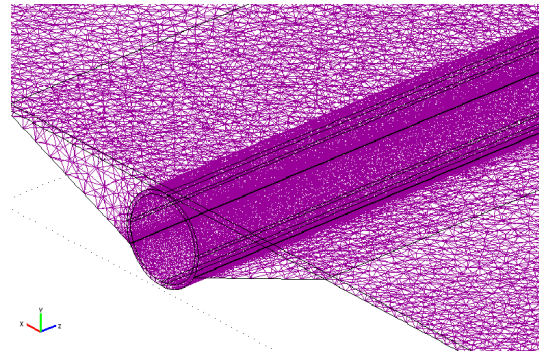

Figure 2: Finite element meshing of FPSC in 3D modeling

3.2 Grid Independent Test

The arrangement of discrete points throughout the domain is simply called a grid. Finite element method can be applied to unstructured grids. This is because the governing equations in this method are written in integral form and numerical integration can be carried out directly on the unstructured grid domain in which no coordinate transformation is required. The mesh is composed of tetrahedral element type with ten nodes in subdomain and triangular element size with six nodes in boundaries. The grid independence test is performed to check validity of the quality of mesh on the solution. There is no significant change in Nu taking element size 27,04,288 but it is time consuming. This is shown in Table 1. The computation procedure runs taking 14,20,465 elements in 3D simulation. Thermo-physical properties are shown in Table 2 according to Nasrin *et al.* [17].

Table 1: Grid Sensitivity Test at $Pr = 5.8$, $I = 215$ W/m^2, $\phi = 2\%$

Elements	4,51,098	7,26,222	14,20,465	27,04,288
Nu (Nanofluid)	2.12154	2.28451	2.433717	2.433807
Nu (Base fluid)	1.89124	2.00312	2.10124	2.10168
Time (s)	1469.587	3846.507	78381.181	99579.254

Table 2: Thermo physical properties of fluid and nanoparticles

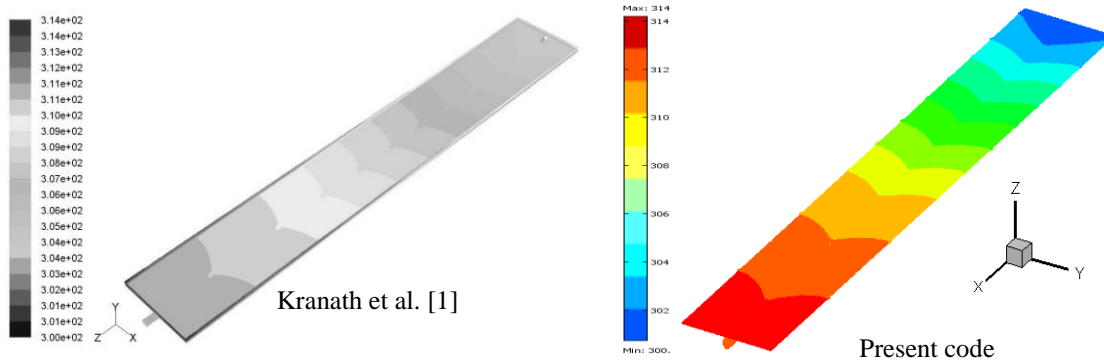| Physical Properties	Fluid phase (Water)	Cu
C_p(J/kgK)	4179	385
ρ (kg/m^3)	997.1	8933
k (W/mK)	0.613	400
$\alpha \times 107$ (m^2/s)	1.47	1163.1

3.2 Code Validation

Figure 3: Code validation of temperature contour of absorber plate

The result obtained from present numerical code is verified against the existing result available in the literature. A comparison of temperature contour plot of absorber plate is shown in figure 3 between the result using present code and Kranath et al. [1]. The numerical study is performed at $I = 800$ w/m^2, inlet velocity = 0.005 m/s, density (copper) = 8900 Kg/m^3, specific heat (copper) = 385 J/kgK, viscosity (water) = 0.000959 Kg/ms,

specific heat (water) = 4179 J/kgK, thermal conductivity (copper) = 387 W/mK and thermal conductivity (water) = 0.6 W/mK. A good agreement is observed from figure 3.

4. Results

The effect of I on the temperature interms of slice plot is presented in figure 4 for 2% concentrated water-Cu nanofluid at Pr = 5.8and mass flow rate 0.0248Kg/s. The considered values of solar irradiation are I (= 200W/m², 215W/m², 230W/m² and 250W/m²). Different colours of slices indicate different temperatures as shown in the figure. Initially at I = 200W/m², irradiation is low, temperature of nanofluid at the outlet edge is low. Colour indicates the probable value of nanofluid temperature. The strength of the thermal current activities is much more activated with escalating I. Slices illustrate that solar irradiation dominant effect plays a critical role on larger heat flow from absorber walls to the passing fluid through the riser pipe. In the temperature distribution of slice plot for different values of solar irradiation shows that absorber temperature as well as nanofluid outlet temperature increases with rising values of I. The values of temperature in slice plots are given in Kelvin unit.
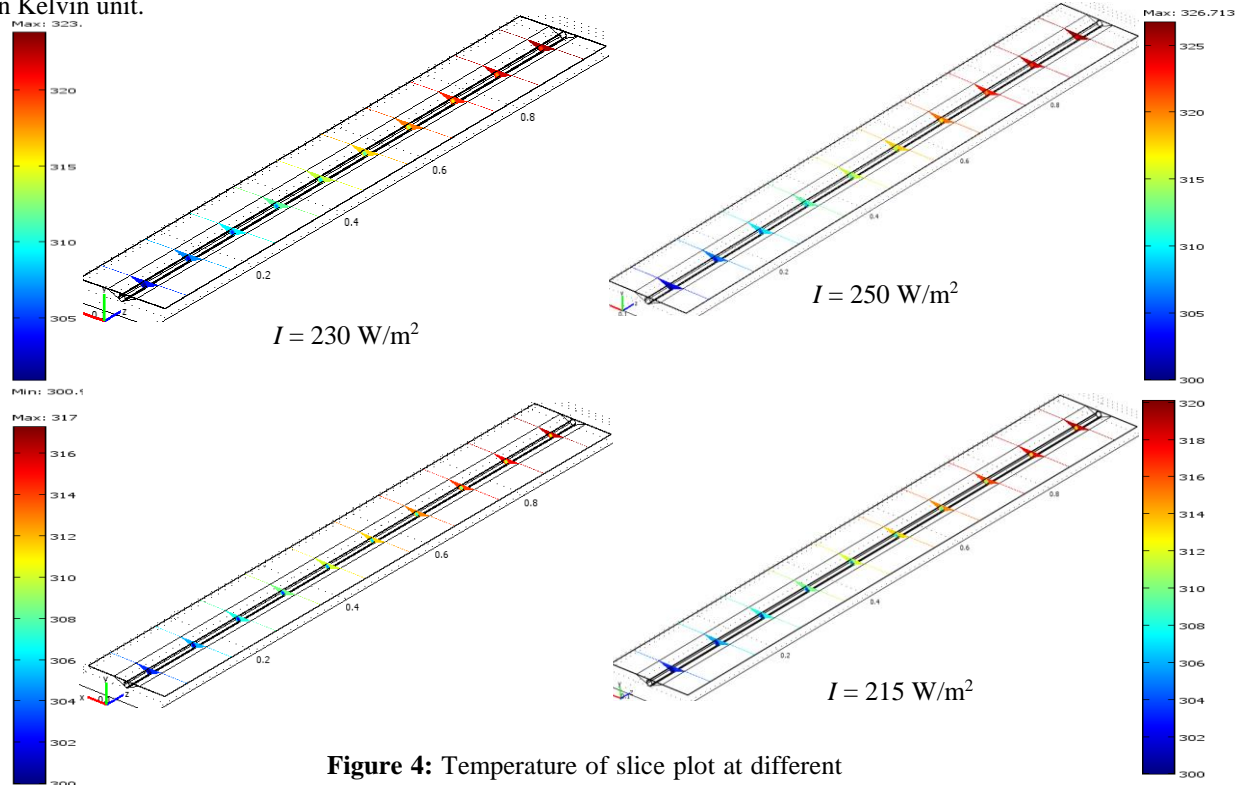

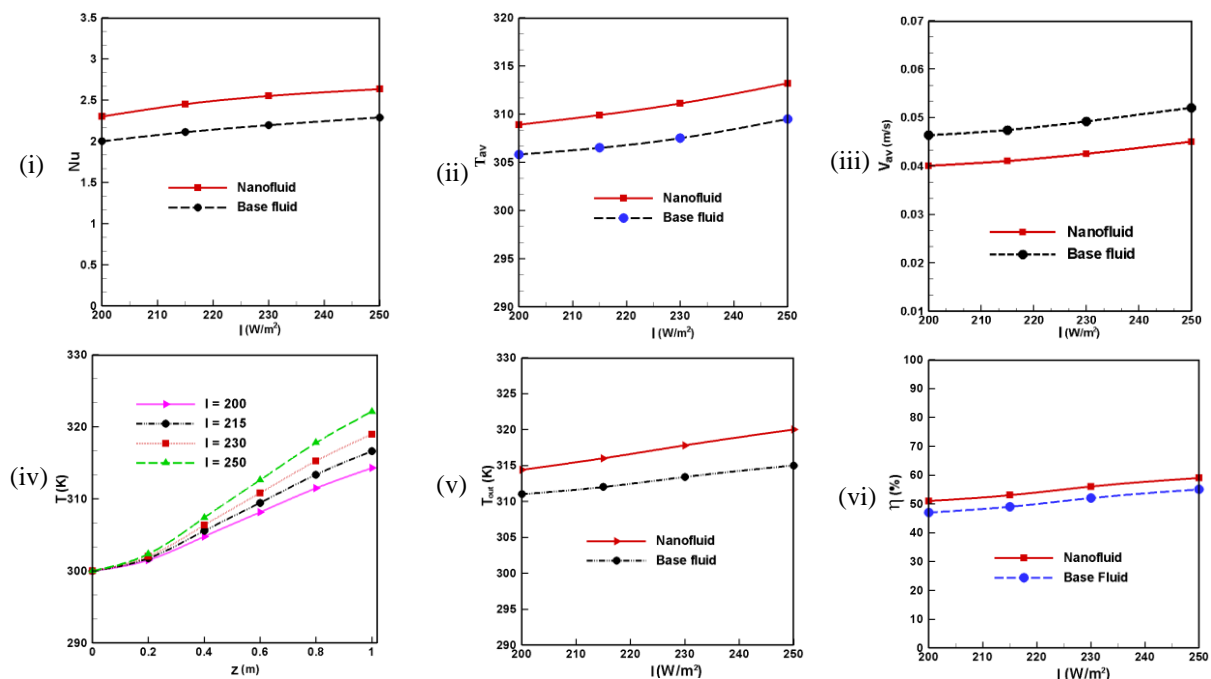**Figure 4:** Temperature of slice plot at different

Figure 5: Effect of I on (i) mean Nusselt number, (ii) mean temperature, (iii) mean velocity, (iv) mid-height temperature, (v) mean output temperature and (vi) collector efficiency

5

Figure 5(i)-(vi) expresses the *Nu-I*, T_{av}-*I*, V_{av}-*I*, mid-height temperature of nanofluid, T_{out}-*I* and η-*I* profiles of fluids through a FPSC. The average Nusselt number increases with mounting solar irradiation (*I*). The rate of radiative heat transfer performance enhances 14% and 10% using water-alumina nanofluid and water respectively for rising solar irradiation from 200W/m^2 to 250W/m^2. It is seen from the figure 5(ii) that T_{av} rises sequentially for growing *I*. It is well known that higher values of solar irradiation (*I*) indicate higher temperature of fluids. Due to escalating values of *I* the absorber as well as the riser pipe becomes more heated. As a result fluids can take more heat from hot walls and become hotter. Here base fluid has lower mean temperature than the water-Cu nanofluid. Magnitude of average subdomain velocity (V_{av}) has noteworthy changes with different values of solar irradiation (*I*). It rises consecutively for growing *I*. Clear water has higher velocity than water-copper nanofluid with 2% solid volume fraction. The temperature water-Cu nanofluid at the middle of the riser pipe is depicted in figure 5(iv). The fluid enters from the left inlet and takes heat form solid surfaces of the riser pipe and finally exits from the right outlet of a FPSC. The temperature increases with growing *I*. From the figure 5(v) it is observed that the inlet temperature of fluid is maintained at 300K and then it increases gradually with the contact of heated solid boundaries of the riser pipe. And finally the mean output temperature of nanofluid becomes 314K, 316K, 318K, 320K and water becomes 311K, 312K, 314K, 316K for I = 200 W/m^2, 215 W/m^2, 230 W/m^2 and 250 W/m^2 respectively. By introducing greater solar irradiation (*I*) the collector efficiency increases. More solar irradiance is able to augment heat transfer system through the riser pipe of a FPSC. In this scheme water/copper nanofluid (ϕ = 2%) performs better than clear water (ϕ = 0%). Thermal efficiency enhances from 51%-59% for nanofluid and 47%-55% for water.

5. Conclusion

The 3D numerical study addresses the heat transfer by water/copper nanofluid as well as base fluid through the riser pipe of a FPSC. Solar irradiation has considerable effect on the flow and temperature field. Stronger solar radiation grows up the heat transfer rate, mean outlet temperatureand the thermal efficiency of the FPSC. The mid height temperature of nanofluid increase steadily while passing through the riser pipe for all values of solar radiation. Average velocity is lower for nanofluid than base fluid.

6. Acknowledgement

7. References

[1] K.V. Karanth, M.S. Manjunath, N.Y. Sharma, Numerical simulation of a solar flat plate collector using discrete transfer radiation model (DTRM) – a CFD approach, *Proc. of the World Cong. on Engg.*, London, U.K., III, 2011.

[2] OA. Bég, A. Bakier, R. Prasad, SK. Ghosh, Numerical modelling of non-similar mixed convection heat and species transfer along an inclined solar energy collector surface with cross diffusion effects*, World J. of Mech.*, Vol. 1, pp. 185-196, 2011.

[3] M.S. Manjunath, K.V. Karanth, N.Y. Sharma, A comparative CFD study on solar dimple plate collector with flat plate collector to augment the thermal performance, *World Academy of Sci., Engg. and Tech.*, Vol. 6, pp. 10-21, 2012.

[4] J. Vestlund, Gas-filled flat plate solar collector, *Ph. D. Thesis*, Building Services Engg., Dept. of Energy and Environ., Chalmers University of Technology, Gothenburg, Sweden, 2012.

[5] P.W. Ingle, A.A. Pawar, B.D. Deshmukh, K.C. Bhosale, CFD analysis of solar flat plate collector, *Int. J. of Emerg. Techn. and Adv. Engg.*, Vol. 3, No. 4, pp. 337-342, 2013.

[6] S. Basavanna and K.S. Shashishekar, CFD analysis of triangular absorber tube of a solar flat plate collector, *Int. J. Mech. Eng. & Rob. Res.*, Vol. 2, No. 1, pp. 19-24, 2013.

[7] I.A. Tagliafico, F. Scarpa, M.D. Rosa, Dynamic thermal models and CFD analysis for flat-plate thermal solar collectors – a review, *Renew. and Sust. Energy Rev.*, Vol. 2, No. 30, pp. 526-537, 2014.

[8] F. Struckmann, Analysis of a flat-plate solar collector, *Project Report 2008 MVK160 Heat and Mass Transport*, 2008, Lund, Sweden.

[9] Soteris A. Kalogirou, Solar thermal collectors and applications, *Progress in Energy and Combustion Science*, Vol. 30, pp. 231–295, 2004.

[10] R. Nasrin and M.A. Alim, Finite element simulation of forced convection in a flat plate solar collector: Influence of nanofluid with double nanoparticles, J. of Appl. Fluid Mech., Vol. 7, No. 3, pp.543-557, 2014.

[11] R. Nasrin and M.A. Alim, Semi-empirical relation for forced convective analysis through a solar collector, *Solar Energy*, Vol. 105, pp. 455-467, 2014.

[12] R. Nasrin and M.A. Alim, Performance of nanofluids on heat transfer in a wavy solar collector, *Int. J. of Engg., Sci. & Tech.*, Vol. 5, No. 3, pp. 58-77, 2013.

[13] HC. Brinkman, The viscosity of concentrated suspensions and solution, *J. Chem. Phys.*, Vol. 20, pp. 571-581, 1952.

[14] J.C. Maxwell-Garnett, Colours in metal glasses and in metallic films, *Philos. Trans. Roy. Soc. A*, Vol. 203, pp. 385–420, 1904.

[15] C. Taylor, P. Hood, A numerical solution of the Navier-Stokes equations using finite element technique, *Computer and Fluids*, Vol. 1, pp. 73–89, 1973.

[16] P. Dechaumphai, Finite element method in engineering, *2nd ed.*, Chulalongkorn University Press, Bangkok, 1999.

[17] R. Nasrin, S. Parvin and M.A. Alim, Heat transfer and collector efficiency through direct absorption solar collector with radiative heat flux effect, *Numerical Heat Transfer, Part A- Application*, Vol. 68, No. 8, pp. 887-905, 2015.

Paper ID: TE-12

Natural convection in a nanofluid filled prismatic cavity with non-isothermal bottom wall

Salma Parvin [1]*, Rehena Nasrin [1] and Raju Chowdhury [1,2]

[1] Department of Mathematics, Bangladesh University of Engineering & Technology,Dhaka-1000, Bangladesh,

[2]Department of Natural Science, Stamford University Bangladesh, Dhaka-1209, Bangladesh.

*E-mail:salpar@math.buet.ac.bd

Abstract

The present paper executes the natural convection flow and heat transfer inside a prismatic enclosure with non-uniform temperature distribution maintained at the bottom wall. The water-Al_2O_3 nanofluid is used as the heat transfer medium through the enclosure. Finite Element Method of Galerkin's weighted residual scheme is used to solve the transport equations with appropriate boundary conditions. Computations are done for various Rayleigh number Ra (10^3 to 10^6) for nanofluid as well as for the base fluid. Isotherms, streamlines and heat lines, local and average heat transfer are presented graphically. Results show that nanofluid gives the higher transfer rate than that of the base fluid for all the considered Ra values.

Keywords: Natural convection; finite element method; heatline, nanofluid; prismatic enclosure; non isothermal wall.

1. Introduction

Natural convection in enclosures finds its applications in geophysics, geothermal reservoirs, insulation of building, heat exchanger design, building structure etc. that motivates many researchers to perform numerical simulation to investigate the flow pattern, temperature distribution, and heat flow. The low thermal conductivity of conventional heat transfer fluids, commonly water, has restricted designers. Fluids containing nanosized solid particles offer a possible solution to conquest this problem. Most of the available literature on this topic concerns regular geometries such as rectangular or square enclosures, while actual applications demand the consideration of irregular shapes. Literature reviews on natural convection inside triangular, trapezoidal and rhombic enclosures are available in [1-5].

The heat recovery system or true path of convective heat transfer can be visualized by 'heatline' method. Heatlines represent heatflux lines which represent the trajectory of heat flow in the system and they are normal to the isotherms for conductive heat transfer. Kimura and Bejan [6] and Bejan [7] first introduced the concept of heatline. Various applications using heatlines were studied in [8-14]. Dalal and Das [15] have used heatline method for the visualization of flow in a complicated cavity. Recently, Yaseen [16] has studied and analyzed numerically the steady natural convection flow in a prismatic enclosure with strip heater on bottom wall. Recently Ahmed et.al [17] performed numerical analysis for natural convection flows within prismatic enclosures based on heatline approach.

Heat transfer in cavities filled with nanofluid is the research interest of many researchers. Parvin et al. [18] studied the natural convection heat transfer in an enclosure with a heated body filled with nanofluid. Nasrin and Parvin [19] investigated numerically the buoyancy-driven flow and heat transfer in a trapezoidal cavity filled with water–Cu nanofluid. In their work, a correlation is developed graphically for the average Nusselt number as a function of the Prandtl number as well as the cavity aspect ratio. Abu- Nada and Chamkha [20] performed a numerical study of natural convection heat transfer in a differentially heated enclosure filled with CuO-EG-Water nanofluid. Heat Transfer and Entropy Generation in an Odd-shaped Cavity filled with Nanofluid is analyzed by Parvin and Chamkha [21]. It must be noticed that, adding nanoparticles into the base fluid does not always increase its thermal conductivity [22]. Parvin et al. [23] numerically investigated the natural convection heat transfer from a heated cylinder contained in a square enclosure filled with water–Cu nanofluid. Their results indicated that heat transfer augmentation is possible using highly viscous nanofluid.

The above literature contains many investigations into the heat transfer performance of natural convection of nanofluid in regular shaped cavities. However, a comprehensive analysis on heat flow during natural convection cooling by nanofluid in irregular enclosure with the heatline approach is yet to appear in the literature. Accordingly, the present study performs a numerical investigation into the natural convection heat flow within a prism shaped cavity containing nanofluid with non isothermal bottom wall. The study focuses specifically on the effects of the free convective parameter on the streamlines, isotherm distribution, heatlines and average Nusselt number for nanofluid as well as water.

2. Governing Equations

The physical domain is shown in Fig. 1. Under the Boussinesq approximation, the governing equations for steady two dimensional laminar incompressible flows in dimensionless form are:

$$\frac{\partial U}{\partial X} + \frac{\partial V}{\partial Y} = 0 \tag{1}$$

$$U\frac{\partial U}{\partial X} + V\frac{\partial U}{\partial Y} = -\frac{\rho_f}{\rho_{nf}}\frac{\partial P}{\partial X} + Pr\frac{v_{nf}}{v_f}\left(\frac{\partial^2 U}{\partial X^2} + \frac{\partial^2 U}{\partial Y^2}\right) \tag{2}$$

$$U\frac{\partial V}{\partial X} + V\frac{\partial V}{\partial Y} = -\frac{\rho_f}{\rho_{nf}}\frac{\partial P}{\partial Y} + Pr\frac{v_{nf}}{v_f}\left(\frac{\partial^2 V}{\partial X^2} + \frac{\partial^2 V}{\partial Y^2}\right) + Ra\,Pr\frac{(1-\chi)\rho_f\beta_f + \chi\rho_s\beta_s}{\rho_{nf}\beta_f}\theta \tag{3}$$

$$U\frac{\partial \theta}{\partial X} + V\frac{\partial \theta}{\partial Y} = \frac{\alpha_{nf}}{\alpha_f}\left(\frac{\partial^2 \theta}{\partial X^2} + \frac{\partial^2 \theta}{\partial Y^2}\right) \tag{4}$$

where, $\rho_{nf} = (1-\chi)\rho_f + \chi\rho_s$ is the density, $(\rho C_p)_{nf} = (1-\chi)(\rho C_p)_f + \chi(\rho C_p)_s$ is the heat capacitance, $\beta_{nf} = (1-\chi)\beta_f + \chi\beta_s$ is the thermal expansion coefficient, $\alpha_{nf} = k_{nf}/(\rho C_p)_{nf}$ is the thermal diffusivity, $\mu_{nf} = \mu_f(1-\chi)^{-2.5}$ is dynamic viscosity and $k_{nf} = k_f\dfrac{k_s + 2k_f - 2\chi(k_f - k_s)}{k_s + 2k_f + \chi(k_f - k_s)}$ is the thermal conductivity of the

nanofluid and $X = \dfrac{x}{L}$, $Y = \dfrac{y}{L}$, $U = \dfrac{uL}{\alpha}$, $V = \dfrac{vL}{\alpha}$, $\theta = \dfrac{T - T_c}{T_h - T_c}$, $P = \dfrac{pL^2}{\rho\alpha^2}$, $Pr = \dfrac{v}{\alpha}$, $Ra = \dfrac{g\beta(T_h - T_c)L^3\,Pr}{v^2}$
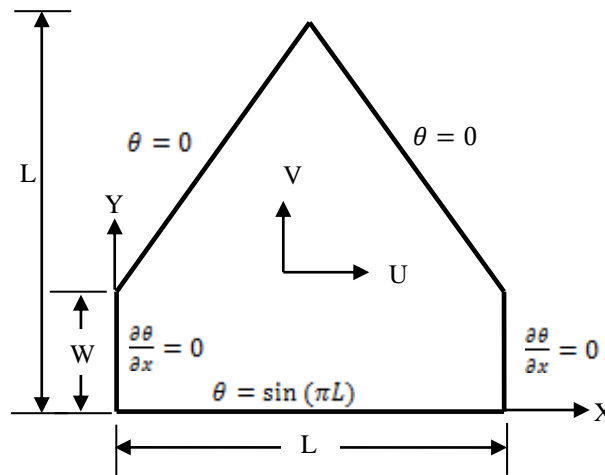

Fig.1: Schematic diagram of the physical system

The boundary conditions can be summarized by the following equations:
- At the bottom wall: $U = 0, V = 0, \theta = \sin(\pi L)$
- For the side walls: $U = 0, V = 0, \dfrac{\partial \theta}{\partial X} = 0$
- For the inclined walls: $U = 0, V = 0, \theta = 0$

The relationships between streamfunction ψ and velocity components U, V for two-dimensional flows are

$$U = \frac{\partial \psi}{\partial Y} \text{ and } V = -\frac{\partial \psi}{\partial X} \quad \text{which give a single equation } \frac{\partial^2 \psi}{\partial X^2} + \frac{\partial^2 \psi}{\partial Y^2} = \frac{\partial U}{\partial Y} - \frac{\partial V}{\partial X} \tag{5}$$

The no-slip condition is valid at all boundaries as there is no cross-flow. Hence $\psi = 0$ is used for boundaries. The heat flow within the enclosure is displayed using the heatfunction Π obtained from conductive heat fluxes $\left(-\dfrac{\partial \theta}{\partial X}, -\dfrac{\partial \theta}{\partial Y}\right)$ as well as convective heat fluxes ($U\theta$, $V\theta$). The heatfunction satisfies the steady energy balance equation such that $\dfrac{\partial \Pi}{\partial Y} = U\theta - \dfrac{\partial \theta}{\partial X}$ and $-\dfrac{\partial \Pi}{\partial X} = V\theta - \dfrac{\partial \theta}{\partial Y}$ which yield a single equation

$$\frac{\partial^2 \Pi}{\partial X^2} + \frac{\partial^2 \Pi}{\partial Y^2} = \frac{\partial}{\partial Y}(U\theta) - \frac{\partial}{\partial X}(V\theta) \tag{6}$$

The local and average Nusselt number may be expressed as $Nu_{local} = -\left(\dfrac{k_{nf}}{k_f}\right)\dfrac{\partial \theta}{\partial N}$ and

$Nu = -\dfrac{1}{S}\displaystyle\int_0^S \left(\dfrac{k_{nf}}{k_f}\right)\dfrac{\partial \theta}{\partial N}\, dN$ where S is the non-dimensional length of the surface.

3. Numerical Method

The numerical procedure used in this study is based on the Galerkin weighted residual method of finite element. The solution domain is discretized into finite element meshes, which are composed of non- uniform triangular elements. Then the nonlinear governing partial differential equations are transferred into a system of integral equations by applying Galerkin weighted residual method. The integration involved in each term of these equations is performed by using Gauss's quadrature method. The nonlinear algebraic equations so obtained are modified by imposition of boundary conditions. These modified nonlinear equations are transferred into linear algebraic equations by using Newton's method. Finally, these linear equations are solved by using Triangular Factorization method. The convergence criterion set to be $\left|\psi^{n+1} - \psi^n\right| \leq 10^{-4}$, where n is the number of iteration and ψ is a function U, V and θ.

3.1 Grid Independent Test

An extensive mesh testing procedure is conducted to guarantee a grid-independent solution for $Ra = 10^5$ and $Pr = 6.2$, $\chi = 0$ in a prismatic enclosure. Five different non-uniform grid systems with the following number of elements within the resolution field: 454, 926, 1504, 2270 and 9948 are examined. The numerical scheme is carried out for highly precise key in the average Nusselt (Nu) number to understand the grid fineness as shown in Fig. 2. The scale of the average Nusselt numbers for 2270 elements shows a little difference with the results obtained for the other elements. Hence, considering the non-uniform grid system of 2270 elements is preferred for the computation.
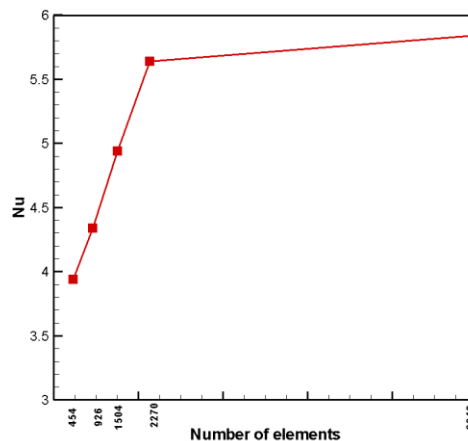

Fig. 2 Grid independent test

4. Result and Discussion

The numerical computation has been carried out through the finite element method to analyze natural convection within a nanofluid filled prismatic enclosure based on heatline concept. Results of isotherms, streamlines and heatlines for various values of Rayleigh number Ra (= 10^3 to 10^6) with Prandtl number $Pr = 6.2$ for both nanofluid and base fluid in the prismatic enclosure are displayed. The Al_2O_3 nanoparticle volume fraction χ is chosen as 5%. In addition, the values of local and average Nusselt number at the bottom have been calculated for the mentioned parameter.

4.1 Effect on Isotherms

The influence of Rayleigh number Ra on isotherms for the present configuration has been demonstrated in Fig. 3(a). The pattern of isotherms is smooth for low Ra and is symmetric to the central vertical line for all the considered values of Ra. At higher Rayleigh number, a thermal plume rises from the middle of the bottom wall because of sinusoidal boundary temperature. The isothermal lines for pure water are more distorted than that of nanofluid.

4.2 Effect on Streamlines

Streamlines corresponding to different Rayleigh number Ra are shown in Fig. 3(b). It is seen from the figure that the trend of streamlines are similar for all cases. There are two symmetric circulation cells formed inside the enclosure. With the increasing value of the Ra, the streamlines are less dense near the central vertical line. It is noteworthy to mention that the central cores of the circulatory cells increase in size for higher values of Ra indicate the greater strength of the flow. Higher flow intensity is seen for the base fluid in comparison to the nanofluid.
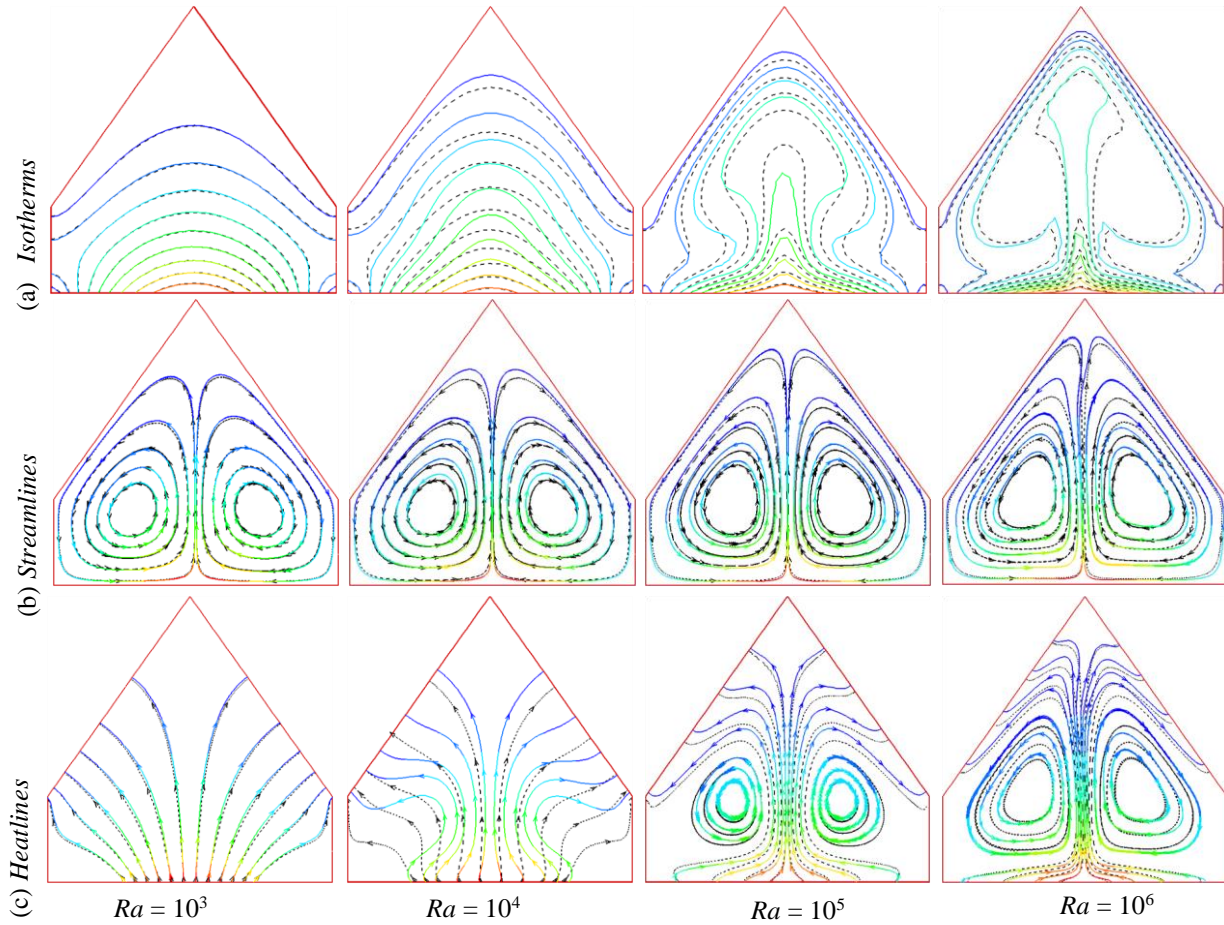

Fig. 3. Effect of Rayleigh number Ra on (a) isothems (b) streamlines and (c) heatlines for base fluid (solid colored lines) and nanodluid (dashed black lines)

4.3 Effect on Heatlines

The heatlines are constructed based on the thermal boundary conditions. As seen from the Fig. 3(c), the heatlines are similar to streamlines at the core signifying convective heat flow and a large amount of heat flow occurs from the middle portion of the bottom wall as seen from dense heatlines. The two heat circulations in the system are observed and a very intense heat flow occurs across the middle of the cavity represented by dense heatline for large Rayleigh number. It is interesting to observe that heat transport in a large regime at the core is due to strong natural convection. The large regime of convection is due to the large amount of heat transport from the bottom wall associated with large intensity of circulations. At Ra = 10^3, heat transfer occur mainly by conduction where, heatlines are perpendicular to the isotherms. Laminar patterns of heatlines are slightly disturbed for Ra = 10^6.

4.4 Local and Average Nusselt number

Fig. 4(a)-(c) shows the distribution of the local and average Nusselt number of the bottom wall versus the Rayleigh number Ra for nanofluid and water. Fig 4(a) and 4(b) present the local heat transfer rate for base fluid and nanofluid respectively. General observation is that the Nusselt number increases sharply for dominant natural convection region ($Ra > 10^4$) for both the fluids. Similar trend of local and average heat transfer rate is seen for both the fluid where as nanofluid shows the higher heat transfer rate. That is adding nanoparticles increases the thermal conductivity which leads to enhanced heat transfer.
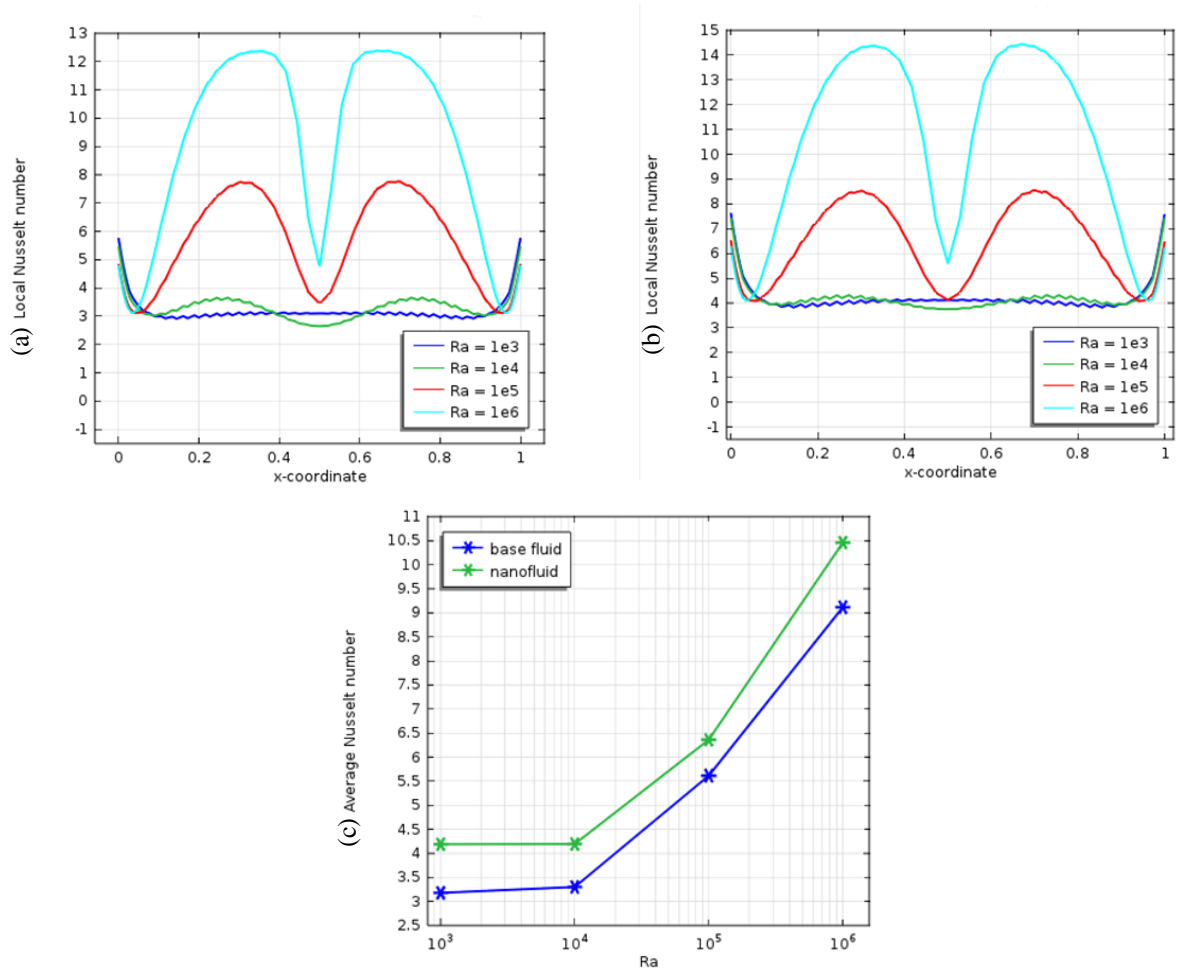
Fig. 4. Effect of Rayleigh number Ra on (a) local Nusselt number for base fluid (b) local Nusselt number for nanofluid and (c) average Nusselt number

5. Conclusion

The current investigation performed a physical as well as computational insight due to heatflow for natural convection within a prismatic enclosure filled with nanofluid. The major conclusions are the following:

- Isotherms, streamlines and heatlines are found to be smooth and the heatlines are seen normal to the isotherm during the lower convection regime.
- For higher Rayleigh number, heat transfer and flow strength increases and heatlines take the flow pattern.
- for nanofluid, heat transfer becomes higher than that of base fluid.

6. Acknowledgement

7. References

[1] T. Basak, G. Arvind and S. Roy, Visualization of heat flow due to natural convection within triangular cavities using Bejan's heatline concept, *Int. J. Heat Mass Transfer*, vol. 52 (11-12), pp. 2824-2833, 2009.

[2] T. Basak, S. Roy, D. Ramakrishna and I. Pop, Visualization of Heat Transport during Natural Convection Within Porous Triangular Cavities via Heatline Approach, *Numerical Heat Transfer, Part A*, vol. 57 (6), pp. 431-452, 2010.

[3] T. Basak, S. Roy and I. Pop, Heat flow analysis for natural convection within trapezoidal enclosures based on heatline

concept, *Int. J. Heat Mass Transfer*, vol. 52 (11-12), pp. 2471–2483, 2009.

[4] R. Anandalakshmi and T. Basak, Heatline based thermal management for natural convection in porous rhombic enclosures with isothermal hot side or bottom wall, *Energy Conversion and Management*, vol. 67, pp. 287–296, 2013.

[5] T. Basak, S. Roy and I. Pop, Heat flow analysis for natural convection within trapezoidal enclosures based on heatline concept, *Int. J. Heat Mass Transfer*, vol. 52, pp. 2471–2483, 2009.

[6] S. Kimura and A. Bejan, The heatline visualization of convective heat-transfer, *ASME J. Heat Transfer*, vol. 105 (4), pp. 916–919, 1983.

[7] Bejan, Convection Heat Transfer, third ed., *Wiley*, Hoboken, NJU, 1984.

[8] F.L. Bello-Ochende, A heat function formulation for thermal convection in a square cavity, *Int. Commun. Heat Mass Transfer*, vol. 15, pp. 193–202, 1988.

[9] V.A.F. Costa, Heatline and massline visualization of laminar natural convection boundary layers near a vertical wall, *Int. J. Heat Mass Transfer*, vol. 43 (20), pp. 3765–3774, 2000.

[10] V.A.F. Costa, Unified streamline, heatline and massline methods for the visualization of two-dimensional heat and mass transfer in anisotropic media, *Int. J. Heat Mass Transfer*, vol. 46 (8), pp. 1309–1320, 2003.

[11] V.A.F. Costa, Bejan's heatlines and masslines for convection visualization and analysis, *Appl. Mech. Rev.*, vol. 59 (3), pp. 126–145, 2006.

[12] Mukhopadhyay, X. Qin, S.K. Aggarwal and I.K. Puri, On extension of heatline and massline concepts to reacting flows through use of conserved scalars, *ASME J. Heat Transfer*, vol. 124 (4), pp. 791–799, 2002.

[13] Mukhopadhyay, X. Qin, S.K. Aggarwal and I.K. Puri, Visualization of scalar transport in non-reacting and reacting jets through a unified ''heatline'' and ''massline'' formulation, *Numer. Heat Transfer, Part A*, vol. 44 (7), pp. 683–704, 2003.

[14] Q.H. Deng and G.F. Tang, Numerical visualization of mass and heat transport for conjugate natural convection/heat conduction by streamline and heatline, *Int. J. Heat Mass Transfer*, vol. 45 (11), pp. 2373–2385, 2002.

[15] Dalal and M.K. Das, Heatline method for the visualization of natural convection in a complicated cavity, *Int. J. Heat Mass Transfer*, vol. 51 (1-2), pp. 263-272, 2008.

[16] S. J. Yaseen, Numerical study of steady natural convection flow in a prismatic enclosure with strip heater on bottom wall using FLEXPDE, *Diyala Journal of Engineering Sciences*, vol. 7 (1), pp. 61-80, 2014.

[17] K. F. U. Ahmed, S. Parvin and Ali J. Chamkha, Numerical analysis based on heatline approach for natural convection flows within prismatic enclosures, *Int. J. Energy & Technology* Vol. 7 (2), pp. 19-29, 2015

[18] S. Parvin, K.F.U. Ahmed, M.A. Alim and N.F. Hossain , Heat transfer enhancement by nanofluid in a cavity containing a heated obstacle, *Int. J. Mechanical and Materials Eng.(IJMME)*, 7 (2) pp. 128-135, 2012.

[19] Rehena Nasrin, Salma Parvin, Investigation of buoyancy-driven flow and heat transfer in a trapezoidal cavity filled with water–Cu nanofluid, *Int. Commun. Heat Mass Transfer* 39 (1) pp. 270–274, 2012.

[20] E. Abu-Nada and A. J. Chamkha, Effect of nanofluid variable properties on natural convection in enclosures filled with a CuO-EG-Water nanofluid, *Int. J. Therm. Sci.* 49 pp. 2339-2352, 2010.

[21] Salma Parvin and A.J. Chamkha, An Analysis on Free Convection Flow, Heat Transfer and Entropy Generation in an Odd-shaped Cavity filled with Nanofluid, *Int. Commun. Heat Mass Transfer* 54 pp. 8–17, 2014.

[22] S. Teja, M. P. Beck, Y. Yuan and P. Warrier, The limiting behavior of the thermal conductivity of nanoparticles and nanofluids, *J. Applied Physics*, 107 pp. 114319, 2010.

[23] Salma Parvin, M.A. Alim, N.F. Hossain, Prandtl number effect on cooling performance of a heated cylinder in an enclosure filled with nanofluid, *Int. Commun. Heat Mass Transfer*. 39, pp. 1220–1225, 2012.

Nomenclature

C_p	specific heat [Jkg^{-1}K^{-1}]	U, V	dimensionless velocity components
g	acceleration due to gravity [ms^{-2}]	x, y	distance along x- and y- coordinates
k	thermal conductivity [Wm^{-1}K^{-1}]	X, Y	dimensionless distance along x- and y- coordinates
L	length of the base and height [m]		**Greek symbols**
Nu	Nusselt number	α	thermal diffusivity [ms^{-2}]
p	dimensional pressure [*Pa*]	v	kinematic viscosity of the fluid[m^{2}s^{-1}]
P	dimensionless pressure	θ	dimensionless temperature
Pr	Prandtl number	χ	nanoparticle volume fraction
Ra	Rayleigh number	ρ	density [kgm^{-3}]
T	temperature [K]	ψ	Stream function
u, v	velocity components [ms^{-1}]	Π	heatfunction

Paper ID: TE-13

Study of Free Convection Heat and Mass Transfer about a Semi-Infinite Vertical Plate with Heat Absorption and Chemical Reaction in Presence of Magnetic Field

M. S. Alam[1]*, M. Ali[2], K. A. Rahman[3]

[1,3]Chittagong University of Engineering and Technology (CUET), Chittagong-4349, Bangladesh
[2]Bangladesh University of Engineering and Technology (BUET), Dhaka-4349, Bangladesh
[1,*]E-mail: shahalammaths@gmail.com, [2]E-mail: ali.mehidi93@gmail.com, [3]E-mail: afzalur99@yahoo.com

Abstract

An analysis is performed to study the free convection heat and mass transfer flow of an electrically conducting incompressible viscous fluid about a semi-infinite vertical plate under the action of heat absorption, chemical reaction in presence of magnetic field with constant heat flux. The effects of magnetic parameter, Prandtl number, Schmidt number, heat absorption parameter and chemical reaction parameter on velocity, temperature and concentration profiles are discussed numerically and shown graphically. Therefore, the results of velocity field increases for increasing values of Prandtl number and chemical reaction parameter but other parameters decrease the velocity profile of the fluid flow. The temperature field decreases in the presence of magnetic parameter and Prandtl number but other parameters increase the temperature profile of the fluid flow. Also, the concentration profile decreases for increasing the values of magnetic parameter, reaction parameter and Schmidt number but there is no effect on concentration profile for heat absorption parameter. To verify the validity and accuracy of the present numerical results for the skin friction coefficient $f''(0)$ and the local Sherwood number $\left[-\varphi'(0)\right]$ are compared with results of Ahmed A. Afify [11] in absence of heat absorption and found to be in very good agreement.

Keywords: MHD, Heat absorption, Chemical reaction, Constant heat flux.

1. Introduction

The boundary layer flow of heat and mass transfer with chemical reaction has a great practical important to engineers and scientist because of its universal occurrence in many branches of science and engineering. Specially, it has a considerable importance in chemical and hydro mathematical industries. In many chemical processes, a chemical reaction occurs between a foreign mass and a fluid in which a plate is moving. These processes has numerous applications such as polymer production, manufacturing of ceramics or glassware and food processing. In recent years, MHD flow problems have become more important industrially. Indeed, MHD laminar boundary layer behavior over a stretching surface is a significant type of flow having considerable practical applications in chemical engineering, electrochemistry and polymer processing. This problem has also an important bearing on metallurgy where magnetohydrodynamic (MHD) techniques have recently been used. In this regard, Sonth *et al*. [1] discussed heat and mass transfer in a visco-elastic fluid flow over an accelerating surface with heat source/sink and viscous dissipation, Tan *et al*. [2] studied heat and mass transfer over an impermeable stretching plate and Sing [3] studied the heat and mass transfer in MHD boundary layer flow past an inclined plate with viscous dissipation in porous medium. The effect of chemical reaction on free-convective flow and mass transfer of a viscous, incompressible and electrically conducting fluid over a stretching sheet was investigated by Afify [4] in the presence of transverse magnetic field. Cortell [5] studied the magneto hydrodynamics flow of a power-law fluid over a stretching sheet. Abel and Mahesh [6] presented an analytical and numerical solution for heat transfer in a steady laminar flow of an incompressible viscoelastic fluid over a stretching sheet with power-law surface temperature, including the effects of variable thermal conductivity and non-uniform heat source and radiation. Iskak *et al*. [7] discussed heat transfer analysis for mixed convection flow through a vertical stretching sheet, Ali *et al*. [8] have analyzed the MHD viscos flow of heat transfer over a permeable shrinking sheet with surface heat flux, Iskak *et al*. [9] also analyzed the heat transfer of unsteady mixed convection flow over vertical stretching sheet, Rajesh [10] have studied the MHD effects on free convection and mass transform flow through a porous medium with variable temperature. Since the study of heat and mass transfer is important in many cases, in the present paper we studied the free convection heat and

mass transfer about a semi-infinite vertical plate with heat absorption and chemical reaction in presence of magnetic field. The boundary layer equations are transformed by a similarity transformation into a system of coupled non-linear ordinary differential equations and which are solved numerically by shooting iteration technique along with Runge- Kutta sixth order method. The study extends the work of Ahmed A. Afify [11] by considering heat absorption effects. Finally, the numerical values of the skin friction and concentration gradient are also shown in a tabular form.

2. Governing Equations of the Present Problem

Consider a two dimensional steady laminar MHD viscous incompressible electrically conducting fluid along a vertical plate. A magnetic field of strength B_0 is introduced to the normal to the direction to the flow. The uniform plate temperature T_w $(>T\infty)$, where T_∞ is the temperature of the fluid far away from the plate. Let u and v be the velocity components along the x and y axis respectively in the boundary layer region. Under the above assumptions and usual boundary layer approximation, the dimensional governing equations of continuity, momentum, concentration and energy under the influence of externally imposed magnetic field are [2]:

Equation of continuity:

$$\frac{\partial u}{\partial x} + \frac{\partial v}{\partial y} = 0 \tag{1}$$

Momentum equation:

$$u\frac{\partial u}{\partial x} + v\frac{\partial u}{\partial y} = v\frac{\partial^2 u}{\partial y^2} + g\beta(T - T_\infty) + g\beta^*(C - C_\infty) - \frac{\sigma B_0^2}{\rho}u \tag{2}$$

Energy Equation:

$$u\frac{\partial T}{\partial x} + v\frac{\partial T}{\partial y} = \frac{\kappa}{\rho c_p}\frac{\partial^2 T}{\partial y^2} + Q^*(C - C_\infty) \tag{3}$$

Concentration Equation:

$$u\frac{\partial C}{\partial x} + v\frac{\partial C}{\partial y} = D_m\frac{\partial^2 C}{\partial y^2} - \lambda^*(C - C_\infty) \tag{4}$$

Boundary conditions are:

$$u = ax, \ v = 0, \frac{\partial T}{\partial y} = -\frac{q}{\kappa}, C = C_w \quad at \ y = 0 \ and \ u = 0, T = T_\infty, C = C_\infty \ as \ y \to \infty$$

where u and v are the velocity components along x and y directions, T, T_w and T_∞ are the fluid temperature, the plate temperature and the free stream temperature respectively while C, C_w and C_∞ are the corresponding concentrations, a is the constant, κ is the thermal conductivity, λ^* is the reaction rate constant, Q^* is the heat absorption rate constant, q is the heat flux, C_p specific heat with constant pressure, v is the kinematic viscosity , σ is the electrical conductivity, ρ is the fluid density, β is the thermal expansion coefficient, β^* is the concentration expansion coefficient, B_0 is the magnetic field intensity, g is the acceleration due to gravity, D_m is the coefficient of mass diffusivity respectively. We introduce the steam function $\psi(x,y)$ as defined by $u = \frac{\partial \psi}{\partial y}$ and $v = -\frac{\partial \psi}{\partial x}$.

To convert the governing equations into a set of similarity equations, we introduce the following similarity transformation:

$$\eta = y\sqrt{\frac{U_0}{\upsilon x}}, \quad \psi = \sqrt{U_0 \upsilon x} f(\eta), \quad \theta = \frac{T - T_\infty}{q}\kappa\sqrt{\frac{U_0}{\upsilon x}}, \quad \phi = \frac{C - C_\infty}{C_w - C_\infty}\sqrt{\frac{U_0}{\upsilon x}}$$

From the above transformations, the non-dimensional, nonlinear and coupled ordinary differential equations are obtained as

$$f''' + \frac{1}{2}ff'' - Mf' + Gr\theta + Gm\phi = 0 \tag{5}$$

$$\theta'' + \frac{1}{2}\Pr(f\theta' - f'\theta) + \Pr R_a \varphi = 0 \tag{6}$$

$$\varphi'' + \frac{1}{2}Sc(f\varphi' - f'\varphi) - ScC_r\varphi = 0 \tag{7}$$

The transform boundary conditions:

$$f = 0, \ f' = 1, \ \theta' = -1, \varphi = 1 \text{ at } \eta = 0 \text{ and } f' = \theta = \varphi \to 0 \text{ as } \eta \to \infty$$

Where f', θ and φ are the dimensionless velocity, temperature and concentration profiles respectively, η is the similarity variable, the prime denotes differentiation with respect to η.

Also the non-dimensional parameters are

$$Gr = \frac{g\beta qx}{U_0^2 \kappa}\sqrt{\frac{\nu x}{U_0}}, Gm = \frac{g\beta^*(C_w - C)x}{U_0^2}\sqrt{\frac{\nu x}{U_0}}, M = \frac{\sigma B_0 x}{\rho U_0}, \Pr = \frac{\nu}{\alpha}, R_a = \frac{\kappa m Q^* x}{q U_0 D_m}, C_r = \frac{\lambda^* x}{U_0}, Sc = \frac{\nu}{D_m}$$

are the Grashof number, modified Grashof number, magnetic parameter, Prandtl number, heat absorption parameter, chemical reaction parameter and Schmidt number respectively.

3. Results and Discussion

Numerical calculation for distribution of the velocity, temperature and concentration profiles across the boundary layer are displayed in Fig. 1- Fig.12 for different values of magnetic parameter M, Prandtl number Pr, heat absorption parameter R_a, chemical reaction parameter C_r and Schmidt number Sc and for fixed values of Gr and Gm. The values of Prandtl number Pr are chosen for 1.00 which correspond to salt water and Schmidt number are taken 0.66 which correspond to water vapor. Throughout the calculations, the bouncy parameter Gr = -5.0 and Gm = -5.0 are taken which correspond to a hot plate and other parameters are chosen arbitrary. The effects of various parameters on velocity profile are shown in Fig. 1- Fig. 4. In Fig. 1 it is observed that the velocity decreases with an increase in the M. The magnetic parameter is found to retard the velocity at all points of the flow field. It is because that the application of transverse magnetic field will result in a resistive type force (Lorentz force) similar to drag force which tends to resist the fluid flow and thus reducing its velocity. Similar effect arises for the increasing values of heat absorption parameter but reverse trend arises for the increasing values of Prandtl number and chemical reaction parameter which are shown in Fig.4, Fig.2 and Fig.3.
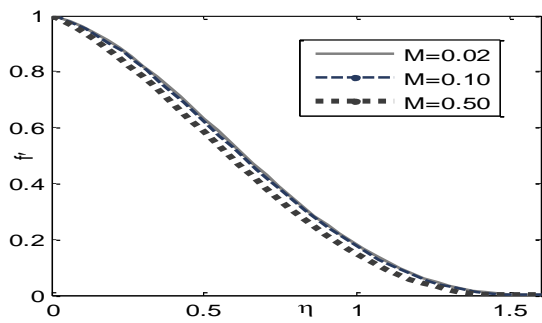
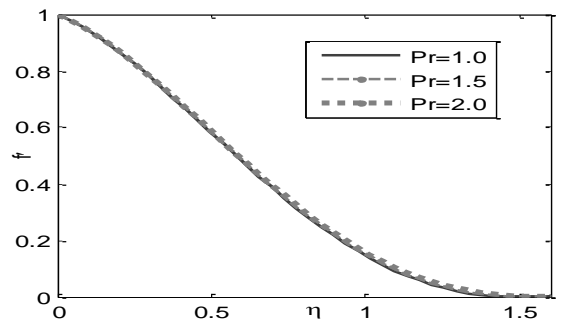

Fig.1. Velocity profile for various values of M

Fig.2. Velocity profile for various values of Pr
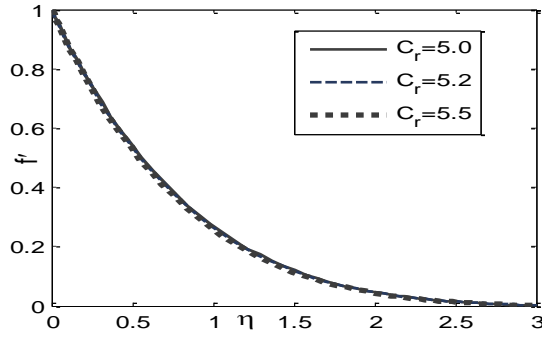
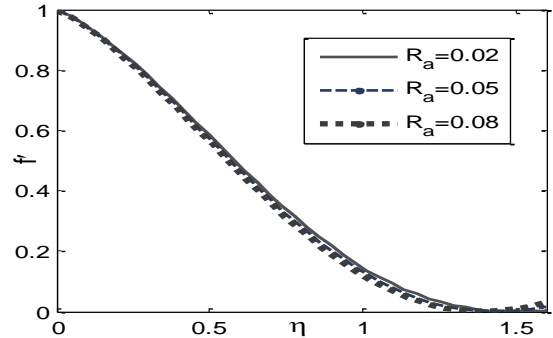**Fig.3.** Velocity profile for various values of C_r

Fig.4. Velocity profile for various values of Ra

The effect of various parameters on temperature profile are shown in Fig.5 - Fig.8. From these figures we see that, the temperature profile is starting at the initial point of the plate surface and then decreasing until it reaches to zero far away from the plate satisfying the boundary condition. Fig.5 shows the temperature distribution for different values of the magnetic field parameter M and observed that the thermal boundary layer decreases as M increases adjacent to the surface of the plate and the effect is not significant far away from the plate. Fig. 6 which illustrate the effect of Prandtl number Pr on the temperature profile. From this figure it is observed that the temperature decreases with an increase in the Prandtl number, which implies viscous boundary layer is thicker than the thermal boundary layer. From these plots it is evident that large values of Prandtl number result in thinning of the thermal boundary layer. In this case temperature asymptotically approaches to zero in free stream region. Fig.7 and Fig.8 indicates the variation of heat absorption parameter and chemical reaction parameter. It is noticed that the thermal boundary layer is increasing.
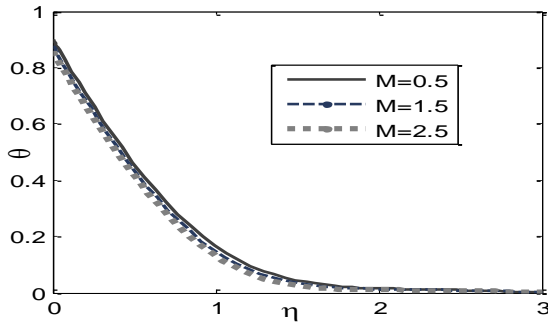
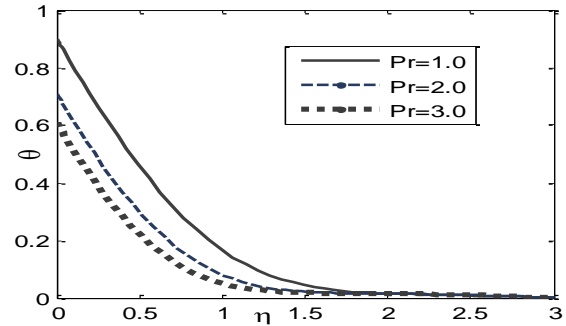Fig.5. Temperature profile for various values of M

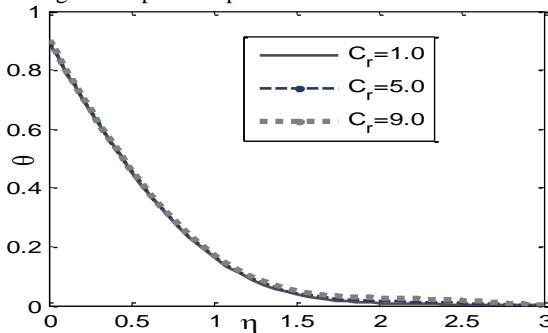Fig.6. Temperature profile for various values of Pr

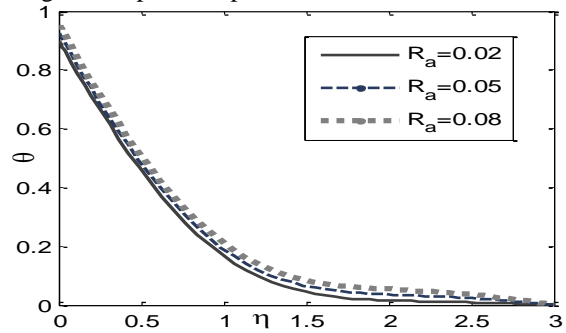Fig.7. Temperature profile for various values of C_r

Fig.8. Temperature profile for various values of R_a

Fig. 9 - Fig. 12 shows the concentration profiles obtained by the numerical simulation for various values of entering non-dimensional parameters. In Fig. 12 the effect of Sc is found to decrease the concentration because increasing in Sc decreases molecular diffusivity which result a decrease of the boundary layer. Hence the concentration of the species in lower for large values of Sc. From the Fig. 9 and Fig.11 it is observed that, the negligible decreasing and increasing effect on concentration profiles for increasing values of M and R_a. The concentration profile is increased for increasing values of chemical reaction parameter which are shown in Fig.10.
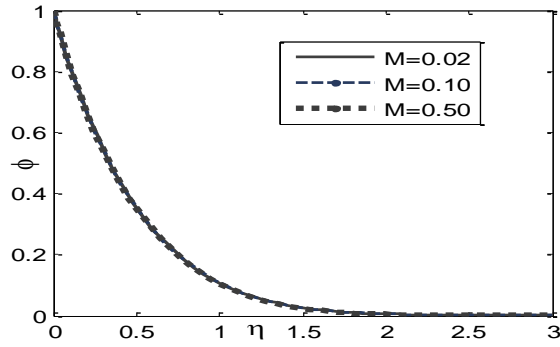
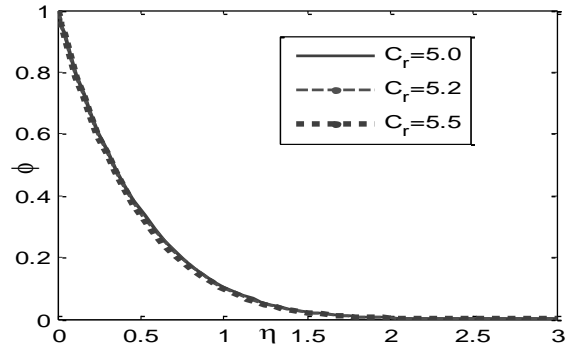Fig.9. Concentration profile for various values of M

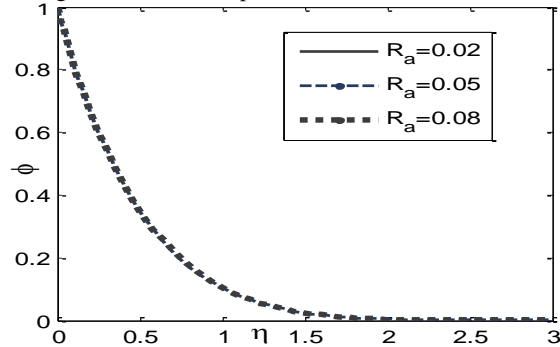Fig.10. Concentration profile for various values of C_r

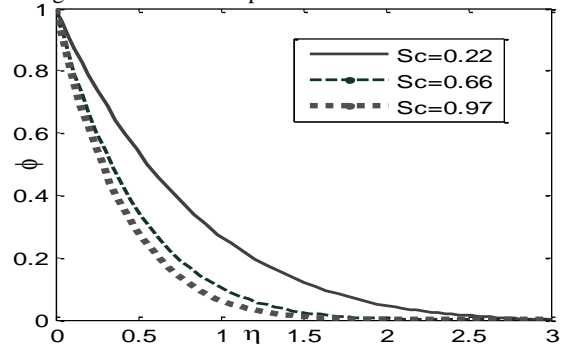Fig.11. Concentration profile for various values of R_a

Fig.12. Concentration profile for various values of Sc

Again, from Table 1 it is observed that the skin friction is decreased for magnetic parameter and heat absorption parameter as a result the momentum boundary layer is decreased but reverse result arises for chemical reaction parameter & Prandtl number. Again, the rate of concentration is increased for magnetic parameter, chemical reaction parameter and Schmidt number as a result the concentration boundary layer is decreased but the rate is constant for heat absorption parameter. Also Table 2 depicts the comparison result for various values of M with Ahmed A. Afify[11] in absence of heat absorption parameter and found to be in good agreement.

Table 1. The skin friction $f'(0)$ and rate of concentration $-\varphi'(0)$ for different values of M, R_a, C_r, Pr and Sc are respectively by considering hot plate

Table 2. The values of $f''(0)$ and rate of concentration transfer $-\varphi(0)$ for different values of M when Pr =0.71, Gr = Gm = 0.5, Sc = 00.1, C_r = 0.1 and R_a = 0 respectively.

M	R_a	C_r	Pr	Sc	$f'(0)$	$\varphi'(0)$
0.02	0.02	5.0	1.0	0.66	-0.2379	1.9799
0.10	0.02	5.0	1.0	0.66	-0.2743	1.9805
0.50	0.02	5.0	1.0	0.66	-0.4461	1.9836
0.5	**0.05**	5.0	1.0	0.66	-0.4675	1.98359
0.5	**0.08**	5.0	1.0	0.66	-0.4868	1.98359
0.5	0.02	**5.2**	1.0	0.66	-0.4258	2.0156
0.5	0.02	**5.5**	1.0	0.66	-0.3912	2.0627
0.5	0.02	5.0	**1.5**	0.66	-0.4423	-
0.5	0.02	5.0	**2.0**	0.66	-0.4378	-
0.5	0.02	5.0	1.0	**0.22**	-	1.1764
0.5	0.02	5.0	1.0	**0.66**	-	1.9836
0.5	0.02	5.0	1.0	**0.97**	-	2.3915

	Ahmed A. Afify[11]		Present results	
M	$f'(0)$	$-\varphi'(0)$	$f'(0)$	$-\varphi'(0)$
0.1	0.39405	0.77174	0.40123	0.76892
0.5	0.94516	0.73770	0.93851	0.74532
1.0	1.45174	0.67701	1.46123	0.67823

4. Conclusions

In the present paper is an investigation of steady MHD free convection, heat and mass transfer flow of an incompressible electrically conducting fluid over a stretching sheet in a rotating system under the influence of an applied uniform magnetic field with Hall current. The leading equations are solved numerically by the shooting method along with Runge- Kutta fourth order integration scheme. The results are presented to display the flow characteristic like velocity, temperature and concentration. Following are the conclusions made from above analysis:

- The magnitude of velocity profile decreases with increasing magnetic parameter. The magnetic parameter is found to retard the velocity at all points of the flow field. As, M, increase, the Lorentz force, which opposes the flow, also increases and leads to enhanced deceleration of the flow.
- The thermal boundary layer decreases as M increases adjacent to the surface of the plate and the effect is not significant far away from the plate. The temperature decreases with an increase in the Prandtl number, which implies viscous boundary layer is thicker than the thermal boundary layer. From these plots it is evident that large values of Prandtl number result in thinning of the thermal boundary layer.
- The effect of Sc is found to decrease the concentration profile because increasing in Sc decreases molecular diffusivity which result a decrease of the boundary layer. Hence the concentration of the species in lower for large values of Sc.
- The skin friction is decreased for magnetic parameter and heat absorption parameter as a result the momentum boundary layer is decreased but reverse result arises for chemical reaction parameter & Prandtl number. Again, the rate of concentration is increased for magnetic parameter, chemical reaction parameter and Schmidt number as a result the concentration boundary layer is decreased but reverse case arises for heat absorption parameter

5. References

[1] S. M. Sonth, S. K. Khan, M. S. Abel, and K. V. Prasad, " Heat and Mass Transfer in a Visco-elastic Fluid Flow over an Accelerating Surface with Heat Source and Viscous Dissipation", *Heat and Mass Transfer*, Vol. 38, pp. 213-220, 2002.

[2] Y. Tan, X. C. You, Xu Hang, and S. J. Liao, "A new Branch of the Temperature Distribution of Boundary Layer Flows over an Impermeable Stretching Plate", *Heat and Mass Transfer*, Vol. 44, pp. 501-504, 2008.

[3] P. K. Singh, "Heat and Mass Transfer in MHD Boundary Layer Flow Past an Inclined Plate with Viscous Dissipation in Porous Medium", *International Journal of Scientific & Engineering Research*, Vol. 3, No. 6, 2012.

[4] A. A. Afify, "MHD Free-Convective Flow and Mass Transfer over a Stretching Sheet with Chemical Reaction", *Heat and Mass Transfer,* Vol.40, pp. 495-500, 2004.

[5] R. Cortell, "A note on Magnetohydrodynamic Flow of a Power-law Fluid over a Stretching Sheet", *Applied Mathematics and Computation,* Vol. 168, pp. 557-566, 2005.

[6] M. S. Abel and N. Mahesha, "Heat Transfer in MHD Viscoelastic Fluid Flow over a Stretching Sheet with Variable Thermal Conductivity, Non-uniform Heat Source and Radiation", *Applied Mathematical Modeling,* Vol. 32, pp. 1965-1983, 2008.

[7] A. Ishak, R. Nazar and I. Pop, "Hydro magnetic Flow and Heat Transfer Adjacent to a Stretching Vertical Sheet", *Heat Mass Transfer*, Vol. 44, 921-927, 2008.

[8] F.M. Ali, R. Nazar and N.M. Arifin, "MHD Viscous Flow and Heat Transfer Induced by a Permeable Shrinking Sheet with Prescribed Surface Heat Flux", *WSEAS Transactions on Mathematics,* Vol. 9, No. 5, 365-375, 2010.

[9] A. Ishak, R. Nazar and I. Pop, "Unsteady Mixed Convection Boundary Layer Flow Due to a Stretching Vertical Surface", *The Arabian Journal for Science and Engineering*, Vol. 31, 165 – 182, 2006.

[10] V. Rajesh, "MHD Effects on Free Convection and Mass Transform Flow through a Porous Medium with Variable Temperature, *International Journal of Applied Mathematics and Mechanics*, Vol. 6, No. 14, pp.1 – 16, 2010.

[11] Ahmed A. Afify, "MHD free convective flow and mass transfer over a stretching sheet with chemical reaction", *Heat and Mass Transfer,* Vol. 40, 495 – 500, 2004.

Paper ID: TE-17

Temperature Distribution and Thermal Comfort Analysis of a Shoe for summer and Winter Season Using CFD Technique: Bangladesh Perspective

Md. Samsul Arefin[1*], Md. Rafiul Hashar[2], Abu Jor[3]

[1, 2, 3] Department of Leather Engineering, Khulna University of Engineering & Technology,
Khulna-9203, Bangladesh
E-mail: arefinkuet@gmail.com*

Abstract

This paper reports a computational fluid dynamics (CFD) analysis in a shoe during wear, under controlled conditions. Simulation of footwear is becoming very popular in recent years for effective shoe designing through heat transfer, heat generation, heat flux etc. analysis. The aims of this study were to analyze the temperature distribution and thermal comfort level of shoes through predicted mean vote (PMV) & percentage person's dissatisfaction (PPD) model by using CFD technique. For this analysis two different temperature seasons such as summer (40°C) and winter (7°C) season of Bangladesh were considered. According to the PMV scale, the human foot felt hot in the summer season and neutral to slightly cool in the winter season within this shoe and their PPD is up to 99.1% and 24% respectively. Thus, from this analysis it can be conclude that the designed shoe model is comparatively best for use in winter season of Bangladesh.

Keywords: CFD, footwear, temperature, comfort, simulation.

1. Introduction

Thermal comfort is increasingly becoming a crucial factor to be considered in shoe design. The climate inside a shoe is controlled by thermal and moisture conditions and is important to attain comfort. Research undertaken has shown that thermal conditions play a dominant role in shoe climate. Development of thermal models that are capable of predicting in-shoe temperature distributions is an effective way forward to undertake extensive parametric studies to assist optimized design [1]. Nowadays, the footwear and textile manufacturers are focused not only on the quality and design of their products, but also on customer comfort, which has also been one of the primary functions of most of textile and leather products [2]. Regarding foot comfort, the movement adaptability of the material, waterproof qualities, weight and the thermal and moisture control would be the main parameters to be taken into account in shoe development [3]. According to the inquiry performed by Kuklane et al. [4] about the main problems related to feet comfort, up to 43% of customers dislike having cold feet and 12% are concerned about sweat problems. Therefore, thermal comfort is an important key when considering comfortable shoes, and it can be achieved by keeping the shoe temperature in the range from 27°C to 33°C [3, 5]. Besides that, according to Covill et al. [6], the amount of heat generated or supplied to the feet must be compensated by heat loss, so the rate of heat generation and release must be similar in order to maintain the temperature in the comfort range. In addition, the heat flux released by the feet could reach values up to 150 W/m^2 during walking and 240 W/m^2 during exercise [3]. In this study, investigate the temperature distribution within the shoe during wear using CFD technique and analyzed their thermal comfort level using PMV and PPD model according to ASHRAE standard [7].

2. Mathematical formulation

The commercial code Autodesk® Simulation CFD 2015 was used to simulate a three-dimensional steady state turbulent flow and heat transfer in the computational model. The partial differential equations governing fluid flow and heat transfer include the continuity equation, the Navier-Stokes equations and the energy equation [8]. A continuity equation ' (1) ' describes the transport of a conserved quantity. Since mass, energy, momentum, electric charge and other natural quantities are conserved under their respective appropriate conditions; a variety of physical phenomena may be described using continuity equations. The continuity equation is given below:

* Corresponding author. Tel.: +88-01814226112
E-mail address: arefinkuet@gmail.com, arefin@le.kuet.ac.bd

$$\frac{\partial u}{\partial t} + \frac{\partial u}{\partial x} + \frac{\partial u}{\partial y} + \frac{\partial u}{\partial z} = 0 \qquad (1)$$

Navier-Stokes equation ' (2) ' is the basic governing equations for a viscous, heat conducting fluid. The Navier-Strokes equations are given below:

$$\rho(\frac{\partial v}{\partial t} + v.\nabla v) = -\nabla p + \mu\nabla 2v + f \qquad (2)$$

For incompressible and subsonic compressible flow, the energy equation ' (3) ' is written in terms of static temperature:

$$\rho Cp(\frac{\partial T}{\partial t} + u\frac{\partial T}{\partial x} + v\frac{\partial T}{\partial y} + w\frac{\partial T}{\partial z}) = \frac{\partial}{\partial x}[k\frac{\partial T}{\partial x}] + \frac{\partial}{\partial x}[k\frac{\partial T}{\partial x}] + \frac{\partial}{\partial x}[k\frac{\partial T}{\partial x}] + qv \qquad (3)$$

3. Material properties

The material properties required for a transient heat transfer shoe model include mass density, specific heat, thermal conductivity, emissivity, transmissivity, electrical resistivity and wall roughness. These properties are also only of importance in transient models, where the change in temperature with respect to time is not zero. The models in this study predominantly used values for these properties that were given in the literature; a list of the material properties used in the heat transfer footwear models and their sources can be seen in Table 1. The thermal property that defines the contact between materials, determines the continuity of temperature distributions and the degree of heat flow between separate materials.

Table 1. Material properties used to assign the CAD model for simulation

Model part	Thermal conductivity (W/m-k)	Specific heat (J/Kg-K)	Mass density (Kg/m³)	Emissivity	Transmissivity	Electrical resistivity (ohm-cm)	Wall roughness (mm)
Shoe upper (leather)	0.16[9]	1500[10]	998[11]	0.95[12]	0.02[12]	1e+16[13]	0.000874[14]
Insole (particle board)[15]	0.078	1300	590	0.8	0	3e+17	0
Occupant (human foot)[15]	50	4182	998	0.98	0	0	0
Air volume[15]	0.02563	1004	--	1	--	--	0

4. Implementation of the simulation model

For this analysis considered two different temperature seasons such as summer and winter season of Bangladesh and also considered the upper material as leather. The process shown in figure 1 was done by generating a geometric model and specifying material properties along with boundary conditions. Next, the model is divided into smaller elements connected at nodes through a process known as meshing and then solved the model. Finally, plots and numerical results are output to provide engineers with insights to the behavior of the model. All the boundary conditions have been assigned for winter season temperature (7°C) and summer season temperature (40°C) of Bangladesh [16].

CAD model
A 3D footwear model with human foot inside it was modeled for this study using CAD software. The detail dimensions of the model can be seen in Table 2.

Materials assignment
Analysis of footwear with Autodesk Simulation CFD relies on the proper assignment of fluid, solid, and occupant materials. It was assigned with leather materials to upper, taxon board to insole, human to foot and air to internal gap.
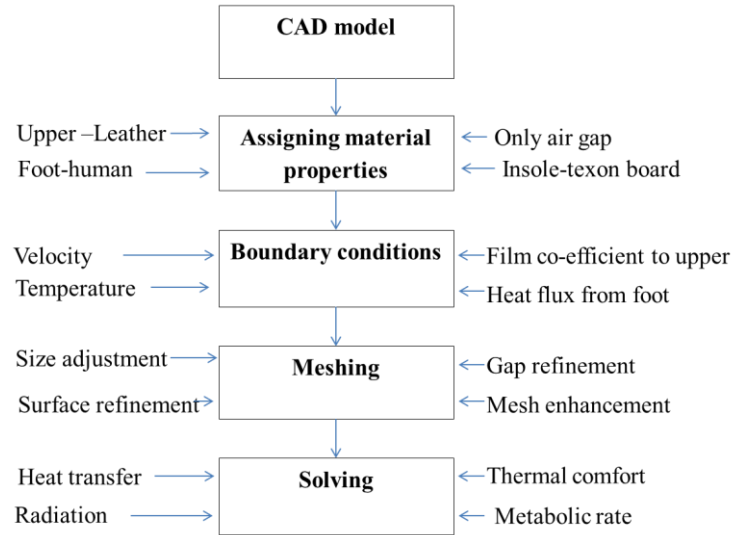
Fig.1. Implementation of the simulation model

Boundary conditions

By assigning boundary conditions such as heat flux, heat generation, film coefficient, velocity, pressure and temperature to openings and other specific locations, we wear effectively "connected" the design with the physical world. Air velocity was assigned at the inlet surface of 0.15 m/s to flow air inside the shoe and a temperature of about 7°C and 40°C was assigned at the inlet section respectively for winter and summer season of Bangladesh.

The outlet surface was defined with atmospheric pressure which allowed the air to move within the model boundary. To simulate heat transfer to the surroundings, without actually modeling the surrounding environment, a boundary condition of film coefficient was applied to the external surfaces. Considering the surrounding air is still, a film coefficient value of 5 W/m² K was used. Reference temperature for film coefficient was equal to ambient temperature of the respective areas which is of around 7°C and 40°C respectively. Heat flux put into the system to represent the heat provided by blood flow. For considering heat flux components in simulation CFD, boundary condition of heat flux was used on the surface of the human foot model. The value for the heat flux wear taken from estimated whole body values of walking (at1.3 m/s) 150 W/m² as presented by cengel. Here the foot surface area was about 7 percent of the whole body surface area [17].

Meshing

The geometry is broken up into small pieces prior to running an Autodesk CFD simulation called elements. The corner of each element is a node. The calculation is performed at the nodes. These elements and nodes make up the mesh. The solution accuracy of any simulation largely depends on grid generation. In figure 2, automatic mesh scheme followed by advanced mesh enhancement was used to generate fine mesh.

Table 2. Detail dimensions of the CAD model

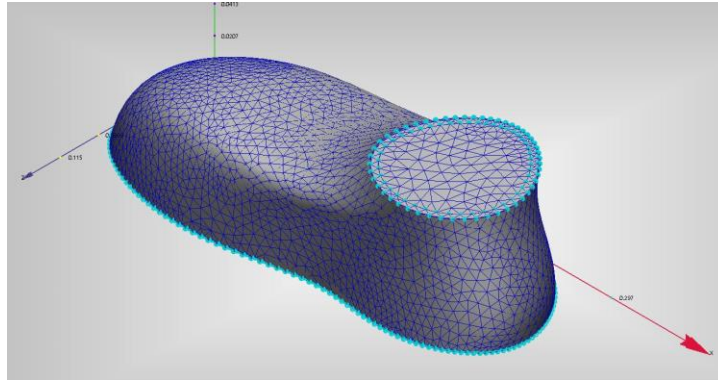| Shoe	Dimension	Unit
Size	43	Paris point
length	28.66	cm
width	9.25	cm
Upper(leather) thickness	0.08	cm
Insole(particle board) thickness	0.20	cm

Fig.2. Meshing view of the CAD model

Solving

The settings to solve the simulation are in table 3. To define how the simulation runs, solve quick edit dialog contains three tabs. The physics tab was used to enable physical models such as flow and heat transfer, the control tab to specify analysis parameters such as steady state or transient and to set the number of iterations and the adaptation tab was used to progressively improve the mesh by running the simulation multiple times. At the end of each run, adaptation modified the mesh based on the results and used the new mesh for the next cycle. The result is a mesh that is optimized for the particular simulation. The mesh is finer for high gradient regions and coarser elsewhere.

Table 3. Solver settings

Solution parameters	Settings/Values
Heat transfer	On
Radiation	On
Thermal comfort	On
Metabolic rate	150 W/m^2
Humidity	50%
Clothing(socks)	0.74 clo
Iterations run	100

5. Results and Discussions

Assigned air of 7°C and 40°C entered into the shoe and came in contact with the heat generating source (i.e. human foot) and got heated. In this way temperature was distributed inside the shoe and increased due to the insulating property of shoe and remained between 8.2°C to 10.3°C and 41.2 to 43.4°C respectively shown in figure 3.
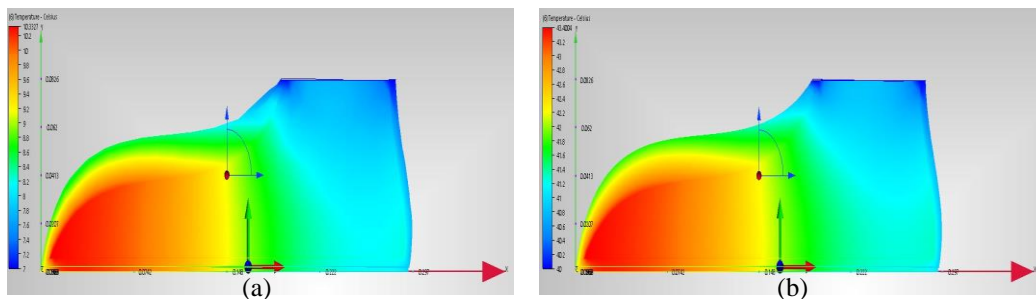

Fig. 3. Temperature distribution (a) for winter and (b) for summer season of Bangladesh

The temperature profile at toe, heel and bottom portion on XY plane was shown in figure 4 for winter season of Bangladesh. It showed the vertical thermal stratification in the shoe. At the toe, heel and bottom portion the temperature was in the range of 10.15°C to 10.34°C, 7.6°C to 8.2°C and 8.2°C to 10.3°C ˗ respectively. In the ˗
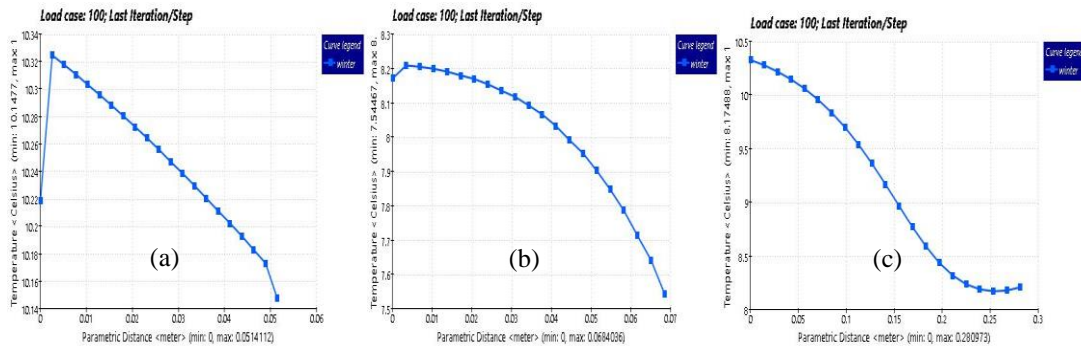
4

Fig. 4. Temperature profile at (a) toe portion, (b) heel portion and (c) bottom portion for winter season of Bangladesh
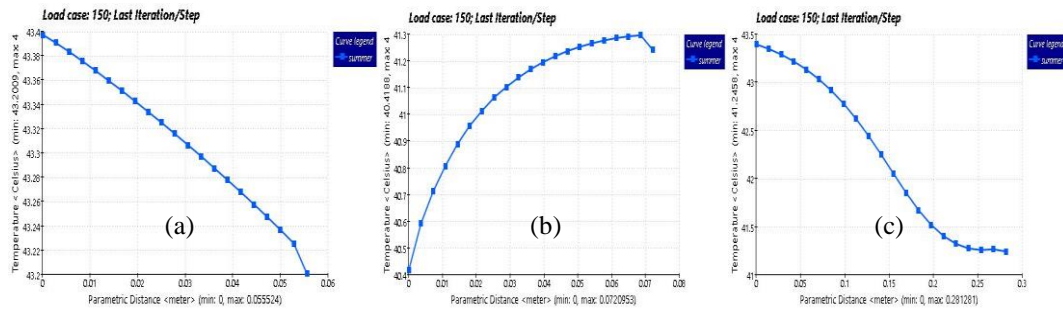

Fig. 5. Temperature profile at (a) toe portion, (b) heel portion, (c) bottom portion in summer season of Bangladesh

same way, the temperature profile at toe, heel and bottom portion on XY plane was shown in figure 5 for summer season of Bangladesh. At the toe, heel and bottom portion the temperature was in the range of 43.2°C to 43.4°C, 40.4°C to 41.3°C and 41.3°C to 43.4°C respectively in summer season of Bangladesh whereas optimum and acceptable ranges of operative temperature for people during 50% relative humidity and mean air speed (≤ 0.15 m/s) are 22°C and 24.5°C for winter and summer respectively according to ASHRAE [18]. The temperatures within the footwear were much more in the toe portion than in the heel portion due to the variation of air circulation within the shoe.

According to PMV, the occupant (human foot) felt neutral to slightly cool in the winter season and felt hot in the summer season of Bangladesh within the shoe and their PPD is up to 99.1% in summer season but up to 24% in winter season of Bangladesh shown in figure 6, that means the shoe is near the comfort range only in winter season of Bangladesh whereas the acceptable thermal environment for general comfort are PMV, -0.5 to + 0.5 and PPD, <10% [19].
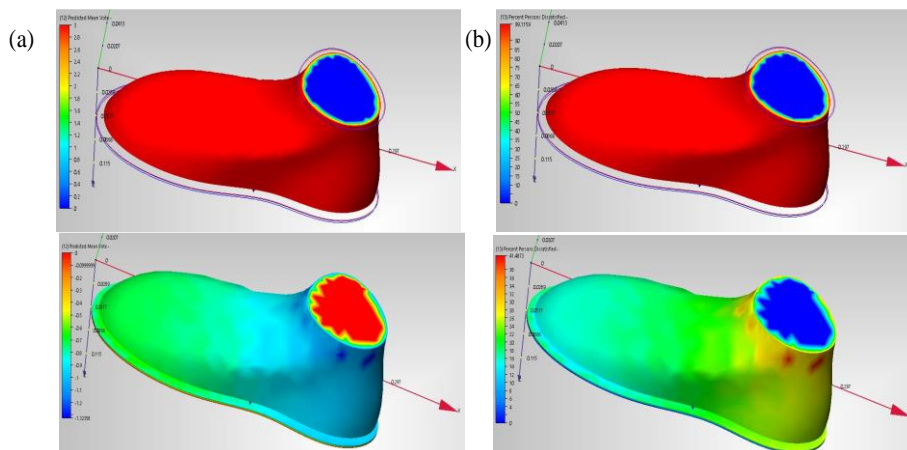

Fig. 6. Comparison of (a) PMV and (b) PPD among two different temperature regions

6. Conclusions

In this research work, thermal comfort aspects of shoe were analyzed for two different temperature seasons such as winter season and summer season of Bangladesh using CFD simulation technique. The main goals of this study were to investigate the temperature distribution inside the shoe and analyze their thermal comfort level and find out a way of verifying optimum comfort for shoe design. The temperatures within the footwear were much more in the toe portion than in the heel portion due to the variation of air circulation within the shoe. Occupant's (human foot) PMV and PPD values were not acceptable according to ASHRAE thermal sensation scale when used in summer season of Bangladesh due to human foot felt hot and experienced 99.1% discomfort in this season. On the other hand PMV and PPD values were quite acceptable when the shoe used in winter season of Bangladesh due to the human foot felt neutral to slightly cool and experienced only 24% discomfort which showed a good accordance with the comfort range. Now it can be conclude that the designed shoe model is comparatively best for use in winter season of Bangladesh. Thus the effectiveness of the shoe design for keeping the human foot comfortable for any kind of design or temperature regions can be assessed. Thus can be analyzed the effects of design changes and develop a design that delivers the desired performance.

7. Acknowledgement

8. References

[1] D. Covill, Z.W. Guan, M. Bailey, and H. Raval, "Development of thermal models of footwear using finite element analysis", Proc. *IMechE Part H: J. Engineering in Medicine*, August 2010, Vol. 225.

[2] N. Sarier, and E. Onder, "Organic phase change materials and their textile applications: an overview", *Thermochim Acta 2012*, 540: 7–60.

[3] K. Kuklane, "Protection of feet in cold exposure", *Ind Health 2009*, 47: 242–253.

[4] K. Kuklane, Y. Holmer, and G. Giesbrecht, "Change foot-wear insulation at various sweating rates", *J Physiol Anthropol Appl Hum Sci 1999*, 18: 161–168.

[5] G.S. Song, "Effect of floor surface temperature on blood flow and skin temperature in the foot", *Indoor Air 2008*, 18: 511–520.

[6] D. Covill, Z.W. Guan, M. Bailey et al., "Development of thermal models of footwear using finite element analysis", *Proc IMechE Part H J Eng*. Med 2011, 225: 268–281.

[7] ANSI/ASHRAE Standard 55-2004, "Thermal Environmental Conditions for Human Occupancy", *American Society of Heating, Refrigerating and Air-Conditioning Engineers, Inc*., 1791 Tullie Circle NE, Atlanta, GA 30329, (www.ashrae.org)

[8] D.C. Sert, "Governing Equations of Fluid Flow and Heat Transfer", *Finite Element Analysis in Thermo fluids*, ME 582.

[9] I. Martinez, "Properties of solids", 1995-2015.

[10] R.J. Kanagy, "Specific Heats of Collagen and Leather", October 1955, Vol. 55, No. 4.

[11] H. Ishii, Y. Sakurai, and T. Maruyama, "Effect of soccer shoe upper on ball behavior in curve kicks", *Scientific reports*, August 2014.

[12] D. Brownleigh, Raleigh, "Basics of non-contact temperature measurement", *MICRO-EPSILON*, 8120, NC 27617 / USA.

[13] E.C. Weir, "Influence of Temperature and Moisture on the Electrical Properties of Leather", *Journal of Research of the National Bureau of Standards*, May 1952, Vol. 48, No. 5.

[14] X. Liu, Z. Yue, Z. Cai, D.G. Chetwynd and S.T. Smith, "Quantifying touch–feel perception: tribological aspects", *Meas. Sci. Technol*., February 2008.

[15] Autodesk® Simulation CFD 2015, Commercial CFD Software, Student Version, © 2014 Autodesk Inc.

[16] S.K. Khanna, and K.N. Shudarshan, "Encyclopedia of South Asia Bangladesh", *S B Nangia, A P H Publishing Corporation*, 5, Ansari road, New Delhi, India

[17] D. Covill, Z.W. Guan, M. Bailey, and H. Raval, "Development of thermal models of footwear using finite element analysis", *Proc. IMechE Part H: J. Engineering in Medicine*, August 2010, Vol. 225.

[18] J.F. Kreider, "Handbook of Heating, Ventilation, and Air Conditioning", CRC Press, Dec 26, 2000 - *Technology & Engineering* - 680 pages.

[19] Proposed Addendum d to Standard 55-2004, "Thermal Environmental Conditions for Human Occupancy", *First Public Review*, Sep 2008.